

Closed-Loop Turbulence Control: Progress and Challenges

Steven L. Brunton

Department of Mechanical Engineering and
eScience Institute,
University of Washington,
Seattle, WA 98195

Bernd R. Noack

Institut PPRIME, CNRS - Université de Poitiers - ENSMA, UPR 3346,
Département Fluides, Thermique, Combustion,
CEAT,
F-86036 Poitiers Cedex, France
Institut für Strömungsmechanik,
Technische Universität Braunschweig,
D-38108 Braunschweig, Germany

Closed-loop turbulence control is a critical enabler of aerodynamic drag reduction, lift increase, mixing enhancement, and noise reduction. Current and future applications have epic proportion: cars, trucks, trains, airplanes, wind turbines, medical devices, combustion, chemical reactors, just to name a few. Methods to adaptively adjust open-loop parameters are continually improving toward shorter response times. However, control design for in-time response is challenged by strong nonlinearity, high-dimensionality, and time-delays. Recent advances in the field of model identification and system reduction, coupled with advances in control theory (robust, adaptive, and nonlinear) are driving significant progress in adaptive and in-time closed-loop control of fluid turbulence. In this review, we provide an overview of critical theoretical developments, highlighted by compelling experimental success stories. We also point to challenging open problems and propose potentially disruptive technologies of machine learning and compressive sensing. [DOI: 10.1115/1.4031175]

1 Introduction

Taming turbulence for engineering goals is one of the oldest and most fruitful academic and technological challenges. One of the earliest examples is the feathers at the tail of an arrow invented several thousand years ago. These feathers stabilize the orientation of the arrow and make the trajectory more predictable and increase its range. Meanwhile, modern turbulence control has applications of epic proportion. Examples include drag reduction of road vehicles, airborne transport, ships and submarines, drag reduction in pipes and air-conditioning systems, lift increase of airfoils, efficiency increase of harvesting wind and water energy, of heat transfer and of chemical and combustion processes—just to name a few examples.

Animal motion has inspired numerous technical advances in engineering flows [1]. The shape of sharks, dolphins, and whales, for instance, yields a low drag per volume [2]. It is not an accident that zeppelins and airplanes have similar shapes. Dolphins are speculated to delay boundary layer transition by a compliant skin. This form of transition delay has been applied to submarines and is under active investigation. Under magnification, the skin of sharks exhibits riblets [3]. Riblets have been found to reduce drag by up to 11% in the laboratory [4]. In-flight tests of riblets on an Airbus passenger airplane have reduced fuel consumption by 2–3%. Some sharks decrease drag by ejecting lubricants during high-speed chases of their prey. A similar skin-friction reduction is used in oil pipelines: one added polymer per 10^6 oil molecules reduces the drag by about 40%. Eagles and other birds have five feathers at the tip of their wings. These feathers increase the lift by reducing the pressure shortcut between the low pressure upper side and the higher pressure lower side. Most modern passenger airplanes have winglets for the same reason.

The environmental benefit of turbulence control can be illustrated with an everyday example: automotive transport. Today, the annual global CO₂ emissions from cars exceed 22×10^9 tons and are expected to increase by 57% by 2030. A large portion of this emission is due to aerodynamic drag [5,6]. At a speed of 50 km/h, the aerodynamic drag accounts for 50% of the total resistance reaching 80% at 130 km/h. A drag reduction of around 25% is currently achievable by active flow control [7]. At a speed of 120 km/h, this would reduce consumption by about 1.8 l and would reduce CO₂ by almost 2 kg per 100 km. In normal traffic, the corresponding reductions are 0.15 l in fuel and 0.73 kg in CO₂. For Europe, this drag reduction would mean a reduction of

23×10^6 tonnes of CO₂ emission in one year. To mitigate pollution, the European government imposes strict norms to car manufacturers. By 2020, the mean CO₂ emission per vehicle must not exceed 95 g CO₂/km. By 2025, the limit is 75 g CO₂/km.

Among the countless technologies that will benefit from turbulence control, we highlight the potential benefits for energy and transportation. Increased lift and reduced drag due to separation control and transition delay would result in increased payloads and decreased runway requirements for aircraft and improved efficiency in nearly all vehicles. Considering that transportation accounts for approximately 20% of global energy consumption, a small improvement would have a dramatic effect [8–10]. Active separation control would also improve the safety of cargo trucks and trains in strong cross-winds [11–13]. Hypersonic vehicles stand to benefit from active control to prevent the undesirable ejection of flames out of the combustion chamber and subsequent quenching. Finally, reducing the amount of turbulent fluctuations on rotor blades would reduce vibration and improve the life of rotor hubs on wind turbines and rotorcraft.

Strategies to control laminar and turbulent flows are classified into three categories [14]: aerodynamic shape optimization, passive, and active control. The first approach for increasing flow performance is the optimization of the aerodynamic shape. Potential flow theory, invented about 150 years ago, provides a simple mathematical foundation. Meanwhile, adjoint-based shape optimization can be numerically performed for the full Navier–Stokes equations. As a second step, passive actuators may improve the performance. Such a device represents a small change of the original configuration. One example is the turbulators on wings of passenger airplanes to delay separation. Such passive devices may come with penalty of parasitic drag. An alternative is the active control devices, such as fluidic vortex generators, which may be turned on and off but require energy for their operation. One advantage is a large dynamic bandwidth, e.g., the excitation of particular frequencies. Active control may be performed in a pre-determined open-loop manner, e.g., periodic blowing and suction, independent of the flow state. The largest gains are, of course, realized in a closed-loop manner when the actuation is informed by the sensors recording the flow state.

Until 1990s, manufacturers have often seen active control as a remedy for a flawed aerodynamic design [15]. Hence, industrial interest has been correspondingly low. Meanwhile, aerodynamic design and passive devices are considered as maturely developed and active control is pursued to further increase the performance, particularly for off-design conditions. Three trends foster closed-loop control. First, the power and reliability of actuators and sensors have dramatically increased, while the price is decreasing.

Manuscript received November 12, 2014; final manuscript received July 25, 2015; published online August 26, 2015. Assoc. Editor: Jörg Schumacher.

Second, a sophisticated control logic can be performed under real-world conditions with increasing computer power and the advancement of mathematical theories. Third, the experimental demonstrations of the benefits of closed-loop over open-loop forcing have become overwhelming (see, e.g., Refs. [16,17]).

Most literature on closed-loop flow control falls in one of three categories: stabilization of laminar flow, adaptive control of turbulence, and model-free tuning of control laws. For the first category, there exists a mature theory for the stabilization of laminar flows with in-time closed-loop control. Early experimental examples are described in Refs. [18,19], while most studies are based on direct Navier-Stokes (DNS) solutions (see, e.g., Refs. [20,21]). “In-time” means that the actuation responds on a time-scale much smaller than the natural time-scale. Most corresponding publications are based on linearization of the evolution equation. The employed evolution equation may be a white-box model, e.g., DNS discretization, resolving all features of the flows, a gray-box model, e.g., proper orthogonal decomposition (POD) models, just describing the coherent structures, or a black-box model, e.g., transfer functions, representing only the input–output behavior. The control logic based on white box models is the most accurate. Gray-box and black-box models are less accurate but allow online-capable control solutions for experiments.

The second category is adaptive control of turbulence usually based on a manipulation of periodic forcing. Most experimental

success stories belong to this class. “Adaptive” means that the change of the actuation parameter, such as amplitude or frequency, is slow compared to the natural time-scale. The third group consists of in-time control of turbulent flows, for instance, by tuning simple laws, e.g., opposition or proportional-integral-derivative (PID) control [22]. The inherent nonlinearities of turbulence pose a challenge for model-based in-time control.

Closed-loop control requires decisions on the hardware, such as the kind, number, location, and dynamic bandwidth of actuators and sensors. Such decisions may be guided by modern adjoint-based techniques for linearized equations, i.e., for laminar flow. For turbulence, these decisions are largely guided by engineering wisdom from the flow control processes and past experiments. The control laws may be guessed based on the flow phenomenology. These aspects will be touched in Sec. 2. The focus of this review is the control logic sketched in Fig. 1. This logic is based on model complexity, e.g., model-free approaches (bottom right of this figure), black-box (left), gray (middle), and white-box models (right). Experimental flow control solutions require a delicate compromise between simplicity and accuracy. Many plants benefit from system reduction approaches. This spectrum of models will be outlined in Sec. 3. The most complete model-based control design techniques are available for linear models. These will be described in Sec. 4. The detailed review of linear control theory may be surprising in a review about control of nonlinear

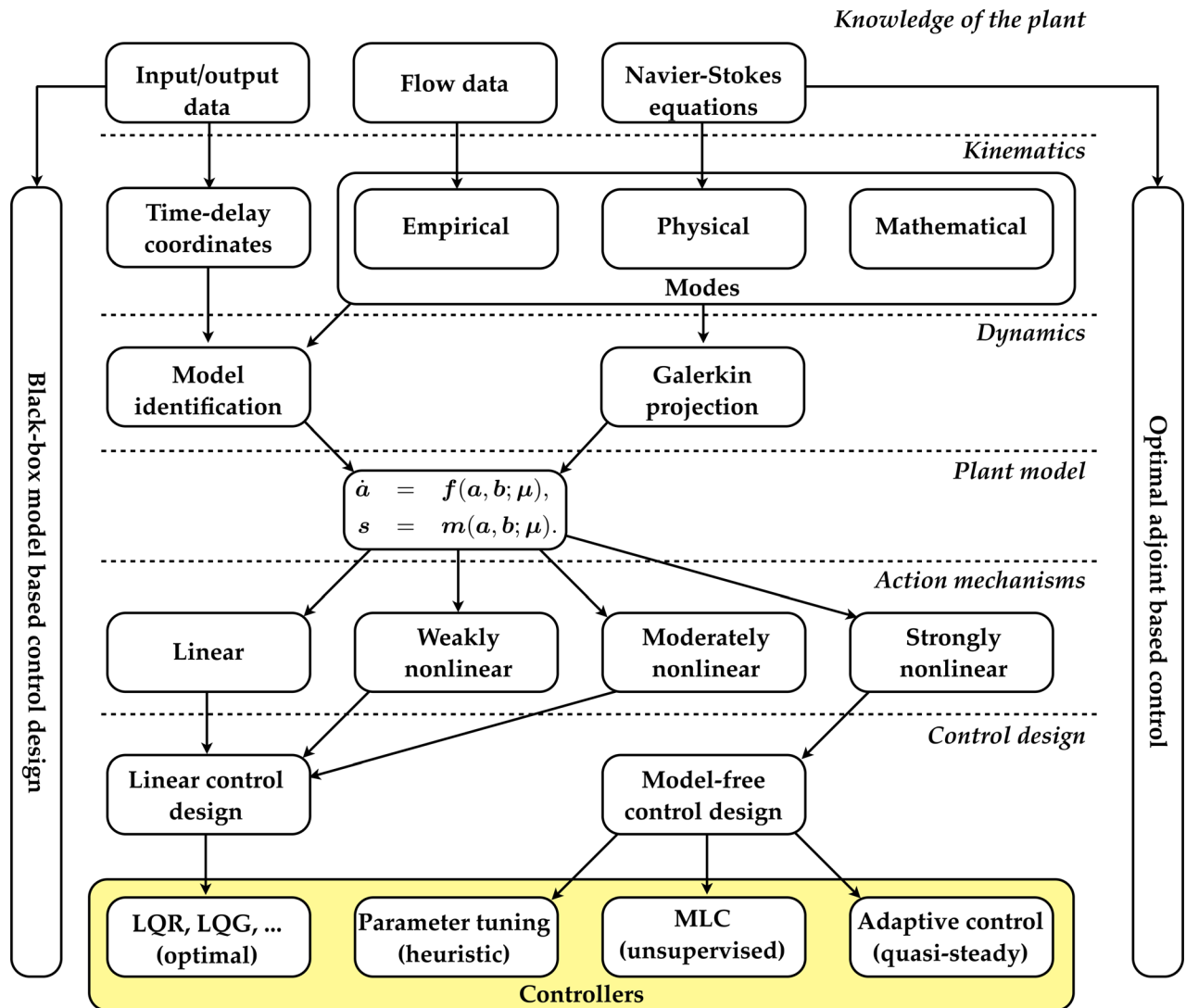


Fig. 1 Turbulence control roadmap. For details, see text and the respective sections.

turbulence processes. We emphasize linear control for three reasons. First, it is a beautiful theory showing clearly the effects of model accuracy and design parameters. Second, the prevention of turbulence, i.e., transition control, can largely be done based on a linear theory. Third, even some strongly nonlinear processes may be tamed with linear control methods, if the nonlinearity is well understood. Examples of such “reducible” nonlinear models are provided in Sec. 5. Model-free approaches for “nonreducible” nonlinear dynamics are reviewed in Sec. 6. In Sec. 7, we summarize good practices of flow control and promising directions of future research are discussed in Sec. 8.

This review focuses on modeling and control methods for nonlinear dynamics associated with turbulent fluid flows. Theoretical and computational aspects of optimal and robust (linear) control are elaborated in Ref. [23]. A large spectrum of linear system approaches is presented in Refs. [20,21,24], and periodic excitation is reviewed in Ref. [25]. We illustrate the performance of the methods by referring to select successful closed-loop control studies. Preference is given to academic studies for simple geometries. There are additional books and reviews in the related fields of flow control for wall flows [26–28], for turbulent mixing [29–31], for turbulent jets [32], for combustion [33], for cavity flows [21,34], for bluff bodies [35], and for actuators [36].

2 Turbulence Control Problem

Turbulence control comprises decisions on the flow control plant, on the cost functional, on the actuation and sensing, and, last but not least, on the control logic. The control logic serves to minimize the cost functional under given constraints. For linear dynamics, there exist adjoint-based methods for the choice of the actuators [21] and the sensors [37]. For turbulent flows, the application of these methods is limited and the choice is generally based on experience and engineering wisdom. In this section, we provide heuristics for turbulence control decisions. Thereafter, a mathematical foundation of the control logic is elaborated.

2.1 The Flow Control Plant and Associated Goals. In the sequel, flow is assumed to be within or around a steady boundary with small unsteady actuators and sensors. Academic flow control configurations strive at geometric simplicity for enhanced reproducibility and for “clean” understandable physical mechanisms. Examples include free shear flows from a bluff body, a mixing layer or a jet and wall-bounded flows in a channel or over a flat plate. Cavity noise, suppression of aeroelastic oscillation, and flame-holder combustion serve as examples for multiphysics flows.

Configurations of industrial importance tend to be geometrically far more complex, such as the flow around a car, truck, train, airplane, or wind-turbine. Internal flows in pipes, diffusers, combustors, mixers, air-conditioning systems, and buildings are further examples. Each of these configurations could profit from closed-loop control and the range of potential applications has epic proportion (see Fig. 2). Yet, many flows with complex geometries can locally be approximated by the above-mentioned academic configurations. Thus, a working flow control experience on simple test cases is advantageous in the design of efficient control for industrial purposes.

The aerodynamic performance of transport vehicles and wind-turbines is based on a *force optimization*, such as drag reduction, lift increase, or reduction of fluctuations to prevent early material fatigue. Examples are transportation trucks (PACCAR), airplane wings, wind turbine blades, helicopter rotor hubs, and reduction in structural loads. Combustors, heat exchangers, and chemical mixers profit from *mixing enhancement*. *Noise reduction* is a common request for greener transport systems. Many of the above applications can be idealized to aim at the stabilization of an unstable fixed point or periodic orbit, which we may refer to as *instability suppression*. Some internal flows require an improved *destabilization*, such as the mixing enhancement in a combustor.

Most control objectives can be formalized in a rigorous mathematical manner. Drag reduction, for instance, reduces by definition the necessary propulsion or towing power. The optimal drag reduction may be defined by the maximum energetic benefit, i.e., the saving in towing power subtracting the investment in actuation power. Note that any well-defined control problem requires a penalization of the actuation power.

Many experimental studies demonstrate that the control is effective for a well-defined operating condition in a noise-free wind-tunnel environment. Engineering applications require additional effectiveness for the intended operating envelope, including various oncoming velocities, a range of angles of attack, free-stream turbulence, just to provide few examples. Ideally, robustness of the control is included upfront in an objective comprising a range of operating conditions, like in linear H_∞ control (see Sec. 4.4). At minimum, the level of robustness needs to be assessed after a single point optimization of actuation. An understanding of the turbulence control mechanisms provides a first hint on the expectable level of robustness.

2.2 Linear Dynamics. Turbulence is known as the last unsolved problem of classical mechanics, largely because the effects of nonlinearity are next to impossible to predict from first principles. Hence, turbulence control can be seen as an even more herculean nonlinear problem as not only the unforced state needs to be predicted but also the effect of a small actuation. Fortunately, there exist a number of configurations for which a linear dynamics has been shown to be a good working assumption. Examples include the following cases:

- *Transition delay.* The transition of a laminar into a turbulent boundary layer is associated with a dramatic rise of skin friction. Hence, engineering applications include transition delay with closed-loop control. The laminar state may still be stabilized based on a linearized model. Evidently, *stabilization of a laminar flow* has benefits for numerous other configurations.
- *Drag reduction in wall turbulence.* At high Reynolds numbers, active control at the wall does not have the authority to stabilize the laminar boundary layer. Yet, up to 11% drag reduction can be achieved with stationary riblets which mitigate sweeps in the viscous sublayer [4]. Over 20% drag reduction can be obtained with linear active control [40]. Arguably, linear control is applicable because the sweep prevention in the viscous sublayer is an effectively laminar process, such as transition control.
- The *in-time actuation response to large-scale coherent structures* may be described by a linear model—extending the examples of drag reduction in wall turbulence. Physically, such a locally linear model may be derived under similar conditions as URANS simulations, i.e., if the effect of the unresolved stochastic velocity component on the dynamically resolved coherent structures is roughly represented by a temporally constant eddy viscosity. An example is the mean-field model for oscillatory fluctuations of turbulence (see Sec. 5.3).
- *Adaptive control* may be subject to a limited linear control. For instance, the change of cost function may respond linearly to small changes of the amplitude and frequency of periodic forcing. This is an implicit working assumption of extremum seeking control (see Sec. 6.2). Thus, tracking may be based on locally linear dynamics.
- Another recently discovered example of linear dynamics is the *ensemble-averaged actuation response of a turbulent shear flow* [41]. The practical relevance of this observation still needs to be explored. Studies of forced nonlinear chaotic systems indicate that the ensemble-averaged effect of a Heaviside actuation may be described by linear system while the amplitude dependency is far from linear [42]. Moreover, the ensemble-averaged response may constitute a small

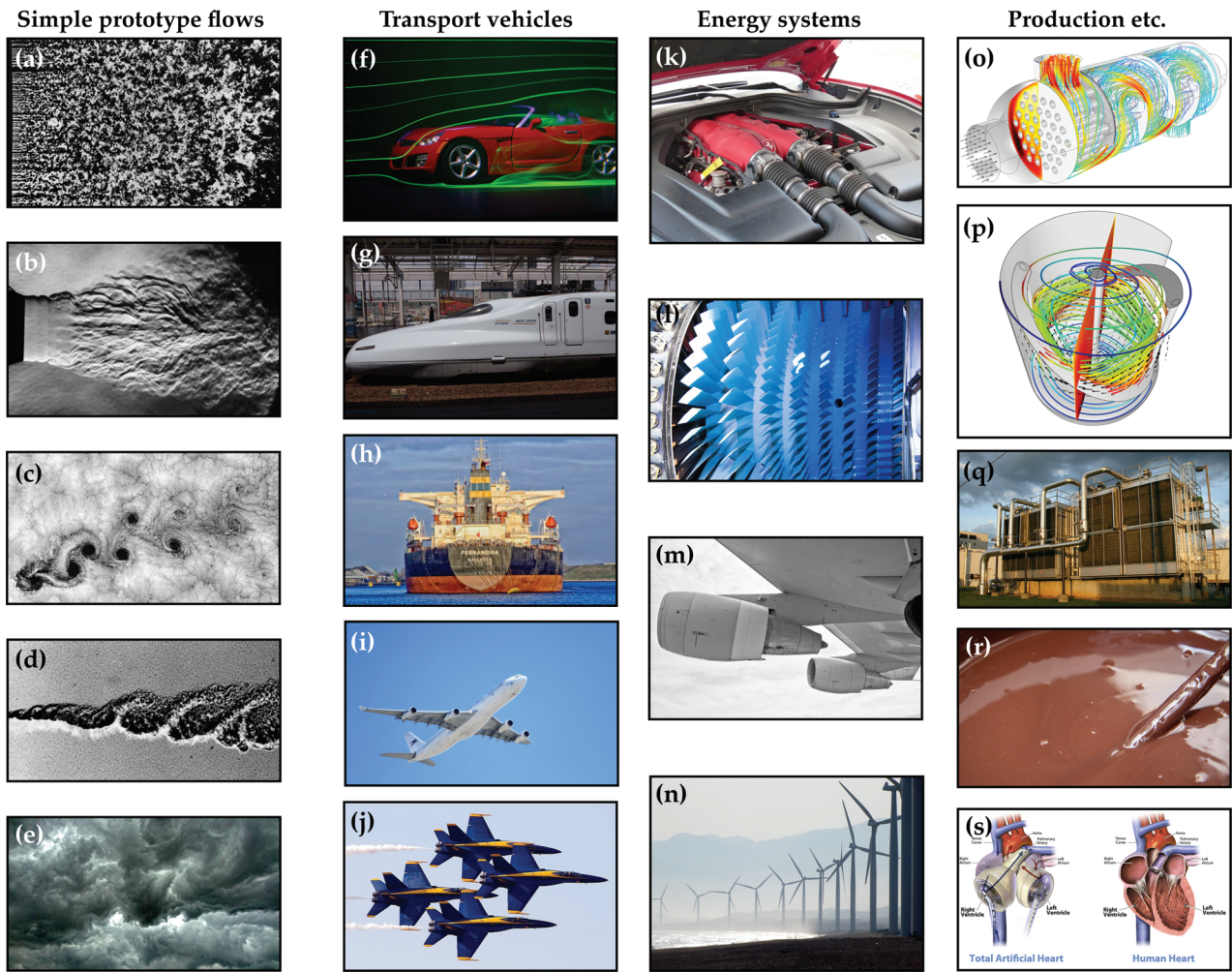


Fig. 2 Applications of closed-loop turbulence control: (a) homogeneous grid turbulence (Reproduced with permission from T. Corke and H. Nagib.); (b) turbulent jet from Bradshaw et al. [38]; (c) Karman vortex street behind a mountain, photo by Bob Cahalan, NASA GSFC; (d) coherent structures in a mixing layer from Brown and Roshko [39]; (e) thunderstorm; (f) automobile in a wind tunnel, photo by Robert G. Bulmahn; (g) high-speed train; (h) cargo ship; (i) passenger jet; (j) Blue Angles fighter jets; (k) automobile engine; (l) turbo jet engine; (m) aircraft engines; (n) wind turbines; (o) heat exchanger flow; (p) rotating mixer; (q) air conditioner; (r) chocolate mixing; and (s) total artificial heart. Images (e) and (g)–(n) are from the website.¹ Images (c), (f), and (q)–(s) are from the website.² Images (o) and (p) were made using the COMSOL Multiphysics® software and are provided courtesy of COMSOL.

portion of the fluctuation energy and may not be very relevant for the control goal.

2.3 Turbulence Control Mechanisms. In the following, common principles of turbulence control are outlined. A *control principle* is understood as a phenomenological rationale based on a simplified physical actuation mechanism. A simple principle has a low-dimensional plant mimicking relevant aspects of turbulence control, including linear and nonlinear dynamics.

We start with stabilizing control. A very simple example is *opposition control*. Let

$$\frac{da}{dt} = a + b$$

be a plant with the unstable fixed point $a=0$ and actuation b . Evidently, the control law $b=-2a$ will “oppose” the natural evolution and stabilize the fixed point. A number of flow control configurations mimic this behavior. Let us consider

Tollmien–Schlichting (TS) waves over a wall. The wall shall have a membrane of which the vertical motion can be controlled. A positive or negative wall-normal velocity fluctuation of a TS wave can be counteracted by a membrane which moves in the opposite direction [18]. Similarly, the transverse centerline motion of a channel flow may be damped by blowing and sucking at opposite sides of the channel wall in order to counteract this fluctuation. Thus, an unstable 2D channel flow may be stabilized. Another example of this category is skin friction reduction. Skin friction is known to increase with sweeps and ejections, both associated with wall-normal velocity fluctuation. A simple opposition control scheme records this velocity fluctuation 10 plus units away from the wall and opposes this motion by local suction or blowing [43].

A slightly more complex principle is *phasor control* based on an oscillatory process. A simple prototypic dynamical system reads

$$\frac{da_1}{dt} = 0.1a_1 - a_2, \quad \frac{da_2}{dt} = 0.1a_2 + a_1 + b$$

Evidently, the fixed point $a_1=a_2=0$ is unstable with respect to an oscillatory instability with unit frequency and growth-rate of 0.1. The control law $b=-0.4a_2$ can be seen to stabilize this fixed

¹<http://pixabay.com>

²<https://commons.wikimedia.org>

point by reducing the fluctuation energy with targeted actuation at the correct phase. Phasor control can also be considered as an opposition control with respect to the amplitude $r = \sqrt{a_1^2 + a_2^2}$. The actuation reduces this amplitude at phases where it is effective. The corresponding energy-based control design will be elaborated in Sec. 5.2. A large class of control laws for suppression of oscillation may be written in the form

$$b = k r \cos(\phi - \beta) \quad (1)$$

where ϕ is the flow phase, β is the phase lag, and k is the gain. In the given example, ϕ is defined by the polar coordinates $a_1 + ia_2 = r \exp(i\phi)$, $\beta = -90$ deg, and $k = 4$. Phasor control (1) is an analogy for virtually any successful stabilization of an oscillatory flow, regardless how the control law is derived. The gains may be constant for assumed linear dynamics or base-flow/energy dependent for weakly nonlinear dynamics. Examples are the stabilization of a laminar cylinder wake with zero net mass flux actuators [44], the stabilization of a turbulent wake in an experiment [45], and the suppression of cavity noise with local forcing [34,46].

A more complex case involves two or few nonlinearly coupled “clock-works” based on the *principle of constructive or destructive frequency cross-talk*. One example is high-frequency forcing which mitigates a target instability [47,48]. Lower frequency forcing may also serve the same purpose [45,49]. Section 5.4 offers a least-order dynamical system for such frequency cross-talk. In the discussed examples, the actuation has a destructive frequency cross-talk with the target instability. However, the frequency interaction may also be constructive. In a mixing layer, the excitation of Kelvin–Helmholtz vortices leads to earlier vortex pairing, i.e., to the excitation of half the actuation frequency. The Kelvin–Helmholtz instability—and thus the vortex pairing—may be mitigated by the excitation of higher frequencies. Without a dynamic model, a careful observation of the flow with respect to period forcing may provide insight into effective control strategies. A sufficiently strong periodic forcing at the right frequency may mitigate the target frequency. The loop may be closed on a long time scale to tune the actuation amplitude to the minimal level. Alternatively, in-time control may destabilize the corresponding oscillator which mitigates the target instability.

The present mechanisms are helpful concepts which can explain many results from the literature and can potentially guide new experiments. Yet, the binary categorization in stabilizing and destabilizing control is an over-simplification. For many control goals, like jet noise reduction, the enabling mechanisms are far from being understood.

In the case of broadband turbulence, no generic simple recipes for the control law can be offered. Yet, we present a highly promising machine-learning strategy in Sec. 6. Figure 3 summarizes all discussed control principles with associated methods. The heuristics for closed-loop turbulence presents a tour de force through the control strategies and methods, which are elaborated throughout this review.

2.4 Actuators and Sensors. The choice of the actuators and sensors, their number, location, frequency range, and amplitude level has a decisive effect on the maximum performance of the control logic. Actuators may include zero-net mass flux actuators [50–52], piezo-electric actuators [53,54], Festo-valves (intermittent blowing), synthetic jets [55–58], plasma actuators [59–65], microelectromechanical systems (MEMS) [66–72], and roughness elements on the wall. Excellent overviews are presented in Refs. [36,55]. Similarly, sensors may measure velocity, pressure, skin-friction, and temperature in various frequency resolutions. These are described in the textbooks of *Experimental Fluid Mechanics*.

Until this day, the choice of the actuators and sensors in experiments is based on engineering experience and on the hypothetical actuation mechanism which shall be exploited. For instance, the sensors are placed before the actuator if the actuation shall counteract upstream perturbations. The sensors are placed downstream

Control mechanism	Control method
Opposition control	Proportional control PID control LQR, LQG control based on a model
Phasor control	PID control Phasor control LQR, LQG control based on a model
Multi-frequency control	Energy-based control Phasor control Low-frequency control High-frequency control
Broadband control	Open-loop control Adaptive control Machine learning control

Fig. 3 Heuristics of turbulence control. Here, s are the sensor signals and b are the actuation signals.

of the actuator, if the actuation mechanism exploits the excited structures. For opposition control, sensors and actuators should be at a similar location. For phasor control, it is important that the actuators are at a high-receptivity point for the oscillatory instability, e.g., a point of geometric separation where the sensors can measure a clean oscillation. The number of rules could easily be extended. For linear dynamics, sophisticated mathematical methods have been developed for actuator and sensor placement, although optimal placement remains elusive. For nonlinear dynamics, heuristic methods for the optimization of sensor placement exist [21]. In this survey, we focus on the control logic.

2.5 Achievable Performance. An important, yet challenging question in turbulence control is the achievable performance. Evidently, any investment in improving a control strategy may be measured in terms of the achievable additional performance. We constrain the discussion to aerodynamic problems. The minimum skin friction in a channel flow is conjectured to be associated with the steady Poiseuille profile. Similarly, the minimum drag of a cylinder wake may also be conjectured to be associated with the steady solution. In fact, most drag reduction strategies are formulated as minimization of the fluctuation energy. Yet, control studies of the cylinder wake exhibit two other potentially desirable flow states. One is the potential solution which is approximated in compliant wall actuation by Wu et al. [73]. Interestingly, Choi et al. [35] reported a better performing optimal control when the cost function for drag reduction contains the difference between the controlled flow and potential solution as opposed to the drag itself. Another solution is closer to the Kirchhoff solution and is achieved by high-frequency forcing [74]. In fact, the drag of high-frequency forcing may even be lower than for the completely

stabilized wake [75]. Yet, both solutions require a significant actuation energy. In fact, the gain in towing power corrected by the actuation energy is less efficient than for complete stabilization. A fourth highly successful drag reduction strategy consists of an aerodynamic shaping of the dead-water region, so that the bluff body and the wake are more streamlined [7].

For high-lift configurations, the potential solution can be conjectured to yield the maximum achievable lift. Similarly, the maximum achievable pressure recovery in diffusers can also be estimated from the potential solution. Summarizing, the hypothesis on achievable performance has not only a theoretical value. The answer may also guide the control strategy.

Finally, we mention mixing enhancement and noise reduction problems in which the cost function explicitly depends on the history of the fluid motion. For such Lagrangian control tasks, an intuition about achievable maximum mixing or the minimum noise emission is still in its infancy.

3 Black-Box, Gray-Box, and White-Box Models

Regardless of the modeling strategy employed below, we assume that we are able to actuate the flow with some input variables $\mathbf{b} \in \mathbb{R}^{N_b}$ and we are able to measure features of the flow with some output variables $\mathbf{s} \in \mathbb{R}^{N_s}$. Once the inputs and outputs are set, there are many choices for the model that links them. For example, we may consider the full discretized Navier–Stokes equations as a high-dimensional nonlinear set of ordinary differential equations. Alternatively, we may relate inputs to outputs through either a statistical description or a set of empirical basis functions. Recent advances in dimensionality reduction techniques and turbulence closures also have exciting implications for the future of turbulence modeling and control.

The choice of model affects nearly every downstream control decision. There are many factors and tradeoffs that must be balanced when deciding on a modeling strategy. These include the accuracy of the model, execution time, generality in other parameter regimes, spatial–temporal resolution relative to disturbances, and the up-front cost to acquire such a model. For example, direct numerical simulation (DNS) is unparalleled at descriptive resolution, generality, and accuracy, but current computational capabilities are decades away from real-time execution for in-time control strategies. Reduced-order models based on data from DNS or experiments provide real-time capable models, but these models are expensive to create and may only work for a small range of training parameters. Fortunately, it may be possible to leverage physical intuition about the structure of the underlying modes, often in terms of linear combinations of full flow fields, to modify the models with additional terms and extend their predictive range. Black-box models based on input–output data are typically faster to generate and require less measured data, but they lack the physical interpretation that goes with having an underlying modal representation.

Figure 4 outlines a model hierarchy for control design, following a classification of Wiener [76] and extending it to include model-free and ultrawhite approaches. These classifications are generally based on the system resolution of the model. Some control laws can be analytically derived from the Navier–Stokes equations. One example is energy-based control to stabilize a flow (see Sec. 5.2). We refer to this control design as “ultrawhite.” An expanded view of the various models and modal decompositions is shown in Fig. 5. This section is not meant to be exhaustive, but rather it includes methods that have either been applied with recent success or methods that have particular promise in the future.

3.1 State-Space Models. In one of the most general frameworks, we will have a state $\mathbf{a} \in \mathbb{R}^{N_a}$ and a nonlinear function f advancing the state forward in time, along with a nonlinear output function \mathbf{m}

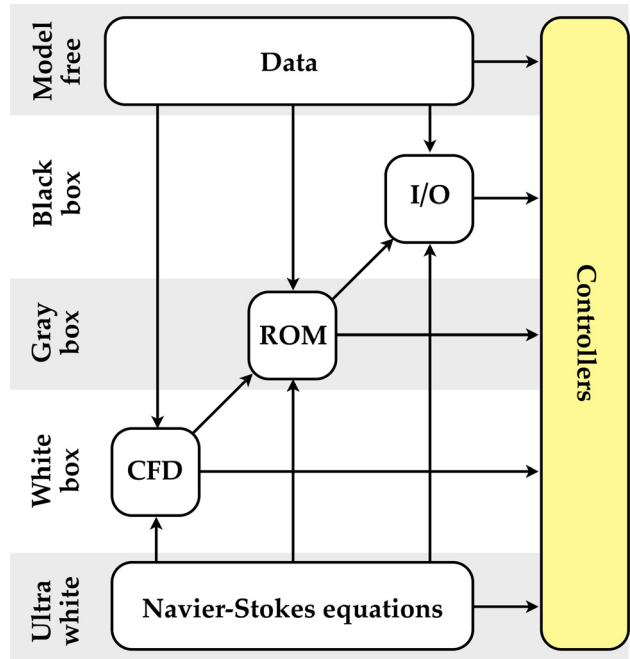


Fig. 4 Model hierarchy for control design based on Wiener [76].

$$\frac{d}{dt}\mathbf{a} = f(\mathbf{a}, \mathbf{b}; \boldsymbol{\mu}) \quad (2a)$$

$$\mathbf{s} = \mathbf{m}(\mathbf{a}, \mathbf{b}; \boldsymbol{\mu}) \quad (2b)$$

In the following, we explore possible state-spaces for \mathbf{a} (Sec. 3.2) and dynamic models for f (Sec. 3.3). Here, the dynamics are assumed to be continuous, and in general the flow state \mathbf{a} in the Navier–Stokes equation is twice continuously differentiable in space and once continuously differentiable in time. The bifurcation parameters $\boldsymbol{\mu}$ may change the qualitative nature of the solutions, and the flow field may not always be continuously differentiable in $\boldsymbol{\mu}$. These parameters include the Reynolds number and Mach number, among others.

The nonlinear dynamics in Eq. (2) may be linearized at a steady fixed point \mathbf{a}^s , where $f(\mathbf{a}^s, \mathbf{0}; \boldsymbol{\mu}) = \mathbf{0}$, away from critical values of the bifurcation parameters. The linearized model may also be converted into a frequency domain representation, as explored in Sec. 4.

3.2 Kinematics: Employed State Spaces. There are numerous choices for the underlying state space in Eq. (2), some of which are shown in the “kinematics” column of Fig. 5. This choice depends strongly on the availability of measurements and the desired model resolution; moreover, it should be considered whether or not the method is *data-driven* or if it requires knowledge of the governing equations. The following represents a non-exhaustive set of possible state-spaces, defining \mathbf{a} in Eq. (2). Note that many of these state-spaces may be used in model-free approaches.

3.2.1 Full-Resolution Description (White-Box). A full description of a fluid flow may include a high-resolution spatial or spectral discretization of the velocity field

$$\mathbf{a} = \mathbb{D}\mathbf{u}(\mathbf{x}, t)$$

Here, \mathbb{D} is a discretization operator, resulting in a high-dimensional state vector representation of a continuous field. Such descriptions are the basis of *white-box* models, which describe every relevant feature of the flow. These representations are

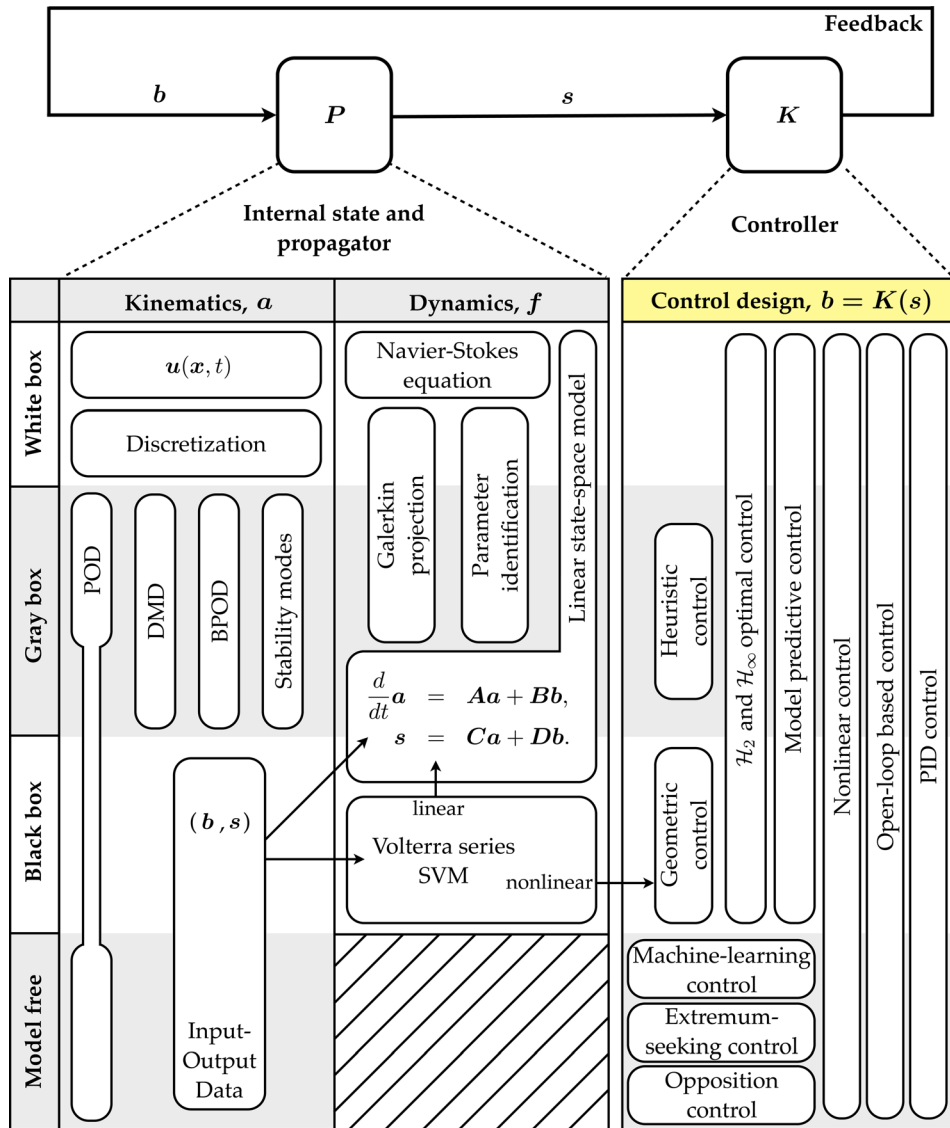


Fig. 5 Schematic illustrating popular choices at the various levels of kinematic and dynamic descriptions of the turbulent system P and choices for designing the controller K .

typically very high dimensional, sometimes exceeding the capacity of computer memory. For example, a high Reynolds number three-dimensional unsteady flow will exhibit important spatial structures that span many orders of magnitude in scale. The Reynolds number can be estimated from the ratio between the largest-scale structures to the smallest structures in the flow. Thus, for a generic geometry, the state dimension will scale with $\text{Re}^{9/4}$, along with the memory cost [77–79]. The computational cost will scale with Re^3 because of the addition of multiple temporal scales, which generally scale with $\text{Re}^{3/4}$. For a channel flow, the scaling may even be worse with Reynolds number, as Re^3 in space and Re^4 in space and time [80,81]. If a spatial discretization is required with 1000 elements in each direction; then, a three-dimensional simulation will contain 10^9 states for every flow variable (velocity, pressure, etc.).

The highest-order fully resolved simulation to date is a wall-bounded turbulent channel flow with $\text{Re}_{\tau} = 5200$ (Reynolds number based on the friction velocity), containing 2.4×10^{11} states [81]. This simulation is about 3.5 times larger than the previous record holder [82], and it uses slightly over 3/4 of a million processors in parallel. Even with Moore's law, it will take nearly 40 yr for this type of computation to become a lightweight "laptop" computation [83] and decades longer before being useful for

in-time control, since the parallel code takes 7 real seconds per simulated time-step, as benchmarked in Ref. [81]. However, impressive and useful for design and optimization, it is unclear that this level of resolution is even necessary for many control applications.

3.2.2 Modal Representation (Gray-Box). Instead of resolving every detail of the flow field at all scales, it is often possible to represent *most* of the relevant flow features in terms of a much lower dimensional state. This state represents the amplitudes of modes, or coherent structures that are likely to be found in the flow of interest. Galerkin models based on modal expansions constitute one class of gray-box models, which resolve the coherent structures of the white-box models while accounting for small-scale fluctuations with subscale closures.

The POD is one of the earliest and most successful modal representations used in fluids [84,85], resulting in dominant spatially coherent structures. POD benefits from a physical interpretation where modes are ordered hierarchically in terms of the energy content that they capture in the flow. There are numerous methods to compute POD, and the snapshot POD [86] is efficient when a limited number of well-resolved full-state measurements are available from simulations or experiments. Snapshot POD is

based on the singular value decomposition (SVD) [87–90], which is both numerically stable and efficient. POD is known under other names: principal components analysis (PCA) [91], the Hotelling transformation [92], Karhunen–Loëve decomposition [93], and empirical orthogonal functions [94]. POD has been widely used for flow control, as in the case of using proportional feedback control to reduce turbulent fluctuations around a turret for aero-optic applications [95]. Extensions of POD specifically designed for closed-loop feedback control, known as balanced (BPOD) [96,97], will be discussed in Sec. 4.5.3.

A recent technique known as dynamic mode decomposition (DMD) combines features of the POD and the discrete Fourier transform (DFT). The resulting spatial-temporal coherent structures oscillate in time at fixed frequencies, possibly with growth or decay [98–101]. Like POD, DMD is a snapshot-based method, making it appealing for simulations and experiments alike. DMD requires time-resolved snapshots of the same quality as needed for a Fourier transform, although recent methods have investigated sub-Nyquist sampled DMD [102]. Finally, DMD has a strong connection to the Koopman operator, which is an infinite dimensional linear operator describing the evolution of an observable function of a nonlinear dynamical system on a manifold [100,103–107].

It is also possible to construct a modal representation of growing and decaying features in the flow based on stability modes of the linearized Navier–Stokes equation and linearized adjoint equations [108–111]. The least damped part of the spectrum determines the coherent structures and their transient dynamics. Although completeness of the stability modes of the linearized Navier–Stokes equation has only been shown for geometrically simple configurations [112,113], it is generally assumed and has also been numerically corroborated. For Stokes eigenmodes, arising from a linearization around vanishing flow, completeness and orthogonality can be shown for a large class of boundary conditions [114].

In many fluid systems, large transient energy growth may be experienced, even in linearly stable systems, because of non-normality of the evolution operator [115,116]. One feature of non-normality can be large transient growth due to the destructive interference of nearly parallel eigenvectors, even with very similar eigenvalues. This phenomenon may be especially pronounced in shear flows, such as channel flows, and is important for flow control.

The modal decompositions discussed above are approximations based on data snapshots of the full system, most likely from a white-box model or experiments. We then have many of the same problems as in the white-box models: since the data may be exceedingly large, even simple tasks, such as computing the inner product of velocity fields, are cumbersome. Fortunately, the expense to compute a modal decomposition is a one-time upfront cost during the training phase, and resulting reduced-order models are generally much faster in the execution phase. There is a new software package in PYTHON, called MODRED from “model reduction,” that efficiently computes various modal decompositions and reduced-order models for systems with large data [117].

The oldest class of gray-box models is based on vortex representations starting with Helmholtz’s vortex laws in 1869. Von Kármán’s kinematic model [118] of the vortex street is one famous example. Some of these vortex models have been used for control applications. The Föppl (1906) vortex model of the cylinder wake has, for instance, been used to design a controller stabilizing the wake [119]. Suh’s vortex model [120] of a recirculation zone has been used for flatness-based control targeting mixing enhancement [121]. Most vortex models, however, are of hybrid nature, i.e., vortices are continually produced, merged, or removed. This implies that the dimension of the state space as well as the meaning of the coordinates continually changes. Such hybrid models are a challenge for almost all control methods. We shall not pause to elaborate these Lagrangian gray box models as there exist excellent textbooks on the topic (see, e.g., Refs. [122–124]) and the control applications are sparse.

3.2.3 Input–Output (Black-Box). Models that are built purely on input–output data are referred to as black-box models because they are opaque with respect to the underlying structure of the fluid. However, what black-box models lack in flow resolution, they make up for in rapid identification and low-overhead implementation. These models may be based on a state space comprised of the sensor and actuator signals

$$\mathbf{a} = [\mathbf{s}^T, \mathbf{b}^T]^T$$

A time-history of sensor signals using time-delay coordinates

$$\mathbf{a} = [\mathbf{s}(t)^T, \mathbf{s}(t-\tau)^T, \mathbf{s}(t-2\tau)^T, \dots, \mathbf{b}(t)^T, \dots]^T$$

or these signals and their derivatives

$$\mathbf{a} = \left[\mathbf{s}^T, \mathbf{b}^T, \frac{d}{dt}\mathbf{s}^T, \frac{d}{dt}\mathbf{b}^T, \dots \right]^T$$

3.3 Dynamics: Classification by System Resolution. Some of the modal representations above are fundamentally linked to a dynamic model. For instance, DMD results in spatial-temporal coherent structures along with a low-order model for how these modes oscillate and/or grow or decay. Likewise, BPOD results in a balanced linear model. For other representations, it is necessary to build a model on top of the data separately. The various methods to determine f in Eq. (2) are illustrated in Fig. 5 under the “dynamics” column.

3.3.1 White-Box Models. For white-box models, the discretized Navier–Stokes equations are used to resolve all flow physics and nonlinearities. When appropriate, e.g., near a fixed point or periodic orbit, the linearized Navier–Stokes equations may be used. As discussed earlier, there are significant hurdles to real-time implementation of these models based on the computational load. In addition, full-state estimation may be required when using a white-box model to control an experiment where measurements are limited. Estimation may be statistical, such as linear stochastic estimation [125–132], or dynamic, as in the Kalman filter [133–136]. However, these models are able to accurately capture important dynamic events, such as bifurcations, which define the phenomenological landscape.

There are a variety of methods in computational fluid dynamics (CFD), including the finite-element method, spectral elements, finite volumes, finite differences, immersed boundaries, point-vortex methods, and many more. As the Reynolds number increases, DNS becomes prohibitively expensive, and it is necessary to use turbulence models for smaller scale fluctuations. Finding turbulence closures to these models is an active field of research, and common methods include Reynolds-averaged Navier–Stokes (RANS) and large eddy simulations (LES). These may be thought of as off-white box models, since they still resolve many orders of magnitude in scale. However, these models must be used with caution and experience.

3.3.2 Gray-Box Models. Reduced-order models may be obtained in terms of the dynamic interaction of coherent structures, such as those obtained through POD, BPOD, DMD, or global stability analysis. The resulting models enable real-time control in experiments since the computational burden is limited and state estimation is often feasible based on limited measurements. However, acceptable accuracy is typically only achieved near the training parameters, for one or a few dominant frequencies, and for a few known nonlinear mechanisms. More robust mathematical reduced-order models may be obtained for simple geometries from Hilbert space considerations without advance data, but at the price of a significantly increased dimension [137,138].

Galerkin projection of the Navier–Stokes equations onto a modal basis is a common technique to obtain nonlinear reduced-order models. The “traditional” Galerkin method [139] requests the same orthogonal modes for the expansion and as test functions for the projection. POD–Galerkin models are the most prominent corresponding example in fluid mechanics [140]. Although BPOD has an associated linear model, it is possible to use BPOD modes for a nonlinear Galerkin projection. Gray-box models will be discussed in more detail in Secs. 4 and 5.

3.3.3 Black-Box Models. Transfer functions and state-space models identified purely from input–output data (i.e., measurements of the sensor and actuation history) are black-box models. They have similar dynamic bandwidth as gray-box models and in fact may have identical input–output characteristics. However, results and predictions lack the clear interpretation available when model states represent modal amplitudes, as is the case with gray-box models. A black-box model may be derived from a gray-box model, and the opposite may also be true if additional snapshot information is available. For example, it may be possible to relate the internal model states with linear combinations of the flow snapshots, resulting in a gray-box model. A major advantage of black-box models is easy experimental identification, particularly for linear and weakly nonlinear dynamics.

There are many techniques available to obtain black-box models, and a full exploration is outside the scope of this review. However, the eigensystem realization algorithm (ERA) [141,142] is a promising algorithm that produces balanced models from input–output data. Other methods are discussed in Refs. [143,144].

The ERA, discussed more in Sec. 4.5.4, results in a linear state-space model based on impulse response data, i.e., sensor measurements in response to an impulsive delta function input in the actuation. The impulse response of a multiple-input, multiple-output (MIMO) system will be given by $\mathbf{h}(t)$, a function of time with N_s rows and N_b columns. It is possible to predict the sensor measurements $s(t)$ in response to an arbitrary input signal $\mathbf{b}(t)$ for linear systems by convolution of the actuation signal with the impulse response

$$s(t) = s(0) + \int_0^t \mathbf{h}(t-\tau) \mathbf{b}(\tau) d\tau \quad (3)$$

The notion of convolution may be extended for generic nonlinear systems, such as in Eq. (2), by a Volterra series [145–147]. To simplify notation, we consider a single-input, single-output (SISO) system

$$\begin{aligned} s(t) &= s(0) + \sum_{k=1}^N \int_0^t \cdots \int_0^t h_k(t-\tau_1, \dots, t-\tau_k) \\ &\quad \times b(\tau_1) \cdots b(\tau_k) d\tau_1 \cdots d\tau_k \end{aligned} \quad (4)$$

The functions h_k are called Volterra kernels, and there are existence and uniqueness theorems for a large class of nonlinear systems [148]. There are also uses of Volterra series in geometric control theory [149]. Notice that the first integral in Eq. (4) for $k=1$ is the linear impulse response from Eq. (3).

As a simple example to demonstrate Volterra series, consider a SISO system with linear dynamics and a quadratic output nonlinearity³

$$\begin{aligned} \frac{d}{dt} \mathbf{a} &= \mathbf{A}\mathbf{a} + \mathbf{B}\mathbf{b} \\ s &= (\mathbf{C}\mathbf{a})^2 \end{aligned}$$

The output $s(t)$ is the square of the convolution in Eq. (3)

$$\begin{aligned} s(t) &= s(0) + \left(\int_0^t h_1(t-\tau) b(\tau) d\tau \right)^2 \\ &= s(0) + \int_0^t \int_0^t h_1(t-\tau_1) h_1(t-\tau_2) b(\tau_1) b(\tau_2) d\tau_1 d\tau_2 \\ &= s(0) + \int_0^t \int_0^t h_2(t-\tau_1, t-\tau_2) b(\tau_1) b(\tau_2) d\tau_1 d\tau_2 \end{aligned}$$

Here, $h_2(t-\tau_1, t-\tau_2) = h_1(t-\tau_1)h_1(t-\tau_2)$, so that static output nonlinearities have simple higher order kernels.

Volterra series have been used with back-stepping and boundary control of PDEs for fluid flow control [150]. They have also been used for general fluid modeling [151], to capture aerodynamic and aeroelastic phenomena [152–154], and to model and control plasma turbulence [155–157].

Support vector machines (SVMs) [158–160] are a new class of supervised nonlinear models that have a tremendous amount of potential for the control of complex dynamical systems. SVMs are supervised models that take input data into a high-dimensional nonlinear feature space, which may then be mapped back down to inputs. They are related to the Volterra series above. Knowledge of the *kernel* is a central part of the algorithm, and in practice, a suite of kernels may be tested to optimize model performance. SVMs have not penetrated the turbulence control literature significantly, but we expect this method to become more prominent in fluids in the future.

3.3.4 Model-Free Approaches. Model-free approaches do not rely on any underlying model description relating inputs to outputs. Instead, these approaches are often based on qualitative steady-state maps and are generally restricted to existing one or few-parameter open-loop control. Steady-state maps typically assume working periodic control and the maps relate input parameters to outcomes in some objective function. However, recent methods allow the identification of controllers using machine learning and adaptive control.

4 Linear Model-Based Control

Many results in closed-loop turbulence control are specific to linear systems. For example, one may stabilize an unstable steady state and delay the transition to turbulence in the boundary layer or channel flow. In this case, the steady (laminar) solution, which becomes unstable for postcritical Reynolds numbers, may be stabilized by feedback control.

Such work has encompassed a significant modeling effort (see Sec. 3) to describe the relevant low-order flow mechanisms to be suppressed or utilized. Performance issues, such as bandwidth, disturbance rejection, and noise attenuation, must be balanced with robustness to model uncertainty and time-delays in sensing, actuation, or computation. For this reason, there has been a recent push to move away from \mathcal{H}_2 optimal control techniques (linear-quadratic regulator (LQR), Kalman estimation, linear-quadratic-Gaussian (LQG), etc.) to the robust \mathcal{H}_∞ controllers [161–164]. These controllers guarantee robust performance by penalizing worst-case performance in the design process. Progress has also been made in the design and modeling of sensors and actuators [36], along with their placement in the flow.

There are many instances when linear control strategies may have significant and direct impact for nonlinear turbulent flows, even away from steady fixed-point solutions. For example, in mean-field models, exciting one oscillatory mode with linear control may suppress other, more energetic, oscillatory modes [48,47]. In addition, ensemble averages of turbulent flow responses may be linear as in Refs. [41,165]. Other examples include the transient control of separation for the fully turbulent boundary layer [41].

The main goal of this section is to develop an overview of the linear control framework and provide context for the related literature in flow control. Ideas, such as control topology (feedback

³This example was adapted from the notes by Nicholas R. Gamroth.

versus feedforward and open-loop versus closed-loop), controllability and observability, state estimation, pole placement, and robustness (sensitivity, bandwidth, stability), are introduced with an emphasis on physical interpretation and engineering implications. Since turbulent flows often have very fast time-scales, many of the topics above are considered in light of computational complexity and the latency of the control decision, leading to a discussion on reduced-order models.

This section is not meant to be an exhaustive overview of either linear control theory or its application in flow control. For more details on control theory, there are two recommended texts, Ref. [166] (*Practical Engineering*) and Ref. [167] (*Mathematical Theory*). There have also been a number of excellent recent reviews involving various aspects of the subject of linear closed-loop flow control [20,34,168–171].

4.1 Linearized Input–Output Dynamics. Often, we are interested in linearizing Eq. (2) about a steady fixed point \mathbf{a}^s , corresponding to a desirable flow state. This leads to a linear system of equations

$$\frac{d}{dt}\mathbf{a} = \mathbf{A}\mathbf{a} + \mathbf{B}\mathbf{b} \quad (5a)$$

$$\mathbf{s} = \mathbf{C}\mathbf{a} + \mathbf{D}\mathbf{b} \quad (5b)$$

where each of the matrices $(\mathbf{A}, \mathbf{B}, \mathbf{C}, \mathbf{D})$ depends on the linearization point \mathbf{a}^s and bifurcation parameter μ . The state vector \mathbf{a} refers to the difference between the current flow and the fixed point \mathbf{a}^s . The system is linearly stable if all of the eigenvalues of \mathbf{A} are in the left-half of the complex plane, having negative real parts. The linear approximation in Eq. (5) will be approximately valid near fixed points without purely imaginary eigenvalues and away from critical values of the bifurcation parameter (i.e., when $\det d\mathbf{f}/d\mu \neq 0$). Fortunately, if control is effective, the flow state should stay close to \mathbf{a}^s , where the linear approximation is valid. Similar linearization may be applied near a periodic orbit of the flow.

It is possible to represent the state-space model in Eq. (5) as a transfer function $\mathbf{P}(\zeta)$ relating the frequency of sinusoidal input forcing to the magnitude and phase of the output response; here $\zeta = i\omega \in \mathbb{C}$ is a Laplace variable

$$\mathbf{P}(\zeta) = \mathbf{C}(\zeta\mathbf{I} - \mathbf{A})^{-1}\mathbf{B} + \mathbf{D} \quad (6)$$

For linear systems, the output frequency will be the same as the input frequency ω , the magnitude is given by $|\mathbf{P}(\zeta)|$, and the phase is given by $\angle\mathbf{P}(\zeta)$. For example, consider a SISO linear system, where an input sinusoid $\sin(\omega t)$ will excite an output measurement $A \sin(\omega t + \phi)$, where A and ϕ are the magnitude and phase angle of the transfer function evaluated at $\zeta = i\omega : A = |\mathbf{P}(\zeta)|$ and $\phi = \angle(\mathbf{P}(\zeta))$. In the context of controls, the system \mathbf{P} is known as the *plant*. The roots of the denominator of \mathbf{P} are referred to as *poles* and the roots of the numerator are referred to as *zeros*. The plant is unstable if any poles have a positive real part; if \mathbf{P} is based on Eq. (6), then the poles of \mathbf{P} correspond to eigenvalues of \mathbf{A} .

Both the state-space and frequency domain representations are useful. It is often beneficial to design specifications and assess controller performance in the frequency domain, although it is often simpler to achieve these goals by manipulating the state-space system [166]. Generally, an effective open-loop plant will have high gain at low frequency for disturbance rejection and reference tracking, low gain at high frequency for noise attenuation, and a good phase margin at crossover for stability.

4.2 Model-Based Open-Loop Control. With a model of the form in Eq. (5) or Eq. (6), it may be possible to design an open-loop control law to achieve some desired specification without the

use of measurement-based feedback or feedforward control. For instance, if perfect tracking of the reference input w_r is desired in Fig. 6, under certain circumstances it may be possible to design a controller by inverting the plant dynamics \mathbf{P} : $\mathbf{K}(\zeta) = \mathbf{P}^{-1}(\zeta)$. In this case, the transfer function from reference w_r to output s is given by $\mathbf{PP}^{-1} = \mathbf{I}$, so that the output perfectly matches the reference. However, perfect control is never possible in real-world systems, and this strategy should be used with caution, since it generally relies on a number of significant assumptions on the plant \mathbf{P} . First, effective control based on plant inversion requires extremely precise knowledge of \mathbf{P} and well-characterized, predictable disturbances; there is little room for model errors or uncertainties, as there are no sensor measurements to determine if performance is as expected and no corrective feedback mechanisms to modify the actuation strategy to compensate.

For open-loop control using plant inversion, the plant \mathbf{P} must also be stable. It is impossible to fundamentally change the dynamics of a linear system through open-loop control, and thus an unstable plant cannot be stabilized without feedback. Attempting to stabilize an unstable plant by inverting the dynamics will typically have disastrous consequences. For instance, consider the following unstable plant with a pole at $\zeta = 5$ and a zero at $\zeta = -10$: $\mathbf{P}(\zeta) = (s+10)/(s-5)$. Inverting the plant would result in a controller $\mathbf{K} = (s-5)/(s+10)$; however, if there is even the slightest uncertainty in the model, so that the true pole is at $5 - \epsilon$; then, the open-loop system will be

$$P_{\text{true}}(\zeta)\mathbf{K}(\zeta) = \frac{s-5}{s-5+\epsilon}$$

This system is still unstable, despite the attempted pole cancellation. Moreover, the unstable mode is now nearly unobservable, a concept that will be discussed later.

In addition to stability, the plant \mathbf{P} must not have any time delays or zeros in the right-half plane, and it must have the same number of poles as zeros. If \mathbf{P} has any zeros in the right-half plane, then the inverted controller \mathbf{K} will be unstable, since it will have right-half plane poles. These plants are called *nonminimum phase*, and there have been generalizations to plant inversion, which provide bounded inverses to these systems [172]. Similarly, time-delays are not invertible, and if \mathbf{P} has more poles than zeros, then the resulting controller will not be realizable and may have extremely large actuation signals \mathbf{b} . There are also generalizations that provide *regularized* model inversion, where optimization schemes are applied with penalty terms added to keep the resulting actuation signal \mathbf{b} bounded. These regularized open-loop controllers are often significantly more effective, with improved robustness.

Combined, these restrictions on the plant \mathbf{P} imply that model-based open-loop control should only be used when the plant is well-behaved, accurately characterized by a model, when disturbances are characterized, and when the additional feedback control hardware is unnecessarily expensive. Otherwise, performance goals must be modest. Open-loop model inversion is often used in manufacturing and robotics, where systems are constrained and well-characterized in a standard operating environment.

4.3 Dynamic Closed-Loop Feedback Control. Feedback control addresses many of the aforementioned issues with open-loop control. Namely, closed-loop feedback, as illustrated in Fig. 7, uses sensor measurements to correct for model uncertainties,

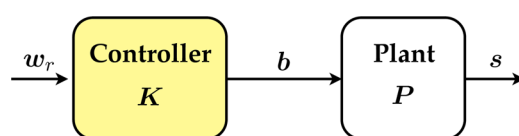


Fig. 6 Open-loop control topology

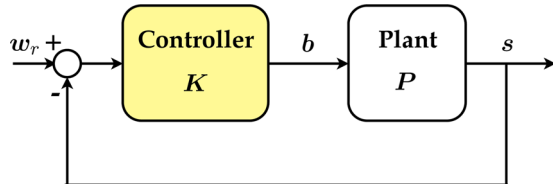


Fig. 7 Closed-loop control topology

reject disturbances, and stabilize unstable system dynamics. Depending on the plant dynamics and system latency, robust performance may be achieved through feedback.

For the linear dynamics in Eq. (5), full-state measurements $s = \mathbf{a}$ and a negative feedback controller $\mathbf{b} = -\mathbf{K}_r \mathbf{a}$ yield

$$\frac{d}{dt} \mathbf{a} = \mathbf{A}\mathbf{a} - \mathbf{B}\mathbf{K}_r \mathbf{a} \quad (7a)$$

$$= (\mathbf{A} - \mathbf{B}\mathbf{K}_r)\mathbf{a} \quad (7b)$$

If the system is *controllable*, as defined in Sec. 4.3.1, the closed-loop poles, given by eigenvalues of $\mathbf{A} - \mathbf{B}\mathbf{K}_r$, may be placed arbitrarily by choice of \mathbf{K}_r . Pole placement has been used to control combustion instabilities [173].

However, full-state measurements of \mathbf{a} may be either infeasible or prohibitively expensive, and so an *estimate* $\hat{\mathbf{a}}$ may be obtained from measurements s . This is of course, only if the system of Eq. (5) is *observable*. An *observer dynamical system* may be constructed as follows:

$$\frac{d}{dt} \hat{\mathbf{a}} = \mathbf{A}\hat{\mathbf{a}} + \mathbf{B}\mathbf{b} + \mathbf{K}_f(s - \hat{s}) \quad (8a)$$

$$\hat{s} = \mathbf{C}\hat{\mathbf{a}} + \mathbf{D}\mathbf{b} \quad (8b)$$

Typically $\mathbf{D} = \mathbf{0}$ for this problem, meaning that there is no direct feedthrough from actuators to sensors, although extensions exist when $\mathbf{D} \neq \mathbf{0}$; see Ref. [166]. Keeping \mathbf{D} in the calculations and combining Eqs. (8a) and (8b)

$$\frac{d}{dt} \hat{\mathbf{a}} = (\mathbf{A} - \mathbf{K}_f \mathbf{C})\hat{\mathbf{a}} + \mathbf{K}_f s + (\mathbf{B} - \mathbf{K}_f \mathbf{D})\mathbf{b} \quad (9)$$

The estimate $\hat{\mathbf{a}}$ will converge to the full state \mathbf{a} if the eigenvalues of $\mathbf{A} - \mathbf{K}_f \mathbf{C}$ are stable. Again, it is possible to place the poles of $\mathbf{A} - \mathbf{K}_f \mathbf{C}$ arbitrarily if the system is observable.

Combined with full-state feedback $\mathbf{b} = -\mathbf{K}_r \hat{\mathbf{a}}$, this results in a dynamical system for the controller

$$\frac{d}{dt} \hat{\mathbf{a}} = (\mathbf{A} - \mathbf{K}_f \mathbf{C} - \mathbf{B}\mathbf{K}_r + \mathbf{K}_f \mathbf{D}\mathbf{K}_r)\hat{\mathbf{a}} + \mathbf{K}_f s \quad (10a)$$

$$\mathbf{b} = -\mathbf{K}_r \hat{\mathbf{a}} \quad (10b)$$

The input to the controller is the sensor signal s , the output is the actuation signal \mathbf{b} , and the state $\hat{\mathbf{a}}$ estimates the full-state of the linear system in Eq. (5). The separation principle in control theory states that the closed-loop system, combining state estimation and full-state feedback, will have combined poles given by the poles of $\mathbf{A} - \mathbf{B}\mathbf{K}_r$ and $\mathbf{A} - \mathbf{K}_f \mathbf{C}$. Thus, \mathbf{K}_r and \mathbf{K}_f may be designed independently to satisfy different stability criteria for the state-feedback and estimation, and they may then be combined without interference.

4.3.1 Controllability, Observability, and Gramians. The ability to place poles of the closed-loop system in Eq. (7) arbitrarily with choice of \mathbf{K}_r relies on the *controllability* of the system in Eq. (5). The system is controllable if and only if the following matrix has full row rank N_a :

$$\mathcal{C} = [\mathbf{B} \quad \mathbf{AB} \quad \mathbf{A}^2\mathbf{B} \quad \cdots \quad \mathbf{A}^{N_a-1}\mathbf{B}] \quad (11)$$

Controllability implies that the system may be steered to an arbitrary state \mathbf{a} with suitable time-history of the control input \mathbf{b} . Similarly, the full state is *observable* if any state \mathbf{a} may be estimated from a suitable time-history of the measurements s . This is true when the observability matrix has full column rank N_a

$$\mathcal{O} = \begin{bmatrix} \mathbf{C} \\ \mathbf{CA} \\ \mathbf{CA}^2 \\ \vdots \\ \mathbf{CA}^{N_a-1} \end{bmatrix} \quad (12)$$

Although the definitions of controllability and observability above are binary, there are *degrees* of controllability and observability, based on how difficult it is to control or estimate a state \mathbf{a} . This is a more physically intuitive notion that some states are easier to control than others. The degree of controllability and observability of a given state in time t_f is quantified by eigenvalues and eigenvectors of the *controllability Gramian*

$$\mathbf{W}_c(t_f) = \int_0^{t_f} e^{\mathbf{A}\tau} \mathbf{B} \mathbf{B}^* e^{\mathbf{A}^*\tau} d\tau \quad (13a)$$

$$\approx \sum_{k=0}^{t_f/\Delta t} (e^{\mathbf{A}\Delta t})^k \mathbf{B} \mathbf{B}^* (e^{\mathbf{A}^*\Delta t})^k \Delta t \quad (13b)$$

and observability Gramian

$$\mathbf{W}_o(t_f) = \int_0^{t_f} e^{\mathbf{A}^*\tau} \mathbf{C}^* \mathbf{C} e^{\mathbf{A}\tau} d\tau \quad (14a)$$

$$\approx \sum_{k=0}^{t_f/\Delta t} (e^{\mathbf{A}^*\Delta t})^k \mathbf{C}^* \mathbf{C} (e^{\mathbf{A}\Delta t})^k \Delta t \quad (14b)$$

Here, the matrices \mathbf{A}^* , \mathbf{B}^* , and \mathbf{C}^* denote the *adjoints* of \mathbf{A} , \mathbf{B} , and \mathbf{C} . Often the Gramians in Eqs. (13) and (14) are evaluated at infinite time, and if the time dependence is not explicitly mentioned, we assume $t_f = \infty$, so that $\mathbf{W}_c \triangleq \mathbf{W}_c(\infty)$ and $\mathbf{W}_o \triangleq \mathbf{W}_o(\infty)$. In this case, if the matrix \mathbf{A} is stable, so that all eigenvalues have negative real part; then, the Gramians are unique solutions to a Lyapunov equation

$$\mathbf{A}\mathbf{W}_c + \mathbf{W}_c\mathbf{A}^* + \mathbf{B}\mathbf{B}^* = \mathbf{0} \quad (15a)$$

$$\mathbf{A}^*\mathbf{W}_o + \mathbf{W}_o\mathbf{A} + \mathbf{C}^*\mathbf{C} = \mathbf{0} \quad (15b)$$

Solving these equations may be quite expensive. Empirical snapshot-based methods, discussed in Sec. 4.5.1, are faster.

The matrices \mathbf{W}_c and \mathbf{W}_o are both symmetric and positive semi-definite. The system is controllable (respectively, observable) if and only if the controllability (respectively, observability) Gramian is invertible. The controllability of a state \mathbf{a} is measured by $\mathbf{a}^*\mathbf{W}_c\mathbf{a}$, which is larger for more controllable states. Physically, if $\mathbf{a}^*\mathbf{W}_c\mathbf{a}$ is large, then it is possible to steer the system state far in the \mathbf{a} direction with a unit control input. Similarly, the observability of a state is measured by $\mathbf{a}^*\mathbf{W}_o\mathbf{a}$. This connection between the Gramians and energy expenditure to move the system toward a state \mathbf{a} at time t_f can be made precise with the notion of *minimum energy control*. The minimum-energy control input $\mathbf{b}(t)$ to steer the system to $\mathbf{a}(t_f)$ from $\mathbf{a}(0) = \mathbf{0}$ is given by

$$\mathbf{b}(t) = \mathbf{B}^T (e^{\mathbf{A}(t_f-t)})^T \mathbf{W}_c(t_f)^{-1} \mathbf{a}(t_f) \quad (16)$$

The total energy expended during this minimum-energy actuation to steer the system to \mathbf{a} in time t_f is given by

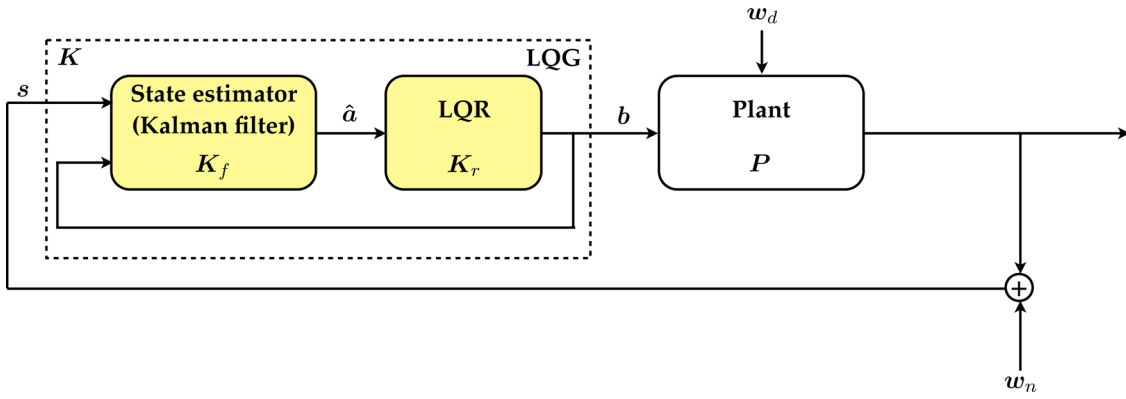


Fig. 8 Linear-quadratic Gaussian controller. The Kalman filter K_f is a dynamical system that takes sensor measurements s and the actuation signal b to estimate the full-state \hat{a} . The LQR gain K_r is a matrix that multiplies the full-state to produce an actuation signal $b = -K_r \hat{a}$ that is optimal with respect to the quadratic cost function in Eq. (18).

$$\int_0^{t_f} \|b(\tau)\|^2 d\tau = \mathbf{a}^T \mathbf{W}_c(t_f)^{-1} \mathbf{a} \quad (17)$$

Thus, if the controllability Gramian is nearly singular; then, tremendous actuation energy is required to control the system. Conversely, if the eigenvalues of the Gramian are large; then, the system is highly controllable.

It is therefore possible to determine a hierarchy of controllable states, in order of controllability, by taking the eigenvalue decomposition of \mathbf{W}_c , which is positive semidefinite. The eigenvectors corresponding to the largest eigenvalues are the most controllable states. This eigendecomposition is closely related to the SVD of the controllability matrix from Eq. (11), but defined from a discrete-time system approximating Eq. (5). This connection to the SVD will be important in model reduction and will be discussed in Sec. 4.5.1. A similar hierarchy of observable states may be determined.

4.3.2 Linear Quadratic Gaussian. Now that we have established conditions enabling arbitrary pole placement of the closed-loop system, we must decide on where to place them. It is mathematically possible to make closed-loop eigenvalues arbitrarily stable (i.e., arbitrarily far in the left-half complex plane) if the system is controllable. However, this may require expensive control expenditure with unrealistic actuation magnitudes. Moreover, very stable eigenvalues may over-react to noise and disturbances, causing the closed-loop system to jitter, much as a new driver over-reacting to vibrations in the steering wheel.

In a LQR controller, the controller K_r is chosen to place the closed-loop poles to minimize a quadratic cost function J . This cost function balances the desire to *regulate* the system state to $\mathbf{a} = \mathbf{0}$ with the added objective of small control expenditure

$$J = \int_0^{\infty} (\mathbf{a}^T \mathbf{Q} \mathbf{a} + \mathbf{b}^T \mathbf{R} \mathbf{b}) dt \quad (18)$$

\mathbf{Q} is a symmetric positive semidefinite matrix that is chosen to penalize deviations of the state \mathbf{a} from the set-point $\mathbf{a} = \mathbf{0}$. Similarly, \mathbf{R} is a symmetric positive definite matrix that is chosen to penalize control expenditure. Often, \mathbf{Q} and \mathbf{R} are chosen to be diagonal matrices, and the magnitude of the diagonal elements may be adjusted to tune the control performance by adjusting relative penalty ratios. For example, to increase the aggressiveness of control, the diagonal entries of \mathbf{R} may be decreased with respect to those of \mathbf{Q} .

The optimal control law that minimizes J in Eq. (18) is given by $\mathbf{b} = -K_r \mathbf{a}$, with $K_r = \mathbf{R}^{-1} \mathbf{B}^T \mathbf{X}$. \mathbf{X} is the unique solution to the algebraic Riccati equation

$$\mathbf{A}^T \mathbf{X} + \mathbf{X} \mathbf{A} - \mathbf{X} \mathbf{B} \mathbf{R}^{-1} \mathbf{B}^T \mathbf{X} + \mathbf{Q} = \mathbf{0} \quad (19)$$

In LQR, a balance is struck between the stability of the closed-loop system and the aggressiveness of control. Taking control expenditure into account is important so that the controller does not over-react to high-frequency noise and disturbances, does not exceed maximum actuation amplitudes, and is not prohibitively expensive.

In practice, to make Eq. (5) more realistic, it must be augmented with the addition of white noise disturbance w_d and measurement noise w_n

$$\frac{d}{dt} \mathbf{a} = \mathbf{A} \mathbf{a} + \mathbf{B} \mathbf{b} + \mathbf{B}_w w_d \quad (20a)$$

$$\mathbf{s} = \mathbf{C} \mathbf{a} + \mathbf{D} \mathbf{b} + \mathbf{w}_n \quad (20b)$$

The matrix \mathbf{B}_w determines the spatial distribution of how disturbances enter the state. Each of these noise inputs has a different covariance matrix: $E(w_d(t)w_d(\tau)^T) = V_d \delta(t - \tau)$ and $E(w_n(t)w_n(\tau)^T) = V_n \delta(t - \tau)$, where $E(\cdot)$ is the expectation value and δ is the Dirac delta function. The addition of disturbances and sensor noise is shown in Fig. 8 and also in Fig. 9 with $w_r = \mathbf{0}$; w_r is the reference input.

In linear-quadratic estimation (LQE), a dual problem to LQR is solved, resulting in an optimal full-state estimator, as in Eq. (9), that balances the relative importance of measurement noise and process noise. The process noise may be an additive stochastic term, or structural uncertainty in the model. A dual Riccati equation is solved for \mathbf{Y} in the observer gain $K_f = \mathbf{Y} \mathbf{C}^T \mathbf{V}_n$

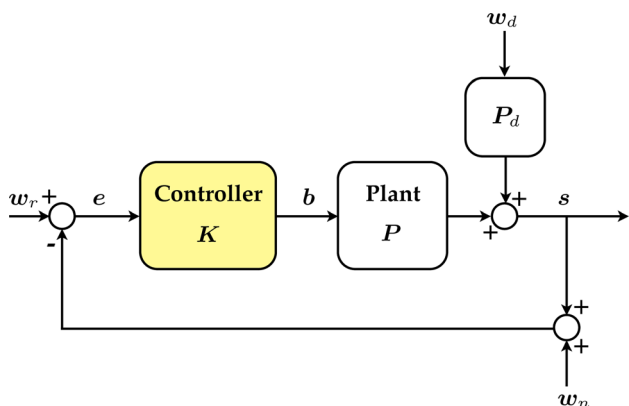


Fig. 9 Feedback control with disturbances and noise

$$YA^T + AY - YC^T V_n^{-1} CY + V_d = \mathbf{0} \quad (21)$$

The so-called *Kalman filter* K_f may be used in the observer in Eq. (9), and it is chosen to minimize $E((\mathbf{a} - \hat{\mathbf{a}})^T(\mathbf{a} - \hat{\mathbf{a}}))$ given known covariance V_d and V_n .

The optimal state-feedback (LQR) and optimal state-estimation (LQE) may be designed independently and then combined. The separation principle guarantees that when combined, the state-feedback and state-estimation will remain stable and optimal. The resulting controller, combining estimation-based full-state feedback, is known as a LQG controller, as shown in Fig. 8.

The combined LQG controller may be written as a more general observer dynamical system, given by

$$\frac{d}{dt}\hat{\mathbf{a}} = \hat{\mathbf{A}}\hat{\mathbf{a}} + \hat{\mathbf{B}}\mathbf{s} \quad (22a)$$

$$\mathbf{b} = \hat{\mathbf{C}}\hat{\mathbf{a}} + \hat{\mathbf{D}}\mathbf{s} \quad (22b)$$

For the LQG controller, we set $\hat{\mathbf{A}} = \mathbf{A} - K_f C - BK_r + K_f DK_r$, $\hat{\mathbf{B}} = K_f$, $\hat{\mathbf{C}} = -K_r$, and $\hat{\mathbf{D}} = \mathbf{0}$, recovering the form of Eq. (10) with K_r as the LQR gain matrix and K_f as the Kalman filter gain matrix.

The resulting controller, known more generally as an \mathcal{H}_2 controller, optimally balances the effect of Gaussian measurement noise with process disturbances. Although LQR controllers may have decent stability margins, there is no guarantee on stability margins for LQG controllers, as famously demonstrated in Ref. [161]. This means that even small uncertainties, such as unmodeled dynamics, unexpected disturbances, or time-delays, may destabilize the closed-loop system.

4.4 Robust Control. The notion of robustness and performance are central in feedback control. The limitations of LQG control have motivated significant advances in the development of controllers with *robust* performance. Robustness typically refers to the ability to maintain control performance despite model uncertainty, unmodeled nonlinear dynamics, and unforeseen disturbances, time-delays, etc., which are all important for turbulence control. A complete discussion of robust control is beyond the scope of this review; instead, our goal is to build an intuition and provide a glimpse of the powerful robust control machinery for flow systems [174]. For a more complete overview with excellent attention to engineering considerations and practical control design, see Ref. [166].

4.4.1 Sensitivity, Complementary Sensitivity, and Robustness. As discussed in Sec. 4.3.2, real systems will always include disturbances \mathbf{w}_d and sensor noise \mathbf{w}_n , as illustrated in Fig. 9. This diagram also includes a commanded reference input \mathbf{w}_r that the controller should track. When designing a robust controller, it is important to understand how these *exogenous* inputs affect the outputs \mathbf{s} , the error signal \mathbf{e} , and the actuation signal, \mathbf{b} . In general, systems will be particularly sensitive to disturbances and noise at certain frequencies.

We may express the output \mathbf{s} in terms of transfer functions on the inputs \mathbf{w}_r , \mathbf{w}_d , and \mathbf{w}_n

$$\begin{aligned} \mathbf{s} &= P_d \mathbf{w}_d + PK(\mathbf{w}_r - \mathbf{s} - \mathbf{w}_n) \\ \Rightarrow (\mathbf{I} + PK)\mathbf{s} &= P_d \mathbf{w}_d + PK\mathbf{w}_r - PK\mathbf{w}_n \end{aligned}$$

Therefore, we have

$$\begin{aligned} \mathbf{s} &= \underbrace{(\mathbf{I} + PK)^{-1}PK}_{T} \mathbf{w}_r + \underbrace{(\mathbf{I} + PK)^{-1}P_d}_{S} \mathbf{w}_d \\ &\quad - \underbrace{(\mathbf{I} + PK)^{-1}PK}_{T} \mathbf{w}_n \end{aligned} \quad (23)$$

S is the *sensitivity*, and T is the *complementary sensitivity*. If we let $L = PK$ be the *loop transfer function*, then we have

$$\mathbf{S} = (\mathbf{I} + \mathbf{L})^{-1} \quad (24a)$$

$$\mathbf{T} = (\mathbf{I} + \mathbf{L})^{-1} \mathbf{L} \quad (24b)$$

Since we are interested in minimizing the error \mathbf{e} (without noise), the following expression is more useful:

$$\mathbf{e} = \mathbf{w}_r - \mathbf{s} = S\mathbf{w}_r - SP_d\mathbf{w}_d + T\mathbf{w}_n \quad (25)$$

The disturbance plant P_d and the system plant P are often closely related. For example, disturbances and control inputs may both be amplified by a natural convective instability in the flow.

Typically, we will choose the controller K so that the open-loop transfer function $L = PK$ has desirable properties in the frequency domain. For example, small gain at high frequencies will attenuate sensor noise. Similarly, high gain at low frequencies will provide good reference tracking performance. These are intimately related to the sensitivity S and complementary sensitivity T . In particular, from Eq. (25), S should be small at low frequencies, and T should be small at large frequencies; note that $S + T = I$, from Eq. (24).

For performance and robustness, we want the maximum peak of S , $M_S = \|S\|_\infty$, to be as small as possible. From Eq. (25), it is clear that in the absence of noise, feedback control improves performance (i.e., reduces error) for all frequencies where $|S| < 1$; thus, control is effective when $|T| \approx 1$. As explained in Ref. [166], p. 37, all real systems will have a range of frequencies where $|S| > 1$, in which case performance is degraded. Minimizing the peak M_S mitigates the amount of degradation experienced with feedback at these frequencies, improving performance. In addition, the minimum distance of the loop transfer function L to the point -1 in the complex plane is given by M_S^{-1} . The larger this distance, the greater the stability margin of the closed-loop system, improving robustness. These are the two major reasons to minimize M_S .

The controller *bandwidth* ω_B is the frequency below which feedback control is effective. This is a subjective definition. Often, ω_B is the frequency where $|S(j\omega)|$ first crosses -3 dB from below. We would ideally like the controller bandwidth to be as large as possible without amplifying sensor noise, which is typically high frequency. However, there are fundamental bandwidth limitations that are imposed for systems that have time delays or right half plane zeros [166].

4.4.2 \mathcal{H}_∞ Robust Control Design. As discussed above, LQG controllers are known to have arbitrarily poor robustness margins. This is a serious problem in turbulence control, where the flow is wrought with uncertainty and time-delays. \mathcal{H}_∞ robust controllers are used when robustness is important. There are many connections between \mathcal{H}_2 and \mathcal{H}_∞ control, and we refer the reader to the excellent reference books expanding on this theory [166,167].

Figure 10 shows the most general schematic for closed-loop feedback control, encompassing \mathcal{H}_2 and \mathcal{H}_∞ optimal control strategies. In the generalized theory of modern control, the goal is to minimize the transfer function from exogenous inputs \mathbf{w} (reference, disturbances, noise, etc.) to the cost function J (accuracy, actuation cost, time-domain performance, etc.). Both \mathcal{H}_2 and \mathcal{H}_∞ control design result in controllers that minimize different norms on this fundamental input–output transfer function. In fact, the symbol \mathcal{H}_2 refers to a Hardy space with bounded two-norm, consisting of stable and strictly proper transfer functions (meaning gain rolls off at high frequency). The symbol \mathcal{H}_∞ refers to a Hardy space with bounded infinity-norm, consisting of stable and proper transfer functions (gain does not grow infinite at high frequencies). The infinity norm is defined as

$$\|\mathbf{P}\|_\infty \triangleq \max_{\omega} \sigma_1(\mathbf{P}(i\omega)) \quad (26)$$

Here, σ_1 denotes the maximum singular value. Since the $\|\cdot\|_\infty$ norm is the maximum value of the transfer function at any

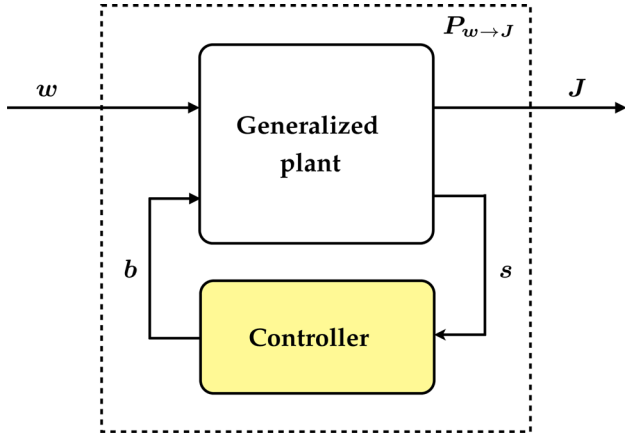


Fig. 10 General framework for feedback control. The input to the controller is the system measurements s , and the controller outputs an actuation signal b . The exogenous inputs w may refer to a reference w_r , disturbances w_d , or sensor noise w_n . The cost function J may measure the cost associated with inaccuracy of reference tracking, expense of control, etc.

frequency, it is often called a *worst-case scenario norm*; therefore, minimizing the infinity norm provides robustness to worst-case exogenous inputs.

If we let $\mathbf{P}_{w \rightarrow J}$ denote the transfer function from w to J ; then, the goal of \mathcal{H}_∞ control is to construct a controller to minimize the infinity norm: $\min \|\mathbf{P}_{w \rightarrow J}\|_\infty$. This is typically difficult, and no analytic closed-form solution exists for the optimal controller in general. However, there are relatively efficient iterative methods to find a controller such that $\|\mathbf{P}_{w \rightarrow J}\|_\infty < \gamma$, as described in Ref. [164]. There are numerous conditions and caveats that describe when this method can be used. In addition, there are computationally efficient algorithms implemented in both MATLAB and PYTHON, and these methods require relatively low overhead from the user.

Selecting the cost function J to meet design specifications is a critically important part of robust control design. Considerations, such as disturbance rejection, noise attenuation, controller bandwidth, and actuation cost, may be accounted for by a weighted sum of the transfer functions S , T , and KS . In the *mixed sensitivity* control problem, various weighting transfer function are used to balance the relative importance of these considerations at various frequency ranges. For instance, we may weight S by a low-pass filter and KS by a high-pass filter, so that disturbance rejection at low frequency is promoted and control response at high-frequency is discouraged. A general cost function may consist of three weighting filters F_k multiplying S , T , and KS

$$\left\| \begin{bmatrix} F_1 S \\ F_2 T \\ F_3 KS \end{bmatrix} \right\|_\infty$$

Another possible robust control design is called \mathcal{H}_∞ loop shaping. This procedure may be more straightforward than mixed sensitivity synthesis for many problems. The method consists of two major steps. First, a desired open-loop transfer function is specified based on performance goals and classical control design. Input and output compensators are constructed to transform the open-loop system to the desired loop shape. Second, the shaped loop is made robust with respect to a large class of model uncertainty. Indeed, the procedure of \mathcal{H}_∞ loop shaping allows the user to design an ideal controller to meet performance specifications, such as rise-time, bandwidth, and settling-time. Typically, a loop shape should have large gain at low frequency to guarantee accurate reference tracking and slow disturbance rejection, low gain at high frequencies to attenuate sensor noise, and a cross-over

frequency that ensures desirable bandwidth. The loop transfer function is then robustified so that there are improved gain and phase margins.

\mathcal{H}_2 control has been an extremely popular control paradigm because of its simple mathematical formulation and its tunability by user input. The advantages of \mathcal{H}_∞ control are increasingly realized in flow control, eminent examples being the collaborative research centers (Sfb 557 and Sfb 1029) lead by King [16,17,175]. Additionally, there are numerous consumer software solutions that make implementation relatively straightforward. In MATLAB, mixed sensitivity is accomplished using the `>>mixsyn` command in the robust control toolbox. Similarly, loop-shaping is accomplished using the `>>loopsyn` command in the robust control toolbox.

4.4.3 Fundamental Limitations With Implications for Turbulence Control. As discussed above, we want to minimize the peaks of S and T . Some peakedness is inevitable, and there are certain system characteristics that significantly limit performance and robustness. Most notably, time-delays and right-half plane zeros of the open-loop system will limit the effective control bandwidth and will increase the attainable lower-bound for peaks of S and T . This contributes to both degrading performance and decreasing robustness.

Similarly, a plant will suffer from robust performance limitations if the number of poles exceeds the number of zeros by more than two. These fundamental limitations are quantified in the *waterbed* integrals, which are so named because if you push a waterbed down in one location, it must rise in another. Thus, there are limits to how much one can push down peaks in S without causing other peaks to pop up.

Time delays are somewhat easier to understand, since a time delay τ will introduce an additional phase lag of $\tau\omega$ at the frequency ω , limiting how fast the controller can respond effectively (i.e., bandwidth). Thus, the bandwidth for a controller with acceptable phase margins is typically $\omega_B < 1/\tau$.

Following the discussion in Ref. [166], these fundamental limitations may be understood in relation to the limitations of open-loop control based on model inversion from Sec. 4.2. If we consider high-gain feedback $b = \mathbf{K}(w_r - s)$ for a system as in Fig. 9 and Eq. (25), but without disturbances or noise, we have

$$b = \mathbf{K}e = \mathbf{K}Sw_r \quad (27)$$

We may write this in terms of the complementary sensitivity T , by noting that since $T = I - S$, we have $T = L(I + L)^{-1} = PKS$

$$b = P^{-1}T w_r \quad (28)$$

Thus, at frequencies where T is nearly the identity I and control is effective, the actuation is effectively inverting the plant P . Even with sensor-based feedback, perfect control is unattainable. For example, if the plant P has right-half plane zeros; then, the actuation signal will become unbounded if the gain K is too aggressive. Similarly, limitations arise with time-delays and when the number of poles of P exceeds the number of zeros, as in the case of open-loop model-based inversion.

As a final illustration of the limitation of right-half plane zeros, we consider the case of proportional control $b = Ks$ in a single-input, single output system with plant $P(\zeta) = N(\zeta)/D(\zeta)$. Here, roots of the numerator $N(\zeta)$ are zeros of the plant and roots of the denominator $D(\zeta)$ are poles. The closed-loop transfer function from reference w_r to sensors s is given by

$$\frac{s(\zeta)}{w_r(\zeta)} = \frac{PK}{1 + PK} = \frac{NK/D}{1 + NK/D} = \frac{NK}{D + NK} \quad (29)$$

For small control gain K , the term NK in the denominator is small, and the poles of the closed-loop system are near the poles of P , given by roots of D . As K is increased, the NK term in the

denominator begins to dominate, and closed-loop poles are attracted to the roots of N , which are the open-loop zeros of P . Thus, if there are right-half plane zeros of the open-loop plant P ; then, high-gain proportional control will drive the system unstable. These effects are often observed in the root locus plot from classical control theory. In this way, we see that right-half plane zeros will directly impose limitations on the gain margin of the controller.

The limitations imposed by a time-delay have significant implications for turbulence control. First, time-delays will be inevitable for many sensor/actuator configurations in convective flows [176], limiting the frequency of disturbances that may be effectively suppressed with feedback. Second, as turbulence time-scales may become extremely fast, the time it takes to compute a control action will introduce a latency that is just as deleterious as a time-delay in the plant. Time-delays and flow time-scales should be primary considerations when designing feedback controllers for turbulent flows.

4.4.4 Two Degrees-of-Freedom Control. With the addition of reference and disturbance feed-forward control, it is possible to improve the control performance at frequencies where feedback control is ineffective due to large sensitivity. This more sophisticated *two-degrees-of-freedom* control is illustrated in Fig. 11.

Again, we may compute the transfer function from inputs to output

$$\begin{aligned} s &= (\mathbf{I} + \mathbf{PK})^{-1} \\ &[\mathbf{P}(\mathbf{K} + \mathbf{K}_{\text{ref}})\mathbf{w}_r + (\mathbf{P}_d - \mathbf{PK}_d)\mathbf{w}_d - \mathbf{PK}\mathbf{w}_n] \end{aligned}$$

Then, the error becomes

$$\mathbf{e} = s - \mathbf{w}_r = -\mathbf{SS}_{\text{ref}}\mathbf{w}_r + \mathbf{SS}_d\mathbf{P}_d\mathbf{w}_d - \mathbf{T}\mathbf{w}_n \quad (30)$$

where the additional feedforward sensitivity functions are

$$\mathbf{S}_{\text{ref}} = \mathbf{I} - \mathbf{PK}_{\text{ref}} \quad (31a)$$

$$\mathbf{S}_d = \mathbf{I} - \mathbf{PK}_d\mathbf{P}_d^{-1} \quad (31b)$$

Two-degrees-of-freedom control may be intuitively understood as the combination of a fast feedforward controller to get close to a desired reference value, followed by a slow feedback controller to mitigate model uncertainty and reject unexpected disturbances. There are explicit bounds on model uncertainty, which determine

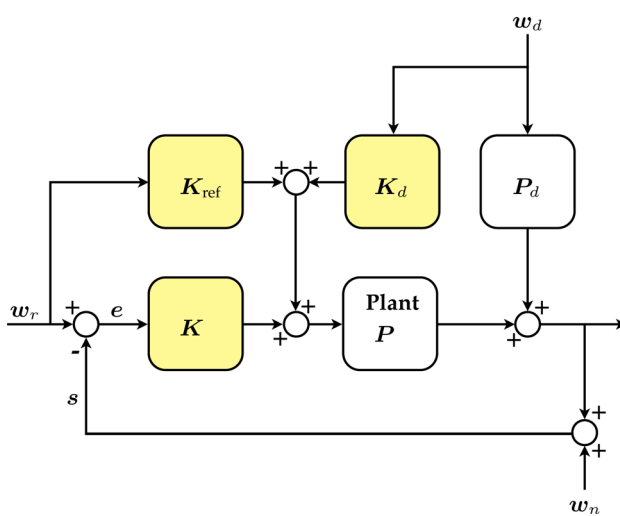


Fig. 11 Two degrees-of-freedom control with reference tracking and disturbance rejection

when combined inverse-based feedforward and feedback will outperform feedback alone [177].

4.5 Balanced Model Reduction. The high-dimensionality and short time-scales associated with turbulent flows make it infeasible to implement the model-based control strategies above in real-time. Moreover, solving for \mathcal{H}_2 and \mathcal{H}_∞ optimal controllers may be computationally intractable, as they involve either a high-dimensional Riccati equation solve, or an expensive iterative optimization. Instead, reduced-order models provide efficient, low-dimensional representations of the most relevant flow mechanisms. These models result in efficient controllers that may be applied in real-time for many systems. An alternative is to develop controllers based on the full-dimensional model and then apply model reduction techniques directly to the full controller [178].

Model reduction is an essential data reduction that respects the fact that the data are generated by a dynamic process. If the dynamic process is a linear time-invariant (LTI) input–output system, then there is a wealth of machinery available for model reduction, and performance bounds may be quantified. Many of these methods are based on the SVD [87,88,179], and the minimal realization theory of Ho and Kalman [180,181]. The general idea is to determine a hierarchical modal decomposition of the flow state that may be truncated at some model order, only keeping the most important coherent structures.

The POD [85,182] orders modes based on energy content, and it has been widely used for a range of fluid dynamic reduced-order models, many for control. POD is guaranteed to provide an optimal low-rank basis to capture the maximal energy or variance in a data set. In some cases, a large number of POD modes may be required to represent non-normal energy growth, as in wall-bounded shear flows, such as in Ref. [183].

Instead of ordering modes based on energy, it is possible to determine a hierarchy of modes that are most controllable and observable, therefore capturing the most input–output information. Such *balanced* models give equal weighting to the controllability and observability of a state, providing a coordinate transformation that makes the controllability and observability Gramians equal and diagonal. It is observed that for many high-dimensional systems, the control input may only excite a few controllable modes, with the remaining modes being stable. These models have been extremely successful in the context of flow control, especially for systems with non-normal growth. However, computing a balanced model using traditional methods is extremely expensive computationally. In this section, we describe the balancing procedure, as well as modern methods for efficient computation of balanced models. A computationally efficient suite of algorithms for model reduction and system identification may be found in Ref. [117].

4.5.1 Discrete-Time Systems and Gramians. Until now, we have considered continuous-time dynamical systems, as in Eq. (5). However, the discussion of model reduction is somewhat simplified using a discrete-time model

$$\mathbf{a}_{k+1} = \mathbf{A}_d\mathbf{a}_k + \mathbf{B}_d\mathbf{b}_k \quad (32a)$$

$$\mathbf{s}_k = \mathbf{C}_d\mathbf{a}_k + \mathbf{D}_d\mathbf{b}_k \quad (32b)$$

The index k may be thought of as the k th sample of a continuous-time system in Eq. (5), sampled every Δt by an analog-to-digital converter. Alternatively, the discrete-time system may be a numerical time-stepper. The discrete-time system may be related to the continuous-time system by the following: $\mathbf{A}_d = \exp(A\Delta t)$, $\mathbf{B}_d = \int_0^{\Delta t} \exp(A\tau)\mathbf{B}d\tau$, $\mathbf{C}_d = \mathbf{C}$, and $\mathbf{D}_d = \mathbf{D}$. Then, $\mathbf{a}_k = \mathbf{a}(k\Delta t)$, and similar for \mathbf{b}_k and \mathbf{s}_k . The assumption that \mathbf{b} is constant during each Δt interval is called a zero-order-hold in control theory.

The Gramians may be approximated by full-state measurements of the direct system in Eq. (32) and adjoint system

$$\text{direct : } \mathbf{a}_{k+1} = \mathbf{A}_d \mathbf{a}_k + \mathbf{B}_d \mathbf{b}_k \quad (33a)$$

$$\text{adjoint : } \mathbf{a}_{k+1} = \mathbf{A}_d^* \mathbf{a}_k + \mathbf{C}_d^* \mathbf{s}_k \quad (33b)$$

It is then possible to determine *empirical* Gramians without solving the Lyapunov equations in Eq. (15).

$$\mathbf{W}_c \approx \mathbf{W}_c^e = \mathcal{C}_d \mathcal{C}_d^* \quad (34a)$$

$$\mathbf{W}_o \approx \mathbf{W}_o^e = \mathcal{O}_d \mathcal{O}_d^* \quad (34b)$$

\mathcal{C}_d and \mathcal{O}_d are snapshot matrices constructed from impulse response simulations of the *discrete* direct and adjoint systems in Eq. (32). The method of empirical Gramians is quite efficient and was used in Refs. [181,184,185]. Note that there are N_s adjoint impulse response experiments required. This becomes intractable when there are a large number of outputs (e.g., full-state measurements).

4.5.2 Goal of Model Reduction. The goal of model reduction is to obtain a related system ($\mathbf{A}_r, \mathbf{B}_r, \mathbf{C}_r, \mathbf{D}_r$)

$$\tilde{\mathbf{a}}_{k+1} = \mathbf{A}_r \tilde{\mathbf{a}}_k + \mathbf{B}_r \mathbf{b}_k \quad (35a)$$

$$\mathbf{s}_k = \mathbf{C}_r \tilde{\mathbf{a}}_k + \mathbf{D}_r \mathbf{b}_k \quad (35b)$$

in terms of a state $\tilde{\mathbf{a}}_k \in \mathbb{R}^{N_r}$ with reduced state dimension, $N_r \ll N_a$. Note that \mathbf{b}_k and \mathbf{s}_k are the same in Eqs. (32) and (35). A balanced reduced-order model should map inputs to outputs as faithfully as possible for a given order.

It is therefore important to introduce an *operator norm* to quantify how similarly Eqs. (32) and (35) act on a given set of inputs. Typically, we consider the infinity norm of the transfer functions $\mathbf{P}(\zeta)$ and $\mathbf{P}_r(\zeta)$ obtained from the full system (32) and reduced system (35), respectively,

$$\|\mathbf{P}\|_\infty \triangleq \max_{\omega} \sigma_1(\mathbf{P}(i\omega)) \quad (36)$$

To summarize, we seek a reduced-order model (35) of low order, $N_r \ll N_a$, so the operator norm $\|\mathbf{P} - \mathbf{P}_r\|_\infty$ is small.

4.5.3 Balanced POD. In balanced truncation (BT) [181], a coordinate transformation is sought that makes the observability and controllability Gramians equal and diagonal. The balancing transformation is given by the matrix \mathcal{B} in the eigendecomposition

$$\mathbf{W}_c \mathbf{W}_o \mathcal{B} = \mathcal{B} \Sigma^2 \quad (37)$$

where Σ is a diagonal matrix containing *Hankel singular values* (HSVs). It is then possible to obtain a reduced-order basis by choosing the first N_r columns of \mathcal{B} corresponding to the N_r largest HSVs. It has been demonstrated that modes with small energy content may be important for control of a given input–output system [97,183]. Therefore, instead of truncating based on energy content, we consider truncating based on HSVs.

In practice, it may be extremely expensive to compute the Gramians \mathbf{W}_c and \mathbf{W}_o by solving a high-dimensional Lyapunov equation, and the subsequent eigendecomposition is also expensive. Instead of solving for Gramians directly, it is possible to construct empirical Gramians using snapshots of direct and adjoint simulations, as discussed in Eq. (34). Strong connections have been established between POD and BT [96,181–185], and in Ref. [96], POD is used to obtain low-rank approximations to the Gramians. However, the early methods combining POD and BT do not scale well with the number of output measurements. In fact, the number of adjoint simulations required is equal to the number of output measurements, N_s , which may be quite large [186].

In Ref. [97], Rowley introduced the method of balanced (BPOD) to address the aforementioned issues associated with snapshot-based BT. There are two major advances introduced in

this method, which make it practical to very large dynamical systems:

- (1) *Method of snapshots*—Instead of computing the balancing transformation by solving the eigendecomposition in Eq. (37), it is possible to construct the transformation by computing the SVD of

$$\mathcal{O}_d \mathcal{C}_d \quad (38)$$

reminiscent of the method of snapshots from Refs. [86,187,188].

- (2) *Output projection*—To avoid computing N_s adjoint simulations, it is possible instead to solve an output-projected adjoint equation

$$\mathbf{a}_{k+1} = \mathbf{A}_d^* \mathbf{a}_k + \mathbf{C}_d^* \mathbf{U}_r s \quad (39)$$

where \mathbf{U}_r is a rank- N_r POD truncation.

First, define the generalized Hankel matrix as the product of the direct (\mathcal{C}_d) and adjoint (\mathcal{O}_d^*) snapshot matrices from Eqs. (11) and (12), for the discrete-time system

$$\begin{aligned} \mathbf{H} &= \mathcal{O}_d \mathcal{C}_d \\ &= \begin{bmatrix} \mathcal{C}_d \mathbf{B}_d & \mathcal{C}_d \mathbf{A}_d \mathbf{B}_d & \cdots & \mathcal{C}_d \mathbf{A}_d^{m_c-1} \mathbf{B}_d \\ \mathcal{C}_d \mathbf{A}_d \mathbf{B}_d & \mathcal{C}_d \mathbf{A}_d^2 \mathbf{B}_d & \cdots & \mathcal{C}_d \mathbf{A}_d^{m_c} \mathbf{B}_d \\ \vdots & \vdots & \ddots & \vdots \\ \mathcal{C}_d \mathbf{A}_d^{m_o-1} \mathbf{B}_d & \mathcal{C}_d \mathbf{A}_d^{m_o} \mathbf{B}_d & \cdots & \mathcal{C}_d \mathbf{A}_d^{m_c+m_o-2} \mathbf{B}_d \end{bmatrix} \end{aligned} \quad (40)$$

Next, we factor \mathbf{H} ⁴ using the SVD

$$\mathbf{H} = \mathbf{U} \Sigma \mathbf{V}^* = [\mathbf{U}_1 \quad \mathbf{U}_2] \begin{bmatrix} \Sigma_1 & 0 \\ 0 & 0 \end{bmatrix} \begin{bmatrix} \mathbf{V}_1^* \\ \mathbf{V}_2^* \end{bmatrix} = \mathbf{U}_1 \Sigma_1 \mathbf{V}_1^* \quad (41)$$

For a given desired model order $N_r \ll N_a$, only the first N_r columns of \mathbf{U} and \mathbf{V} are kept, along with the first $N_r \times N_r$ block of Σ . This yields a bi-orthogonal set of modes given by

$$\text{direct modes : } \Phi_r = \mathcal{C}_d \mathbf{V}_r \Sigma_r^{-1/2} \quad (42a)$$

$$\text{adjoint modes : } \Psi_r = \mathcal{O}_d^* \mathbf{U}_r \Sigma_r^{-1/2} \quad (42b)$$

These modes are bi-orthogonal, $\Psi_r^* \Phi_r = \mathbf{I}_{N_r \times N_r}$, and Rowley [97] showed that the direct and adjoint modes, Φ and Ψ , establish the change of coordinates that balance the empirical Gramians: $\mathcal{B} = \Phi \triangleq \mathcal{C}_d \mathbf{V} \Sigma^{-1/2}$ and $\mathcal{B}^{-1} = \Psi^* \triangleq \Sigma^{-1/2} \mathbf{U}^* \mathcal{O}_d$. Moreover, Φ_r and Ψ_r are the first N_r -columns of the balancing transformation.

Now, these modes allow us to project our original system onto a (balanced) reduced-order model of order N_r

$$\mathbf{A}_r = \Psi_r^* \mathbf{A}_d \Phi_r \quad (43a)$$

$$\mathbf{B}_r = \Psi_r^* \mathbf{B}_d \quad (43b)$$

$$\mathbf{C}_r = \mathcal{C}_d \Phi_r \quad (43c)$$

One of the key benefits of BT is that there is an upper bound on the error of a given order truncation

$$\text{Upper bound : } \|\mathbf{P} - \mathbf{P}_r\|_\infty < 2 \sum_{j=N_r+1}^n \sigma_j$$

⁴The powers m_c and m_o in Eq. (40) signify that data must be collected until the matrices \mathcal{C}_d and \mathcal{O}_d^* become full rank, after which the controllable/observable subspaces have been sampled.

A BPOD model may not exactly satisfy this upper bound due to errors in the calculation of empirical Gramians. In addition, there is a lower bound that is universal to all models with N_r states

$$\text{Lower bound : } \|\mathbf{P} - \mathbf{P}_r\|_\infty > \sigma_{N_r+1}$$

4.5.4 ERA. Balanced POD requires expensive full-state measurements and adjoint simulations, which are not feasible for experiments. The ERA makes it possible to obtain equivalent balanced models directly from input–output measurements. ERA is based on the minimal realization theory of Ref. [180], and it was developed to identify structural models for various spacecraft [141]. It has been shown that ERA models are equivalent to BPOD models [189]. ERA is a system identification method based on impulse response measurements and does not require prior knowledge of the high-dimensional model in Eq. (32) or access to adjoint simulations.

Similar to BPOD, we take the SVD of the Hankel matrix \mathbf{H} . However, instead of collecting snapshot matrices \mathcal{C}_d and \mathcal{O}_d^* to obtain modes Φ and Ψ , we proceed directly to the reduced-order model, without modes. Introducing another Hankel matrix \mathbf{H}' advanced one time-step in the future

$$\mathbf{H}' = \mathcal{O}_d \mathbf{A}_d \mathcal{C}_d \quad (44)$$

A model is constructed as follows:

$$\mathbf{A}_r = \Sigma_r^{-1/2} \mathbf{U}_r^* \mathbf{H}' \mathbf{V}_r \Sigma_r^{-1/2} \quad (45a)$$

$$\mathbf{B}_r = \text{first } p \text{ columns of } \Sigma_r^{1/2} \mathbf{V}^* \quad (45b)$$

$$\mathbf{C}_r = \text{first } q \text{ columns of } \mathbf{U} \Sigma_r^{1/2} \quad (45c)$$

It is simple to verify that Eqs. (43a) and (45a) are equal. The expressions (43b) and (45b) for \mathbf{B}_r are equivalent, since $\Sigma_r^{-1/2} \mathbf{U}_r^* \mathbf{H} = \Sigma_r^{1/2} \mathbf{V}_r^*$. Similarly, the expressions for \mathbf{C}_r are equivalent.

\mathbf{H} and \mathbf{H}' are constructed from impulse response simulations/experiments, without the need for storing direct or adjoint snapshots. However, if direct snapshots are available, for example, by collecting velocity fields in simulations or particle image velocimetry (PIV), then it is possible to construct direct modes.

ERA and BPOD balance the empirical Gramians, so unless we collect a very large amount of data, the true Gramians are only approximately balanced. However, instead of collecting long tails of data, it is possible to collect data until the Hankel matrix is full rank, balance the full-rank identified model, and then truncate. This is more efficient than collecting snapshots until all of the transients have decayed.⁵

4.5.5 Observer/Kalman Filter Identification (OKID). OKID was developed to compliment the ERA for lightly damped experimental systems with noise [142,192–194]. This method addresses the general problem of identifying an approximate impulse response (i.e., Markov parameters) from arbitrary, noisy input–output data. Typically, one would obtain reduced-order models according to the following general procedure:

- (1) Collect output response to a pseudorandom input,
- (2) This information is then passed through the OKID algorithm to obtain the linear impulse response,
- (3) The impulse response is passed through the ERA to obtain a reduced-order state-space system.

The OKID method identifies an approximation to the impulse response of a system from noisy input–output data using an asymptotically stable Kalman filter. Although this method is quite powerful, it has not been broadly adopted because of the

algorithmic complexity as well as nonintuitive theoretical elements. However, a recent method extending DMD to systems with control inputs provides similar models as ERA/OKID, but with a more intuitive and computationally simple algorithm [195]. This follows recent results that DMD and ERA may be seen as equivalent, up to a coordinate transformation, for certain types of input–output data [101].

4.6 Case Study: Transition Delay in a Boundary Layer and Stabilizing Steady States.

For many canonical flows, such as pipe flow or Couette flow, the underlying laminar steady solution is stable for all Reynolds numbers [196–198], and turbulent fluctuations arise as transient events due to perturbations and wall roughness. However, many fully turbulent flows are characterized by saturated nonlinear dynamics and the existence of a desirable underlying unstable fixed point or periodic orbit. For example, in the laminar-to-turbulent transition of a flat plate boundary layer or channel flow, the unstable fixed point corresponds to steady, laminar flow with significantly decreased drag. The existence of these remnant unstable steady-states is consistent with the Hopf-bifurcation route to turbulence [199]. In addition, linearization may also work in the viscous sublayer in wall turbulence.

Linear control is ideal for such systems, because successful regulators keep the system in a state that is near the fixed point, where the linear assumption remains valid. Therefore, linear control has largely been applied to transition delay and stabilizing unstable steady-states. It is also possible to *destabilize* a system to enhance mixing by reversing the sign of a stabilizing controller [200]. It is worth noting that there are numerous examples where linear model-based control has been successfully applied to flows that are in a nonlinear regime. Often times turbulence is considered a disturbance term in a slower dynamical system, such as the rigid body equations of an aircraft, space shuttle, or rocket. In this case, turbulent fluctuations may be seen as inevitable and operating on a time scale that is faster than controller bandwidth. Instead of trying to change the nature of the turbulence itself, the controller may be designed to obtain some other objective while robustly managing the uncertain turbulent disturbance. Here, we consider the problem of actively controlling the turbulent dynamical system.

The field of linear model-based flow control has experienced exceptional growth, largely due to the close alignment of challenges in engineering fluid dynamics with the sophisticated machinery in model reduction and control theory. There are a number of excellent reviews of linear flow control [20], for transition delay in spatially developing wall-bounded flows [170,171,201], and for the control of cavity oscillations [34]. A good overview of drag reduction by control of turbulence boundary layers is also found in Ref. [10], with a quantification of potential fuel savings in transportation. The discussion here is not meant to be complete, but rather is designed to clarify the choices and historical progress of linear model-based flow control, especially in turbulence.

4.6.1 Early Work. Early progress in model-based flow control is closely tied to advances in computational resources, enabling the simulation of large-scale dynamical systems, such as in fluid dynamics. Currently, the majority of model-based flow control employing \mathcal{H}_2 and \mathcal{H}_∞ techniques are applied to numerical simulations. In Ref. [202], gradient-based optimal control techniques were introduced to control the flow in a channel using boundary condition control. Adjoint methods have also been used extensively for aerodynamic shape optimization based on CFD [203–206].

A suboptimal control approximation was introduced by Choi et al. [207] using a very short time horizon that allowed convective terms to be neglected, resulting in a controller based on a Stokes flow model. This method was then applied to a turbulent channel flow by Bewley and Moin [208], resulting in a 17% drag reduction. Suboptimal control with more physically realizable

⁵This idea is developed in Ref. [190], inspired in Ref. [191].

measurement was analyzed for a turbulent channel flow in Ref. [209]. Without the suboptimal approximation, a model-predictive control (MPC) framework may be used for receding-horizon optimal control, although this is computationally intensive. MPC has been used in Refs. [210,211] and is discussed in more detail in a recent review [171].

In Bewley and Liu [212], both \mathcal{H}_2 and \mathcal{H}_∞ controllers were developed and applied to single wavenumber pairs in a plane channel flow with three-dimensional perturbations. In Ref. [213], robust control was applied to the extended problem of 2D multi-wavenumber control with localized actuation and sensing in plane Poiseuille flow. Höglberg et al. [214] extended the analysis of Bewley and Liu [212] to include multiple wavenumbers and state estimation using a Kalman filter based on wall measurements. Their three-dimensional DNS used boundary condition forcing, and it was shown that state-estimation was not as effective as full-state feedback.

Höglberg and Henningson [215] demonstrated the effectiveness of linear \mathcal{H}_2 optimal control in spatially developing boundary layers, even with moderately strong nonlinearities present. In a follow-up work [216], they extended this analysis to include full-state estimation based on a number of wall measurements, similar to Ref. [214].

4.6.2 Use of Reduced-Order Models. As discussed earlier, the development of controllers for high-dimensional linear systems may be extremely computationally intensive since they depend on the solution to Riccati equations, involving $\mathcal{O}(N_a^3)$ operations, or expensive iterations. Further, once a high-dimensional controller has been designed, it is expensive to compute the resulting control action, introducing unwanted latency in the control loop. This latency significantly limits control bandwidth and may prevent real-time control of high-dimensional systems with fast time-scales. These issues are especially pronounced in flow control.

In the timely work of Akervik et al. [217], reduced-order models were developed by using a few non-normal global eigenmodes of the linearized Navier–Stokes equations as a basis for Galerkin projection. Based on the reduced-order model, an LQG controller is able to attenuate global oscillations in a separated boundary layer. The use of non-normal global modes has been important to capture the transient energy growth associated with wall-bounded shear flows. Yet, these approaches have limited applicability to unstable advection-dominated flows. Transient growth implies a sensitivity issue: a small difference in the initial condition or a small perturbation in the system can give rise to significantly different solutions. Hence, unavoidable truncation errors of reduced-order models based on global modes may cause similar

differences in the solutions. The sensitivity problem is less pronounced at lower Reynolds numbers or for weakly unstable flows.

After the seminal work of Rowley [97], introducing a computationally efficient method to compute balanced reduced-order models, the use of balanced models has become a mainstay in model-based linear flow control. The resulting models are able to capture transient energy growth with significantly fewer modes than POD, as demonstrated in Ref. [183] on the transitional channel flow. BPOD was also shown to outperform standard POD/Galerkin methods for the separation control of an airfoil at low Reynolds number [218], using an immersed-boundary method [219,220].

The paper of Bagheri et al. [221] provides one of the most complete and clearly presented narratives on closed-loop control based on balanced models. In this work, they develop models using snapshot-based BT. Snapshot-based methods are necessary when the state dimension N_a is large, since the A matrix is size N_a^2 , which may not be representable in system memory. The matrix-free methods advocated in Ref. [221] use the CFD time-stepper to find the next flow state, rather than explicitly computing a large A matrix. These methods may be used to solve large eigenvalue problems, for instance, using Arnoldi iteration, thus bypassing the creation and factorization of a large matrix. In this paper, \mathcal{H}_2 control is developed to suppress two-dimensional boundary layer perturbations. Reference [222] presents a three-dimensional generalization of Ref. [221] using LQG to delay transition in a boundary layer.

As described in Sec. 4.5.4, the ERA produces balanced models that are equivalent to BPOD, but without the need for adjoint simulations [189]. ERA has been rapidly adopted in flow control because of the fact that it is based purely on input–output data, making it a system identification method, rather than a model reduction method. ERA was used to study and control cavity flow oscillations and combustion oscillations [223,224]. In Semeraro et al. [225], ERA models were used to develop LQG control to suppress three-dimensional TS waves in a transitional boundary layer using a volume force actuation. This paper is well-written and thought provoking, and an illustration of the closed-loop control topology is shown in Fig. 12. Interestingly, one of the earliest experimental demonstrations of active feedback suppression of turbulence was applied to cancel TS waves using a downstream heating element and a phase-shifted measurement feedback, resulting in an increase in the transition Reynolds number [18].

4.7 Case Study: Wall Turbulence Control and Skin-Friction Reduction. There is a tremendous industrial motivation to reduce turbulent skin-friction drag. This problem has thus

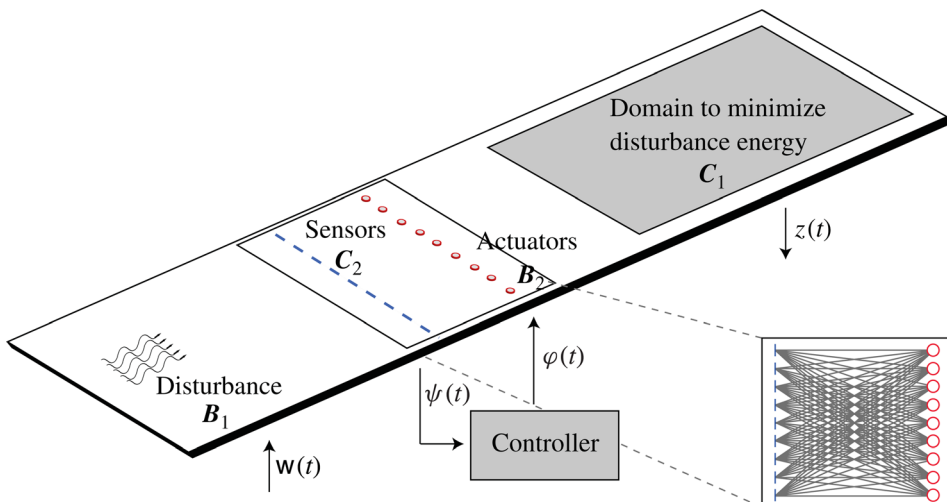


Fig. 12 Schematic of the closed-loop controller for transition delay of a flat-plate boundary layer (Reproduced with permission from Semeraro et al. [225]. Copyright 2013 by Cambridge University Press).

received significant attention, and corresponding progress has been made [10,40,226]. Reduced-order models for control based on LQG and the robustifying loop-transfer recovery were used to reduce skin-friction drag in a channel flow [227,228], resulting in eventual relaminarization of the flow. Reduced-order models were also used with blowing/suction at the wall to reduce skin friction in simulations [229], and reduced-order Kalman filters were developed based on BT models [133].

In addition to the mechanisms and techniques discussed, there have been many efforts to reduce turbulent skin friction drag [230–234] using various techniques, such as traveling-wavelike actuation including blowing/suction and wall deformation. Increasing heat transfer while decreasing drag is also an important area of research [235]. In addition, system identification and control were used for the linear feed-forward control of turbulent boundary layer fluctuations by exploiting coherent structures and predicting their behavior downstream [236]. The same reduction in turbulent boundary layer fluctuations was explored using model-based control in an experiment using an array of synthetic jet actuators [237].

4.8 Case Study: Cavity Flow Control. The work surrounding the control of open cavity flows represents one of the most complete and compelling success stories in active flow control [238]. Cavity flow control has many applications, such as the suppression of oscillations in weapons bays in high-speed flight [239], which is an inherently high Reynolds number phenomena. A more complete discussion of the cavity flow control problem is discussed in reviews [34,240,241].

Suppression of cavity oscillations has benefited from a combination of new physical insights combined with simulations [242], advances in advanced Galerkin modeling [243,244], and the practical implementation of control in experiments [245–248]. Exciting new methods, such as control based on neural networks [46,249] and the use of ERA [225], have also been investigated.

In some regimes, oscillations are self-sustained and inherently nonlinear. To identify models suitable for control, Rowley et al. [245] stabilized the oscillations using Nyquist plots to tune the phase of controllers based on experimentally obtained frequency response data. A model was then obtained for the closed-loop system using system identification, and model for the unstable system was derived.

4.9 Potential Impact and Challenges. All of the models discussed above, and therefore the corresponding controllers, depend on the placement of actuators and sensors, as these directly affect \mathbf{B} and \mathbf{C} in Eq. (5). Actuator and sensor placement was recently investigated for boundary layer transition delay [250]. Importantly, this study provides a clear comparison of feedforward (sensor upstream of actuator) versus feedback (sensor downstream of actuator) control. In particular, it is shown that disturbance-feedforward control is effective sometimes, but is sensitive to additional disturbances and uncertainty. Feedback, on the other hand, effectively rejects disturbances and compensates for unmodeled dynamics. However, if the sensor is too far downstream, the time-delay between actuation and sensing dramatically limits robust performance, which is consistent with the discussion above.

Given the performance of drag reduction, in the neighborhood of 20%, and transition delay cited in the literature, it may be somewhat surprising that active closed-loop control is not being utilized on mainstream aircraft, trains, or automobiles. There are a number of reasons why the studies above are largely numerical. First, many model-reduction techniques require extensive and invasive information about the plant, although ERA is less invasive. Second, the time-scales associated with real experimental and industrial turbulence are extremely fast, so that reducing time delays is a significant challenge. Time delays may originate from latency involved in the computation of a control decision, and they may also arise from convective time scales from actuators to

sensors. Finally, the development of advanced sensor and actuator hardware will be a major enabling factor in the practical implementation of these methods.

5 Prototypes for Linear and Nonlinear Dynamics

Despite the powerful tools for linear model reduction and control, the assumption of linearity is often overly restrictive for real-world fluids. Turbulent fluctuations are inherently nonlinear, and often the goal is not to stabilize an unstable fixed point but rather to change the nature of a turbulent attractor. Moreover, it may be the case that the control input is either a bifurcation parameter itself, or closely related to one, such as the control surfaces on an aircraft.

The degree of nonlinearity is most easily characterized in a Galerkin modeling framework (Sec. 5.1). The subsequent sections (Sects. 5.2–5.5) provide prototypic examples of linear, weakly, moderately, and strongly nonlinear dynamics as evidenced in many fluid flows and corresponding control strategies. Section 5.6 concludes with enablers and show-stoppers of nonlinear model-based control design.

5.1 Galerkin Model. In this section, different degrees of system nonlinearity are introduced. For simplicity, we consider an incompressible velocity field $\mathbf{u}(\mathbf{x}, t)$ in a finite steady domain $\mathbf{x} \in \Omega$. Let $\mathbf{a} = [a_1, a_2, \dots, a_{N_a}]^T$ represent an N_a -dimensional approximation of the flow state. The coordinates a_i , $i = 1, \dots, N_a$ may, for instance, represent the coefficients in a Galerkin expansion

$$\mathbf{u}(\mathbf{x}, t) = \mathbf{u}^s(\mathbf{x}) + \sum_{i=1}^{N_a} a_i(t) \mathbf{u}_i(\mathbf{x}) \quad (46)$$

where \mathbf{u}^s represents the steady Navier–Stokes solution, and \mathbf{u}_i , $i = 1, \dots, N_a$ are suitable expansion modes.

Let $\mathbf{b} = [b_1, b_2, \dots, b_{N_b}]^T$ characterize the actuation. One example involves N_b volume forces $\sum_i^{N_b} b_i(t) \mathbf{g}_i(\mathbf{x})$ with the individual fields \mathbf{g}_i , $i = 1, \dots, N_b$. To simplify the discussion, only a single component is assumed, $N_b = 1$, and $b = b_1$ denotes its amplitude.

The sensor signals $\mathbf{s} = [s_1, s_2, \dots, s_{N_s}]^T$ may represent velocity components. In this case, they are affinely related to expansion coefficients via Eq. (46). The sensing plays no role in this section. Focus is placed on finding a proper linearized system whenever possible.

For the sake of simplicity, we assume the structure of a Galerkin system with a single volume force as actuation. Then, the dynamics in Eq. (2) take the form

$$f_i(\mathbf{a}, b) = \sum_{j=1}^{N_a} l_{ij} a_j + \sum_{j,k=1}^{N_a} q_{ijk} a_j a_k + g_i b \quad (47)$$

The constant term of the dynamics vanishes since the basic mode \mathbf{u}^s is assumed to be the steady Navier–Stokes solution.

Near the fixed point $\mathbf{a} \approx \mathbf{0}$, the quadratic term may be neglected yielding the linear dynamics (5) of Sec. 4. Physically meaningful linearizations may also be effected far away from the origin. The critical element is the notion of “fast” and “slow” modes. The fast modes describe the evolution of coherent structures and may best be considered as a fluctuation. Let us assume $i = 1, \dots, N_a^f$ represent the indices of the fast modes. The slow modes have significantly lower frequencies and may best be attributed to a base-flow variation. Let the remaining indices $i = N_a^f + 1, \dots, N_a$ represent such slow modes. By a trivial operation, the dynamics have the form

$$f_i = c_i^B + \sum_{j=1}^{N_a^f} l_{ij}^B a_j + h_i^B + g_i b$$

where

$$\begin{aligned}c_i^B &= \sum_{j=N_a^f+1}^{N_a} l_{ij} a_j + \sum_{j,k=N_a^f+1}^{N_a} q_{ijk} a_j a_k \\l_{ij}^B &= \sum_{k=N_a^f+1}^{N_a} (q_{ijk} + q_{ikj}) a_k \\h_i^B &= \sum_{j,k=1}^{N_a^f} q_{ijk} a_j a_k\end{aligned}$$

Here, the quasi-constant c_i^B measures the distance to the fixed point $\mathbf{a} \equiv \mathbf{0}$, the quasi-linear term with the coefficients l_{ij}^B incorporates slow base-flow changes, and h_i^B represents a quadratic nonlinearity in the fluctuating modes. h_i^B has slow and fast components. If the volume force is in feedback with the fluctuations, $c_i^B + h_i^B \approx 0$ in a short-term average. In this case, $f_i = \sum_{j=1}^{N_a^f} l_{ij}^B a_j + g_i b$, $i = 1, \dots, N_a$ may be a suitable linear representation of the fast dynamics.

The slow modes are slaved to an approximate manifold in state space defined by $da_i/dt = f_i(\mathbf{a}) \approx 0$, $i = N_a^f + 1, \dots, N_a$ and are driven by the Reynolds stress contributions of the fast modes, or, equivalently, by the slow component of h_i^B .

In Secs. 5.2 through 5.5, four prototypic examples are discussed: (A) an oscillation around the fixed point; (B) a self-excited amplitude-limited oscillation; (C) frequency cross-talk with two different frequencies over the base-flow deformation; and (D) the remaining irreducible cases.

5.2 Linear Dynamics. First, a small oscillatory fluctuation around a steady solution is considered. Examples include the flow over a backward-facing step [251] at subcritical Reynolds number with noise, transition delay of a boundary layer [252], or stabilization of a cylinder wake [19,253]. In Sec. 5.2.1, a control-oriented oscillator model is presented as a least-order description. Section 5.2.2 exemplifies the powerful method of energy-based control design for this model.

5.2.1 Oscillator Model. The considered flows can be described by

$$\mathbf{u}(\mathbf{x}, t) = \mathbf{u}^s(\mathbf{x}) + \mathbf{u}^u(\mathbf{x}, t) \quad (48a)$$

$$\mathbf{u}^u(\mathbf{x}, t) = a_1(t) \mathbf{u}_1(\mathbf{x}) + a_2(t) \mathbf{u}_2(\mathbf{x}) \quad (48b)$$

Here, \mathbf{u}_i , $i = 1, 2$, correspond to the cosine and sine contribution of the first harmonic or the real and imaginary part of the unstable complex eigenmode. Higher harmonics are neglected. By construction, the stable or unstable fixed point is $\mathbf{a}^s = \mathbf{0}$.

The linearized version of the dynamics (47) reads

$$\frac{d}{dt} \mathbf{a} = \mathbf{A}_0 \mathbf{a} + \mathbf{B} b \quad (49)$$

where

$$\begin{aligned}\mathbf{A}_0 &= \begin{bmatrix} \sigma^u & -\omega^u \\ \omega^u & \sigma^u \end{bmatrix} \\ \mathbf{B} &= \begin{bmatrix} 0 \\ g \end{bmatrix}\end{aligned}$$

Without loss of generality, the modes can be rotated so that the gain in the first component vanishes. A similar equation holds for the measurement equation. As discussed in Sec. 4.1, the matrices \mathbf{A}_0 and \mathbf{B} depend on the fixed point \mathbf{a}^s and the bifurcation parameters μ .

The linear dynamics (49) may also be an acceptable approximation for turbulent flows with dominant oscillatory behavior. In the

triple decomposition, the velocity field is partitioned into the mean flow \mathbf{u}_0 , the periodic oscillation \mathbf{u}^u , and an uncorrelated stochastic fluctuation \mathbf{u}^r . The periodic fluctuation may be described by two modes (48b), again. Equation (49) is obtained by substituting the velocity field $\mathbf{u} = \bar{\mathbf{u}} + \mathbf{u}^u + \mathbf{u}^r$ in the Navier–Stokes equation, projecting onto the modes \mathbf{u}_i , and filtering out anything but the dominant frequency. In this case, the growth-rate $\sigma^u = 0$ has to vanish and the amplitude selection mechanism cannot be resolved by the two-dimensional Galerkin model. In particular, the fixed point $\mathbf{0}$ of the Galerkin model represents the mean flow which is not the steady solution of the Navier–Stokes equation. Yet, the model may be good enough to predict the right actuation for increasing or decreasing the fluctuation near the limit cycle.

5.2.2 Energy-Based Control Design. Control design of the linear system (49) can be performed with the methods of Sec. 4. Here, we illustrate the idea of energy-based control which is particularly suited for nonlinear dynamics. Moreover, energy-based control has a kinematic relation to phasor control and an energetic relation to opposition control.

The growth-rate σ^u is assumed positive and small enough so that the time-scale of amplitude growth is small compared to the time-scale of oscillation. In this case, the state can be approximated by $a_1 = r \cos \theta$ and $a_2 = r \sin \theta$, where r and $\omega = d\theta/dt$ are slowly varying functions of time. The amplitude evolution is given by

$$\frac{dr^2}{dt} = 2a_1 \frac{da_1}{dt} + 2a_2 \frac{da_2}{dt} = 2\sigma^u r^2 + 2g a_2 b$$

The control goal is an exponential decay of the amplitude with $\sigma^c < 0$, i.e.,

$$\frac{dr^2}{dt} = 2\sigma^c r^2$$

Eliminating the time-derivative in both equation yields

$$\frac{dr^2}{dt} = \sigma^c r^2 = \sigma^u r^2 + g a_2 b$$

The control command b increases (decreases) the energy $r^2/2$ if it has the same (different) sign as a_2 . To prevent wasting actuation energy with the wrong phase, the linear ansatz $b = -k a_2$ is made. The gain $k > 0$ is determined by substituting $a_2 = r \cos \theta$ in the energy equation and averaging over one period. The resulting control law reads

$$b = 2 \frac{\sigma^c - \sigma^u}{g} a_2 \quad (50)$$

The gain increases with the difference between the natural and design growth rate $\sigma^c - \sigma^u$ and decreases with the forcing constant g in the linear dynamics. The factor 2 arises from the fact that the actuation is only effective in the $[0, 1]^T$ direction.

It may be emphasized that the achieved decay of the fluctuation energy is an average value over one period. When $a_2 = 0$, no change of the energy is achievable. Second, the construction of the control law is based on designing a dissipative term $ga_2 b$ in the power balance. Hence, the actuation mechanism may be considered an energetic opposition control. Third, the actuation command b scales with fluctuation amplitude r . Its phase lags 270 deg with respect to the first coordinate a_1 . Hence, on a kinematical level, the actuation describes a phasor control. Figure 13 describes the corresponding unactuated and actuated solution of Eq. (49).

The described energy-based control design is very simple and immediately reveals the physical mechanism. It is easy to generalize for nonlinear systems, particularly if the fluctuation is composed of clean frequency components. Related approaches are called Lyapunov control design and harmonic balance.

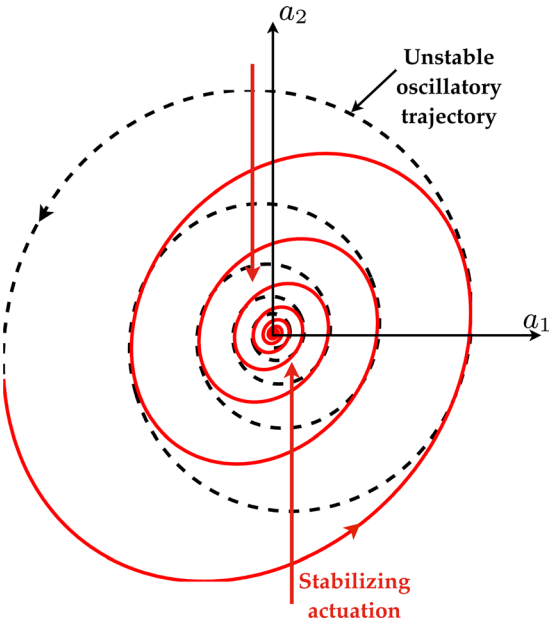


Fig. 13 Phase portrait of oscillatory linear dynamics (49). The dashed trajectory corresponds to the unactuated dynamics while the solid trajectory corresponds to actuated dynamics with Eq. (50). The chosen parameters are $\sigma^u = 0.1$, $\sigma^c = -0.1$, $\omega^u = 1$, $g = 1$ implying $k = 0.4$.

5.3 Weakly Nonlinear Dynamics. As a refinement to the linearization, mean-field theory is recapitulated [254,255] providing an important nonlinear amplitude selection mechanism. The onset of vortex shedding behind a cylinder is one well investigated example fitting this description [256]. The following two sections outline the dynamical model and corresponding control design, respectively.

5.3.1 Mean-Field Model. Qualitatively, mean-field theory describes the feedback mechanism between the fluctuations and the base flow. The fluctuation gives rise to a Reynolds stress which changes the base flow. The base-flow deformation generally reduces the production of fluctuation energy with increasing fluctuation level until an equilibrium is reached. The resulting evolution equations are also referred to as *weakly nonlinear dynamics*, as they describe a mild form of nonlinearity.

The fluctuation has the same representation as in Sec. 5.2. However, the base flow is allowed to vary by another mode \mathbf{u}_3 , called the zeroth, base-deformation or shift mode. This mode can be derived from the (linearized) Reynolds equation and it is assumed to be slaved to the fluctuation level. The resulting velocity field ansatz reads

$$\mathbf{u}(\mathbf{x}, t) = \mathbf{u}^s(\mathbf{x}) + \mathbf{u}^u(\mathbf{x}, t) + \mathbf{u}^\Delta(\mathbf{x}, t) \quad (51a)$$

$$\mathbf{u}^u(\mathbf{x}, t) = a_1(t) \mathbf{u}_1(\mathbf{x}) + a_2(t) \mathbf{u}_2(\mathbf{x}) \quad (51b)$$

$$\mathbf{u}^\Delta(\mathbf{x}, t) = a_3(t) \mathbf{u}_3(\mathbf{x}) \quad (51c)$$

The evolution equation is given by

$$\frac{d}{dt} \begin{bmatrix} a_1 \\ a_2 \end{bmatrix} = \mathbf{A}(a_3) \begin{bmatrix} a_1 \\ a_2 \end{bmatrix} + \mathbf{B} b \quad (52a)$$

$$a_3 = \alpha^u (a_1^2 + a_2^2) \quad (52b)$$

where

$$\mathbf{A}(a_3) = \mathbf{A}_0 + a_3 \mathbf{A}_3$$

$$\mathbf{A}_0 = \begin{bmatrix} \sigma^u & -\omega^u \\ \omega^u & \sigma^u \end{bmatrix}$$

$$\mathbf{A}_3 = \begin{bmatrix} -\beta^u & -\gamma^u \\ \gamma^u & -\beta^u \end{bmatrix}$$

$$\mathbf{B} = \begin{bmatrix} 0 \\ g \end{bmatrix}$$

Without loss of generality, $\alpha^u > 0$. Otherwise, the sign of the mode \mathbf{u}_3 must be changed. A nonlinear amplitude saturation requires the Landau constant to be positive $\beta^u > 0$.

For $a_3 \equiv 0$, Eq. (52) is equivalent to Eq. (49). However, Eq. (52) has a globally stable limit cycle with radius $r^\infty = \sqrt{\sigma^u / \alpha^u \beta^u}$ in the plane $a_3 = a_3^\infty = \sigma^u / \beta^u$, and with center $[0, 0, a_3^\infty]$.

In the framework of weakly nonlinear stability theory, the growth-rate is considered a linear function of the Reynolds number $\sigma_u = \kappa(\text{Re} - \text{Re}_c)$, where Re_c corresponds to its critical value. The other parameters are considered to be constant. This yields the famous Landau equation for the amplitude $dr/dt = \sigma^u r - \beta r^3$, $\beta = \alpha^u \beta^u$ and a corresponding equation for the frequency. In particular, the Landau equation explains the famous square-root amplitude law $r \propto \sqrt{\text{Re} - \text{Re}_c}$ for supercritical Reynolds numbers assuming a soft bifurcation. We refer to the literature for a discussion of the hard subcritical bifurcation with quintic nonlinearity [255].

Mean-field theory explains the stabilizing feedback mechanism between the harmonic oscillatory structure and the mean-field deformation. A refined weakly nonlinear expansion also takes higher harmonics into account. The first harmonic, via the quadratic Navier–Stokes term, generates not only a mean-flow deformation but also a second harmonic which changes, in turn, the mean flow. The nonlinear interaction of the first and second harmonics produces a third harmonic, etc. Dusek et al. [257] derived a corresponding harmonic expansion from the Navier–Stokes equation in the neighborhood of a supercritical Hopf bifurcation. Let $\epsilon > 0$ be the small amplitude of the first harmonic; then, the n th harmonics are shown to scale in geometric progression, i.e., with ϵ^n . Hence, higher harmonics may be neglected near the onset of fluctuations. Even for periodic flow far beyond the onset, the second harmonic is observed to be 1 order of magnitude smaller than the corresponding harmonic component. A similar observation holds for turbulent flow with dominant periodicity.

Intriguingly, even turbulent flows with dominant periodic coherent structures may be described by Eq. (52). One example is the wake behind a finite cylinder [258]. In this case, the rationale is the velocity decomposition with an added uncorrelated stochastic fluctuation \mathbf{u}^r : $\mathbf{u} = \mathbf{u}^s + a_3 \mathbf{u}_3 + \mathbf{u}^u + \mathbf{u}^r$. In this case, Eq. (52) remains valid if \mathbf{u}^r scales with the oscillatory fluctuation level and the base flow deformation is slaved to this level as well.

5.3.2 Nonlinear Control Design. The mean-field model and variants thereof have been successfully used for the model-based stabilization of the cylinder wake at $\text{Re} = 100$ [44,259,260]. In these studies, an energy-based control design as discussed in Sec. 5.2 has been used to prescribe a fixed decay rate of the model. Figure 14 illustrates an unactuated and actuated transient.

It may be noted that Eq. (52) can be considered a linear parameter varying model with the shift-mode amplitude a_3 , or, equivalently, with the fluctuation level r^2 as the parameter. Thus, the linear control design of Sec. 4 is immediately applicable for the linear system corresponding to the actual value of this parameter. King et al. [261] elaborated other nonlinear control design techniques for the mean-field model employing input–output linearization, Lyapunov-based synthesis, and backstepping. The mean-field model has also been the basis for optimal control of the Navier–Stokes equation [262], using the simulation to improve the model and the model as a surrogate plant for control design.

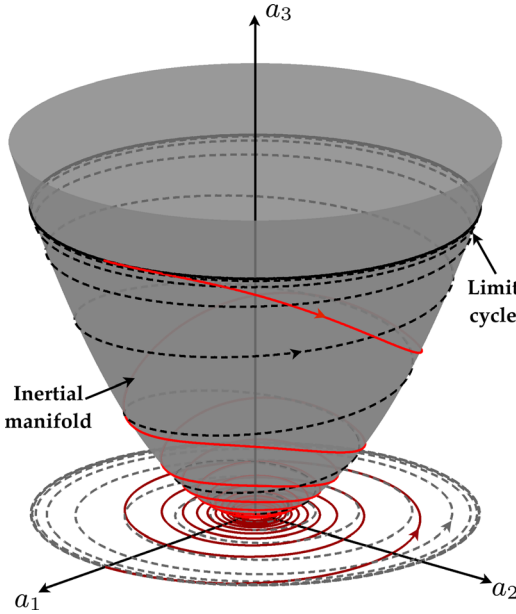


Fig. 14 Phase portrait of weakly nonlinear dynamics. The dashed trajectory corresponds to the unactuated dynamics while the solid trajectory corresponds to actuated dynamics. The chosen parameters of Eq. (52) are $\sigma^u = 0.1$, $\omega^u = 1$, $\alpha^u = 1$, $\beta^u = 1$, $\gamma^u = 0$, and the forced decay rate $\sigma^c = -0.1$. The globally stable limit cycle lies on the parabolic inertial manifold.

5.4 Moderately Nonlinear Dynamics. Some oscillatory flows may be tamed by direct mitigation with models and methods described in Sec. 5.3. Not all plants, particularly turbulent flows, have the actuation authority for such a stabilization. However, periodic forcing at high frequency has mitigated periodic oscillations in a number of experiments. Examples are the wake stabilization with a oscillatory cylinder rotation [74], suppression of Kelvin–Helmholtz vortices in transitional shear layers [263], reduction of the separation zone in a high-lift configuration [48], and elongation of the dead-water region behind a backward facing step [47]. Also a periodic frequency at 60–70% of the dominant shedding frequency may substantially delay the vortex formation in wall-bounded shear-layers [49] and D-shaped cylinders [45]. Sections 5.4.1 and 5.4.2 outline a corresponding modeling and control strategy.

5.4.1 Generalized Mean-Field Model. Here, a generalized mean-field model for such frequency-cross talk phenomena is reviewed from Ref. [48]. Let \mathbf{u}^u denote the natural self-amplified oscillation represented by two oscillatory modes \mathbf{u}_1 and \mathbf{u}_2 . Analogously, the actuated oscillatory fluctuation \mathbf{u}^a is described by two modes \mathbf{u}_3 and \mathbf{u}_4 . The base-flow deformation due to the unstable natural frequency ω^u and stable actuation frequency ω^a is described by the shift-modes \mathbf{u}_5 and \mathbf{u}_6 , respectively. The resulting velocity decomposition reads

$$\mathbf{u}(\mathbf{x}, t) = \mathbf{u}^s(\mathbf{x}) + \mathbf{u}^\Delta(\mathbf{x}, t) + \mathbf{u}^u(\mathbf{x}, t) + \mathbf{u}^a(\mathbf{x}, t) \quad (53a)$$

$$\mathbf{u}^u(\mathbf{x}, t) = a_1(t) \mathbf{u}_1(\mathbf{x}) + a_2(t) \mathbf{u}_2(\mathbf{x}) \quad (53b)$$

$$\mathbf{u}^a(\mathbf{x}, t) = a_3(t) \mathbf{u}_3(\mathbf{x}) + a_4(t) \mathbf{u}_4(\mathbf{x}) \quad (53c)$$

$$\mathbf{u}^\Delta(\mathbf{x}, t) = a_5(t) \mathbf{u}_5(\mathbf{x}) + a_6(t) \mathbf{u}_6(\mathbf{x}) \quad (53d)$$

Generalized mean-field arguments yield the following evolution equation:

$$\frac{d}{dt} \begin{bmatrix} a_1 \\ a_2 \\ a_3 \\ a_4 \end{bmatrix} = \mathbf{A}(a_5, a_6) \begin{bmatrix} a_1 \\ a_2 \\ a_3 \\ a_4 \end{bmatrix} + \mathbf{B} b \quad (54a)$$

$$a_5 = \alpha^u(a_1^2 + a_2^2) \quad (54b)$$

$$a_6 = \alpha^a(a_3^2 + a_4^2) \quad (54c)$$

where

$$\mathbf{A}(a_5, a_6) = \mathbf{A}_0 + a_5 \mathbf{A}_5 + a_6 \mathbf{A}_6$$

$$\mathbf{A}_0 = \begin{bmatrix} \sigma^u & -\omega^u & 0 & 0 \\ \omega^u & \sigma^u & 0 & 0 \\ 0 & 0 & \sigma^a & -\omega^a \\ 0 & 0 & \omega^u & \sigma^u \end{bmatrix}$$

$$\mathbf{A}_5 = \begin{bmatrix} -\beta^{uu} & -\gamma^{uu} & 0 & 0 \\ \gamma^{uu} & -\beta^{uu} & 0 & 0 \\ 0 & 0 & -\beta^{au} & -\gamma^{au} \\ 0 & 0 & \gamma^{au} & -\beta^{au} \end{bmatrix}$$

$$\mathbf{A}_6 = \begin{bmatrix} -\beta^{ua} & -\gamma^{ua} & 0 & 0 \\ \gamma^{ua} & -\beta^{ua} & 0 & 0 \\ 0 & 0 & -\beta^{aa} & -\gamma^{aa} \\ 0 & 0 & \gamma^{aa} & -\beta^{aa} \end{bmatrix}$$

$$\mathbf{B} = \begin{bmatrix} 0 \\ 0 \\ 0 \\ g \end{bmatrix}$$

It should be noted that a vanishing actuation implies $a_3 = a_4 = a_6 = 0$ and yields the mean-field model of Eq. (52) modulo index numbering. In the sequel, we assume that the fixed point is unstable ($\sigma^u > 0$) and the limit cycle is stable ($\beta^{uu} > 0$). Similarly, a vanishing natural fluctuation $a_1 = a_2 = a_5$ yields another mean-field model, again modulo index numbering. In the sequel, we assume that the actuated structures vanish after the end of actuation, implying $\sigma^{aa} < 0$ and $\beta^{aa} > 0$ in the model.

An interesting aspect of Eq. (54) is the frequency cross-talk. The effective growth-rate for the natural oscillation reads

$$A_{11} = \sigma^u - \beta^{uu} \alpha^u (a_1^2 + a_2^2) - \beta^{ua} \alpha^a (a_3^2 + a_4^2) \quad (55)$$

The forcing stabilizes the natural instability if and only if $\beta^{ua} > 0$. Complete stabilization implies $A_{11} \leq 0$. From Eq. (55), such complete stabilization is achieved with a threshold fluctuation level at the forcing frequency

$$a_3^2 + a_4^2 \geq \frac{\sigma^u}{\alpha^a \beta^{ua}}$$

Thus, increasing the forcing at higher or lower frequency can decrease the natural frequency.

The generalized mean-field model has been fitted to numerical URANS simulation data of a high-lift configuration [48] with high-frequency forcing. This model also accurately describes the experimental turbulent wake data with a stabilizing low-frequency forcing [264], as shown in Fig. 15.

5.4.2 Nonlinear Control Design. The model above may guide in-time control [265] and adaptive control design providing the minimum effective actuation energy [266].

Figures 16 and 17 show an unactuated and stabilizing transient with the parameters of Table 1. For simplicity, all nonlinear

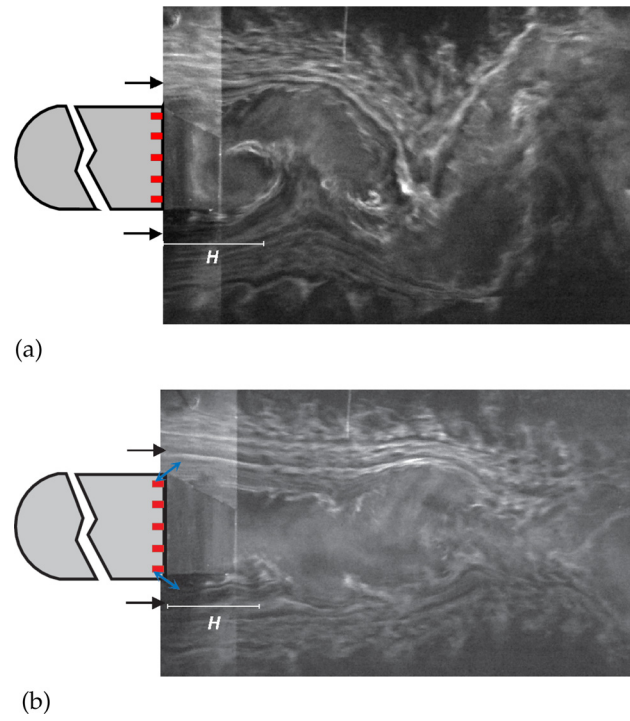


Fig. 15 Flow visualization of the experimental wake behind a D-shaped body without (a) and with symmetric low-frequency actuation (b) (Reproduced with permission from Mark Pastoor.) The D-shaped body is shown with five pressure sensors on the rear face, and the arrows at the corners indicate the employed zero net mass flux actuators. (a) Natural wake with vortex shedding and (b) actuated partially stabilized wake.

terms of the forced oscillator are assumed to vanish, since the linear term is already stabilizing. For the same reason, all nonlinear frequency terms are set to zero as the frequency cross-talk is not affected by small frequency variations. In principle, Eq. (54) can be generalized for an arbitrary number of frequencies.

It should be noted that linear, weakly nonlinear, and moderately nonlinear systems show different actuation response which may be tested in experiments. For the linear system, a *global superposition principle* for the actuation response holds: Let $\mathbf{b}^1(t)$ and $\mathbf{b}^2(t)$ be two open-loop actuation commands and $\mathbf{a}^1(t)$ and $\mathbf{a}^2(t)$ be the corresponding solutions. Let the linear combination $\mathbf{b} = \lambda\mathbf{b}^1 + \mu\mathbf{b}^2$ with real coefficients λ and μ be a new actuation command. Then, $\mathbf{a} = \lambda\mathbf{a}^1 + \mu\mathbf{a}^2$ is a corresponding new solution. The weakly nonlinear system has a similar *local superposition principle* for an infinitesimal perturbation of the stable unforced limit cycle. In contrast, the frequency cross-talk mechanism of the moderately nonlinear system is not resolved by a local linearization around the stable unforced limit cycle. The linearization of Eq. (55) removes the frequency cross-talk.

5.5 Strongly Nonlinear Dynamics. Sections 5.5.1 and 5.5.2 outline examples of strongly nonlinear dynamics not fitting in the previous categories and examples of corresponding control design, respectively.

5.5.1 Examples of Strongly Nonlinear Dynamics. In the case of moderately nonlinear dynamics, different frequencies interact over the slowly varying base flow. The corresponding solutions are well described by the local linearization around the short-term averaged flow. In other words, the solution lives on a manifold in state space and evolves according to a locally linear dynamical

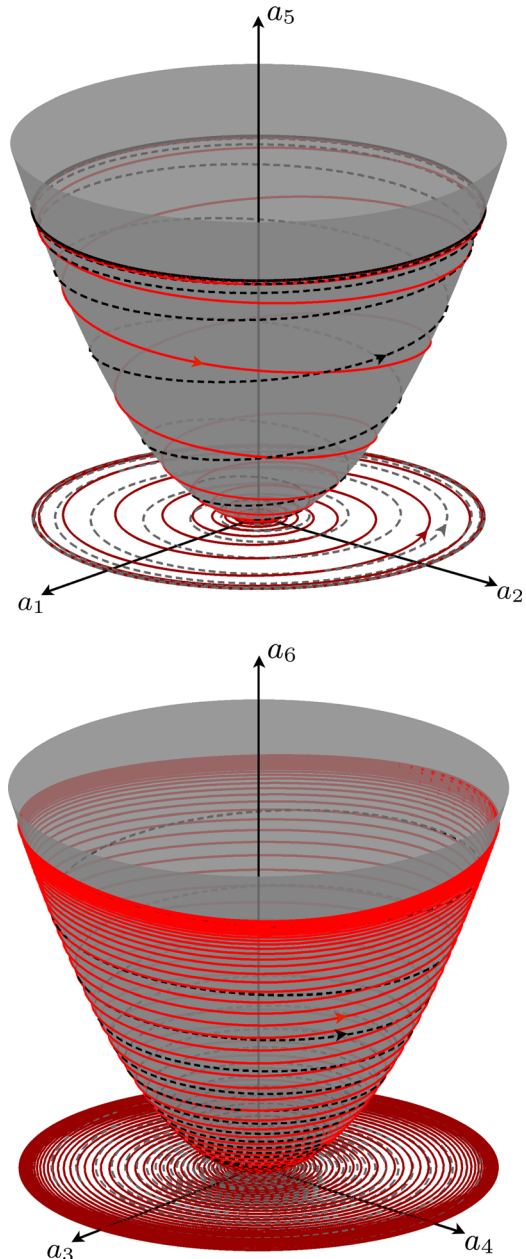


Fig. 16 Phase portrait of moderately nonlinear dynamics (54). The dashed trajectory corresponds to the unactuated dynamics while the solid trajectory corresponds to actuated dynamics with Eq. (50). The chosen parameters are enumerated in Table 1.

system. This may be a useful approximation even for turbulent flows with one or few dominant frequencies. The turbulence cascade is, however, dominated by triadic interactions involving non-vanishing frequencies. The corresponding energy flow from large scales (low frequencies) to small scales (high frequencies) is not well characterized by moderately nonlinear dynamics. No linearization is able to describe such a cascade. A similar behavior applies to the inverse cascade from dominant to larger scales, e.g., via vortex pairing. We shall call such dynamics “strongly nonlinear” implying that they are irreducible to even locally linear systems. The decay of 2D turbulence by optimal initial conditions is a beautiful configuration illustrating the complexity associated with strong nonlinearity [267].

Mathematically, strong nonlinearity may be cast in a form similar to the linear dynamics in Eq. (5), but with

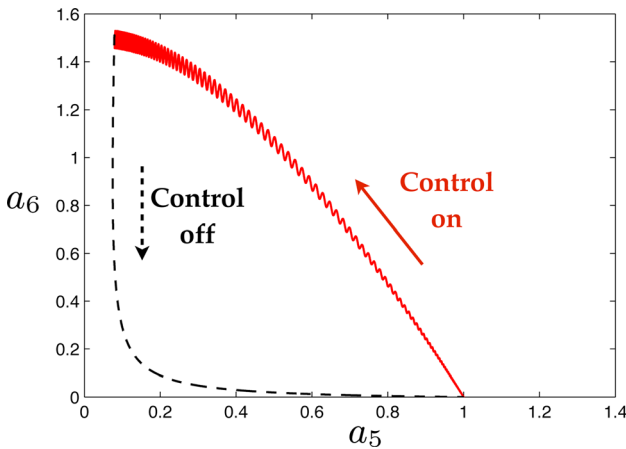


Fig. 17 Phase portrait of the shift-mode amplitudes a_5 and a_6 , i.e., the slow dynamics in Eq. (54). Same transient solutions as in Fig. 16.

Table 1 Parameters of the generalized mean-field model illustrated in Fig. 16

Unstable oscillator	Stable oscillator
$\sigma^u = 0.1$	$\omega^u = 1$
$\beta^{uu} = 1$	$\gamma^{uu} = 0$
$\beta^{ua} = 1$	$\gamma^{ua} = 0$
$\alpha^u = 1$	$\alpha^a = 1$
	$\sigma^a = -0.1$
	$\beta^{au} = 0$
	$\beta^{aa} = 0$
	$\gamma^{aa} = 0$
	$g = 1$

$$A = A_0 + \sum_{i=1}^{N_a} a_i A_i \quad (56)$$

The variation of the matrix A can neither be ignored nor considered slowly varying—in contrast to linear, weakly nonlinear or moderately nonlinear behavior.

We arrive at the following classification of system dynamics (see Fig. 18). The dynamics are either linearizable near the fixed point, or they are locally linearizable with one or few frequencies, or they belong to the reducible cases. The boundaries between two neighboring cases are, of course, a bit blurred depending on the considered error tolerance of the model.

5.5.2 Nonlinear Control Design. The above classification is based on a spectrum of periodic processes (clock-works). There

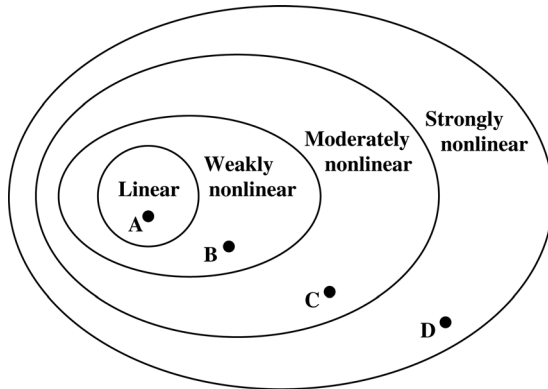


Fig. 18 Venn diagram for the classification of nonlinearities. Prototypic examples are for (A), the subcritical flow over backward-facing step with noise excitation [251]; for (B), the supercritical onset of vortex shedding [256]; for (C), the suppression of Kelvin–Helmholtz vortices by high-frequency forcing [47]; and for (D), the decay of 2D turbulence [267].

exists an analog classification for event-based control. Model-based control strategies for strongly nonlinear dynamics are scarce. One programmatic general approach is suboptimal control in which the optimal control actuation is chosen just for the next time step [43]. In Ref. [268], a corresponding Lyapunov-based control strategy has been found effective to suppress jet noise events. For some well understood configurations, the physical mechanism can be exploited. For instance, skin-friction of wall turbulence is known to increase with sweeps and ejections. Hence, a wall-normal blowing or suction counteracting the wall-normal velocity at 10 plus units has been found to be a very effective closed-loop opposition control [43].

Figure 19 displays examples of the single input (one actuator) and single output (one sensor) system for the four kinds of system dynamics. The first row shows the excitation of a frequency for a stable linear system. The second example is the energization of a stable limit cycle. The third row shows the suppression of a low frequency by high-frequency forcing, and the last example indicates how a single excitation frequency can change the whole frequency spectrum.

There is a strong increase of complexity as one moves from taming few frequency peaks to broadband dynamics. For the latter, even developing reduced-order models suitable for control design constitutes an unattainable goal with modern techniques.

5.6 Enablers and Challenges of Nonlinear Model-Based Control. In this section, enablers and challenges of nonlinear model-based control are discussed. The beauty of the linear (49), weakly nonlinear (52), and moderately nonlinear models (54) is that each mode and each dynamical system coefficient have a clear physical meaning. Moreover, the nonlinear systems have an inherent tunable robustness. Evidently, more sophisticated models with more frequencies can be constructed in a similar spirit. Alternatively, a POD model with, say, 100 dimensions may be more accurate but the modes and the system coefficients have no physical meaning. Moreover, each mode and each coefficient act as a noise amplifier for estimation and control design tasks. Thus, more accurate models for a given operating condition tend to be less effective for control design [44].

In the sequel, a validated recipe for control-oriented least-order modeling is provided giving preference to the most simple methods. Focus is placed on the generalized mean-field model which incorporates the other models as special cases. In addition, an experimental plant is assumed, which gives access to less data and thus makes model identification more difficult.

- **Modes**—The domain of the modes should be large enough to provide instantaneous phase information and small enough to ignore pure convection effects. The size of the recirculation region or one or two wavelengths is a good indicator. The first two modes $\mathbf{u}_{1,2}$ may be a pair of Fourier cosine and sine modes at the natural frequency ω^u of the unactuated flow. Similarly, the second pair $\mathbf{u}_{3,4}$ may be Fourier cosine and sine modes at the actuated frequency ω^a under periodic forcing. The dominant POD or DMD modes of unactuated and forced flow are good candidates [48]. Filtering techniques may be equally suited [269]. The shift modes $\mathbf{u}_{5,6}$ are more difficult as the unstable steady solution \mathbf{u}^s is generally not accessible from experiments. However, base-flow changes from modulations and unforced transients may provide \mathbf{u}_5 , for instance, via a POD of low-pass filtered flows [258]. Now, \mathbf{u}_s may be inferred from the fixed point of a calibrated Galerkin model with the averaged flow \mathbf{u}_0 and the expansion modes $\mathbf{u}_{1,2,5}$. The second shift mode \mathbf{u}_6 points from \mathbf{u}_s to the average actuated flow $\langle \mathbf{u}^a \rangle$. An orthonormalization completes the construction of the basis.
- **Coefficients of the dynamical system**—The 4D Var method is a powerful technique that is generally applicable for parameter identification [270]. One significant advantage is that no time-derivative information from flow snapshots is needed.

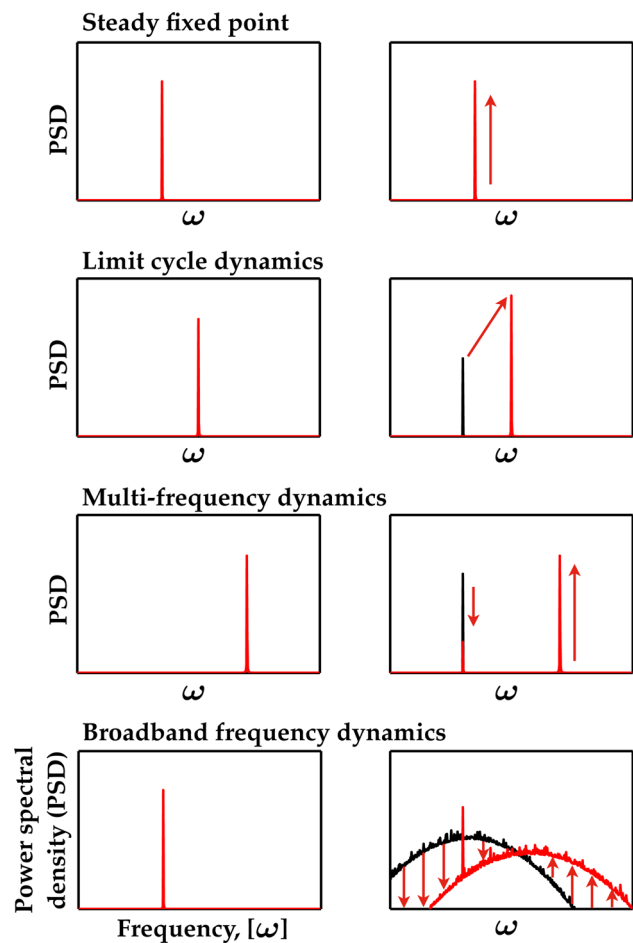


Fig. 19 Input/output characteristics of different dynamics. Left: actuation command; right: sensor signal without forcing (dark), and sensor signal under periodic forcing (light). From top to bottom: a stable fixed point with periodic excitation (linear dynamics); a stable limit cycle with locking periodic forcing (weakly nonlinear dynamics); a stable limit cycle with high-frequency forcing (moderately nonlinear dynamics); and broadband turbulence under periodic forcing (strongly nonlinear dynamics).

One actuation off-on-off transient (from unforced to forced state) can provide information about unforced and periodically forced solutions as well as growth-rates and frequencies. Generally, the parameter identification problem tends to be ill-posed, i.e., significantly different dynamical system coefficients can yield similar Galerkin solutions. Hence, a critical enabler is a regularization, i.e., a weak penalization of the difference from a reference dynamical system. This reference system may be obtained for a Navier-Stokes-based Galerkin projection (ignoring the third flow dimension for 2D PIV data) or from a simple propagator calibration technique.

- **Sensor-based estimation**—Good sensor placement can easily be inferred from the actuation mechanism. A destabilizing sensor-based control, for instance, requires knowledge of the phase of the forced structures and the amplitude of the natural shedding for gain scheduling. Developing more general techniques for sensor optimization is a recent area of active research. No generally applicable robust optimization strategy has emerged yet (see Sec. 8).
- **Control design**—A control law for the model can easily be designed following conventional wisdom of control theory. However, any control design should respect the narrow limitations of the model. For instance, the generalized mean-field

model can be stabilized in a tiny fraction of the shedding period. The shed vortices in the experiment, however, need a minimum time to leave the observation domain. In particular, the model is only applicable for slow transients with the design frequency content. For most shear flows, the resolvable frequencies are hard-coded by the wavelength of the vorticity in the expansion modes and the convection of the mean flow.

These recipes for model-based control design follow increasingly powerful data-driven methods. The danger of overfitting needs to be mitigated by a cross-validation with data not used for the parameter identification. The modeling may also be based on first principles, i.e., a Navier-Stokes-based Galerkin projection, subgrid turbulence closures, actuation modes, deformable expansion modes, and other auxiliary methods. This path provides additional physical insight at the price of larger effort and the necessity of a more extensive experience [271].

Reduced and least-order Galerkin models can provide a crisp analytical description of the actuation mechanism and thus guide the design of control laws. As such, they can serve as light houses for terra incognita. However, the construction of robust control-oriented models is more often an art rather than a fool-proof methodology. By construction, Galerkin models are elliptic, i.e., a local change of the flow is immediately communicated via the expansion modes in the whole domain. Moreover, Galerkin models can build up unbounded fluctuation energy. Shear flows, however, are hyperbolic, i.e., dominated by convection. Excited structures convect out the observation domain. Thus, the fluctuation level is naturally stabilized. Galerkin models lack this convective stabilization mechanism. This can be considered the root-cause of the narrow dynamic bandwidth of Galerkin models. Another related challenge is the change of flow structures under natural or actuated transients. In simple cases, such as structures with dominant frequencies, these changes may be tracked in deformable base-flow dependent modes [272,273]. In broadband turbulence, as in turbulent jets, there is no rationale for such cure. Physically, an evolving vortex configuration convects downstream and it constitutes a significant challenge to robustly embed a relevant ensemble of such vortex dynamics in a modal framework.

Some challenges of Galerkin models can be avoided by choosing a suitable sensor-based state space (see, e.g., Sec. 3). The structure of the linear, weakly nonlinear, and moderately nonlinear models has been derived purely from the linear-quadratic structure of the Navier-Stokes equation and from frequency filtering arguments. Hence, similar models may be constructed from the sensor history. These sensor-based models keep all relevant informations which are accessible in the control experiment and bypass Galerkin modeling problems with the observation domain, the unknown steady solution, base-flow dependent expansion modes, etc. ERA/OKID is a powerful realization of this path for linear dynamics (see Sec. 4.5.4).

6 Model-Free Control

Often, developing a detailed dynamical system model for a given set of high-dimensional nonlinear phenomena may not be the best use of time and resources. After an attractor has been identified and dynamics painstakingly determined, applying control strategies will usually shift the attractor significantly, rendering models inaccurate. The obvious exception is linear stabilization of a fixed point, whereby effective control makes the model *more* accurate. Alternatively, one may apply adaptive or model-free approaches to control a complex high-dimensional system.

There are a wide range of model-free control options, and we explore a number of methods that have been widely applied in turbulence control. First, open-loop forcing is perhaps the most pervasive model-free control strategy, based on its simplicity. Next, adaptive control may be used as a slow parameter tuning feedback

wrapped around a working open-loop control to modify controller behavior in response to changing environmental conditions. Extremum-seeking control (ESC) is among the most widely used adaptive controllers for flow control. Third, in-time control may be achieved by first specifying a given parameterized control structure, such as PID control, and then employing tuning methodologies to improve performance. Finally, machine-learning control constitutes a growing collection of data-driven techniques for structure identification and parameter identification of controllers.

Machine learning (ML) is a rapidly developing field of computer science whereby a complex system may be *learned* from observational data, rather than first-principles modeling [274–277]. There is a tremendous potential to incorporate data-driven modeling techniques, especially for the control of high-dimensional complex systems, such as turbulence. ML control, the use of machine-learning techniques to determine effective output–input maps (i.e., the controller), is a relatively new innovation [278]. The specific machine learning methods discussed here include adaptive neural networks, genetic algorithms (GA), and genetic programming (GP) control.

Figure 20 provides an organization of these model-free control methods. In each method, the structure of the control law must be determined and the parameters are identified to optimize the control law. Many of the methods (open-loop forcing, in-time control, and neural networks) specify the structure of the control law, while other methods (adaptive control, gradient search, and GA) identify optimal parameters once the structure has been identified. Thus, once a given structure has been assumed, there is a choice of parameter identification algorithm. Among the methods discussed here, GP control is the only method where both the structure and the parameters of the control law are identified. Other important considerations include whether or not the method adaptation or learning occurs predominantly online or offline, and whether the parameter optimization finds local extrema or has the possibility of exploring the global parameter space.

It is important to note that model-free control methodologies may be applied to numerical or experimental systems with little modification. All of these model-free methods have some sort of macroscopic objective function, typically based on sensor measurements (past and present). The objective may be drag reduction, mixing enhancement, or noise reduction, among others.

6.1 Open-Loop Forcing. Periodic forcing is widely used in turbulence control, largely because of its ease of implementation and the lack of the need for a model of the flow [25]. Periodic

forcing may be used to modify the dominant frequency of a flow, resulting in a lock-on with the forcing frequency. Alternatively, the forcing may modify the broadband frequency content, exploiting nonlinear frequency cross-talk.

In either case, open-loop forcing does not take advantage of sensor measurements, including reference or disturbance measurements for feedforward control and downstream sensors for feedback control. This limits the ability of open-loop forcing to reject disturbances, adapt to slow variations in flow parameters, or compensate for unmodeled dynamics. Most importantly, open-loop strategies are unable to stabilize unstable flows, regardless of the forcing strategy.

6.2 Adaptive Control

6.2.1 ESC Methodology. There are numerous adaptive control techniques, although ESC [279,280] has gained the most traction in fluid dynamics. ESC is attractive for complex systems because it does not rely on an underlying model and it has guaranteed convergence and stability under certain well-defined conditions [279,280]. ESC may be applied to track local maxima of an objective function, such as mixing enhancement or drag reduction, despite disturbances, and varying system parameters. Although adaptive control may generally be implemented in-time, it is overwhelmingly used in flow control as a slower feedback tuning the parameters of a working open-loop controller. There are a number of reasons for this, including sensor and actuator bandwidth, the fact that turbulent fluctuations may be viewed as a fast disturbance, and the fact that many objective functions, such as mixing, require integration over a slow time-scale. However, this slow feedback has many benefits, such as maintaining performance despite slow changes to environmental conditions.

ESC is an advanced method of perturb-and-observe, whereby a sinusoidal input perturbation is used to estimate the gradient of an objective function J to be maximized (or minimized). The objective function is typically based on sensor measurements, s , although it ultimately depends on the choice of input signal b , via the plant dynamics relating b to s . Often, for ESC, the variable b may be a parameter that describes the actuation signal, such as the frequency of periodic forcing.

A schematic of the extremum seeking control architecture is shown in Fig. 21 for a single scalar input b , although the methods readily generalize to vector-valued inputs \mathbf{b} . A schematic objective function $J(b)$, for static plant dynamics, is shown in Fig. 22.

In ESC, a sinusoidal perturbation is added to \hat{b} , the best approximation of the input that maximizes the objective function

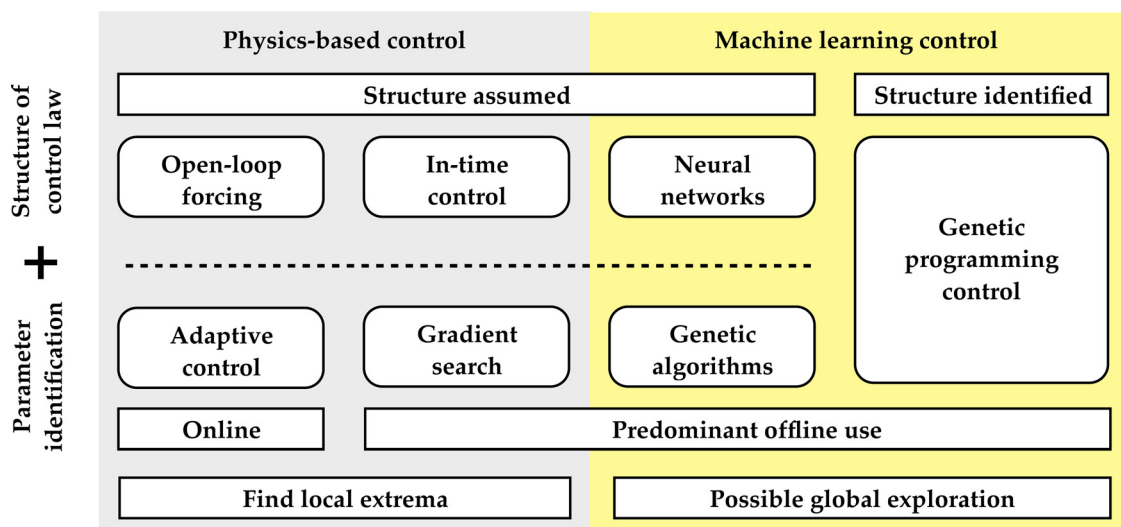


Fig. 20 Overview of model-free control methods discussed in Sec. 6. Model-free control involves the choice of control law structure as well as the optimization of controller parameters.

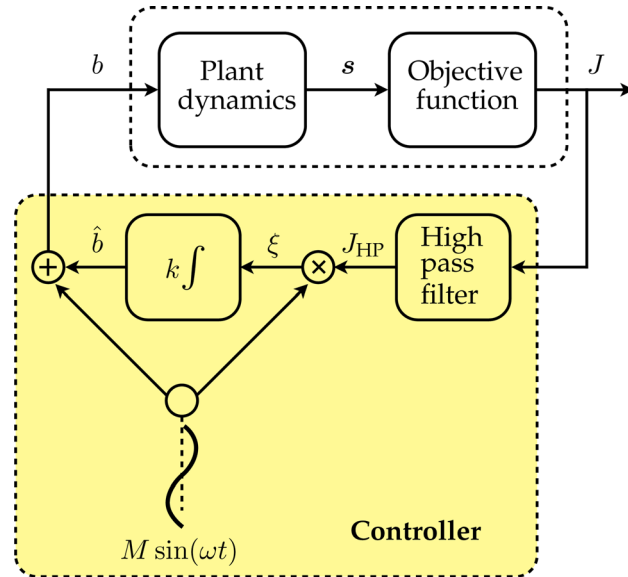


Fig. 21 Schematic illustrating the components of an ESC. A sinusoidal perturbation is added to the best guess of the input b , passing through the plant, and resulting in a sinusoidal output perturbation. The high-pass filter removes the DC gain and results in a zero-mean output perturbation, which is then multiplied (demodulated) by the same input perturbation. This demodulated signal is finally integrated into the best guess \hat{b} for the optimizing input b .

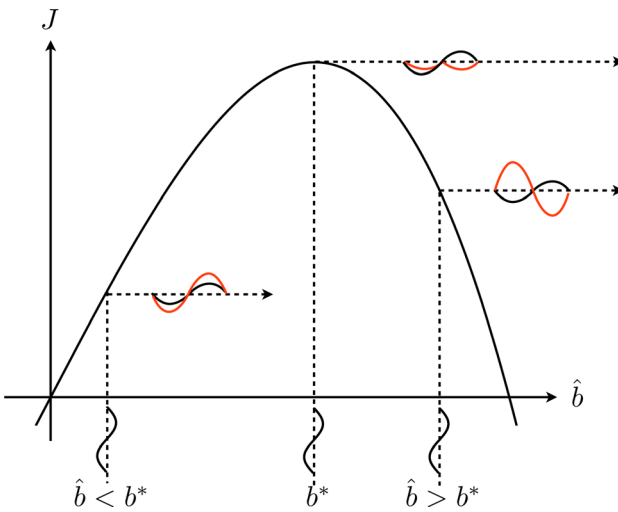


Fig. 22 Schematic illustrating ESC on for a static objective function $J(b)$. The output perturbation (light) is in phase when the input is left of the peak value (i.e., $b < b^*$) and out of phase when the input is to the right of the peak (i.e., $b > b^*$). Thus, integrating the product of input and output sinusoids moves b toward b^* .

$$b = \hat{b} + M \sin(\omega t) \quad (57)$$

This input perturbation passes through the system dynamics, resulting in an output signal J that varies sinusoidally about some mean value. To remove the mean, the output is high-pass filtered, resulting in J_{HP} . A simple high-pass filter is represented in the frequency domain as

$$\text{HP}(\zeta) = \frac{\zeta}{\zeta + \omega_{\text{HP}}} \quad (58)$$

where ζ is the Laplace variable, and ω_{HP} is the filter frequency, chosen to be slow compared with the perturbation frequency ω . It

is possible to multiply the high-pass filtered output signal by the input sinusoid, resulting in a *demodulated* signal ξ , which is mostly positive if the input b is to the left of the optimal value b^* and which is mostly negative if b is to the right of the optimal value b^*

$$\xi = M \sin(\omega t) J_{\text{HP}} \quad (59)$$

Finally, the demodulated signal ξ is integrated into \hat{b} , the best estimate of the optimizing value

$$\frac{d}{dt} \hat{b} = k \xi \quad (60)$$

so that the system estimate \hat{b} is steered toward the optimal input b^* . Here, k is the integral gain, which determines how aggressively the actuation responds to a nonoptimal input.

The demodulated signal ξ measures the gradient of the objective function, so that the algorithm converges more rapidly when the gradient is larger. To see this, first assume constant plant dynamics, so that $J(s)$ is simply a function of the input $J(b) = J(\hat{b} + M \sin(\omega t))$. Expanding $J(b)$ in the perturbation amplitude M , which is assumed to be small, yields

$$\begin{aligned} J(b) &= J(\hat{b} + M \sin(\omega t)) \\ &= J(\hat{b}) + \left. \frac{\partial J}{\partial b} \right|_{b=\hat{b}} \cdot M \sin(\omega t) + \mathcal{O}(M^2) \end{aligned}$$

The leading-order term in the high-pass filtered signal is $J_{\text{HP}} \approx \partial J / \partial b|_{b=\hat{b}} \cdot M \sin(\omega t)$. Averaging ξ over one period yields

$$\begin{aligned} \xi_{\text{avg}} &= \frac{\omega}{2\pi} \int_0^{2\pi/\omega} M \sin(\omega t) J_{\text{HP}} dt \\ &= \frac{\omega}{2\pi} \int_0^{2\pi/\omega} \left. \frac{\partial J}{\partial b} \right|_{b=\hat{b}} M^2 \sin^2(\omega t) dt \\ &= \frac{M^2}{2} \left. \frac{\partial J}{\partial b} \right|_{b=\hat{b}} \end{aligned}$$

Thus, for the case of trivial plant dynamics, the average signal ξ_{avg} is proportional to the gradient of the objective function J with respect to the input b .

In general, J may be time-varying and the plant relating b to s may have nonlinear dynamics that operate on a faster timescale than the perturbation ω , complicating the simplistic averaging analysis above. This general case of ESC applied to a nonlinear dynamical system was analyzed by Krstić and Wang [279], where they developed powerful stability guarantees based on a separation of timescales and a singular perturbation analysis. It is also possible to modify the basic algorithm outlined above by adding a phase ϕ to the sinusoidal input perturbation in Eq. (59). In Ref. [279], there was an additional low pass filter $\omega_{LP}/(\zeta + \omega_{LP})$ placed before the integrator to extract the DC component of the demodulated signal ξ . Finally, there is an extension to extremum-seeking called slope-seeking, where instead of a zero slope, a specific slope is sought [280]. Slope-seeking is preferred when there is not an extremum, as in the case when control inputs saturate. Often extremum-seeking is used for frequency selection and slope-seeking is used for amplitude selection.

6.2.2 Examples of Adaptive Control in Turbulence. Extremum-seeking has been widely applied in turbulence control, largely because of its ease of use and equation-free implementation. ESC was used in Refs. [281,282] to reduce the drag over a bluff-body in an experiment at moderate Reynolds number ($Re = 20,000$). The objective function weighted drag reduction against energy expended by the actuation, a rotating cylinder on the upper trailing edge of the backward facing step, to obtain efficient drag reduction.

In Ref. [283], ESC was used for separation control on a high-lift configuration. The experiment consisted of spanwise pressure

sensors and pulsed jets on the leading edge of the single-slotted flap for actuators. This work demonstrated enhanced lift over open-loop forcing, both at large angles of attack where the flow was separated and at moderate angles of attack where flow remained attached. They use the slope-seeking extension of ESC. This work also developed both SISO and MIMO controllers.

ESC has also been used to control thermoacoustic modes across a range of frequencies in an industrial scale, 4 MW gas turbine combustor [284,285]. It has also been utilized for separation control in a planar diffusor that is fully turbulent and stalled [286], and to control jet noise [287].

The ESC relies on a separation of timescales where the system dynamics are the fastest, the periodic perturbation is moderate, and the high-pass filter cut-off is slow. Changes to the plant dynamics, either varying parameters or disturbances, are assumed to the slowest timescale. It is possible to improve the performance of ESC in some instances by adding additional filters and phase delays. For example, extended Kalman filters were used as the filters in Ref. [288] to control thermoacoustic instabilities in a combustor experiment. The dramatic performance improvement of the modified ESC algorithm from Ref. [288] is reproduced in Fig. 23. Kalman filters were also used in Ref. [289] to reduce the flow separation and increase the pressure ratio in a high-pressure axial fan using an injected pulsed air stream. The use of a Kalman filter improved the controller speed by a factor of 10 over traditional ESC. The implication is that the controller may compensate for disturbances and changes in environmental conditions that are ten times faster than before.

The external perturbation used in ESC may be infeasible for some applications, such as optimizing aircraft control surfaces for efficient flight. In Ref. [290], atmospheric turbulent fluctuations were used as the perturbation for optimization of aircraft control based on ESC. The strategy of using natural system perturbations for ESC is promising. ESC has also been used for parameter tuning in PID controllers [291] as well as to tune PI controllers to stabilize a model of nonlinear acoustic oscillation in a combustion chamber [292].

6.3 In-Time Control

6.3.1 Control Law Parameterizations and Tuning Methodologies. Often, the structure of a control law may be decided by an expert in the loop with engineering intuition based on previous

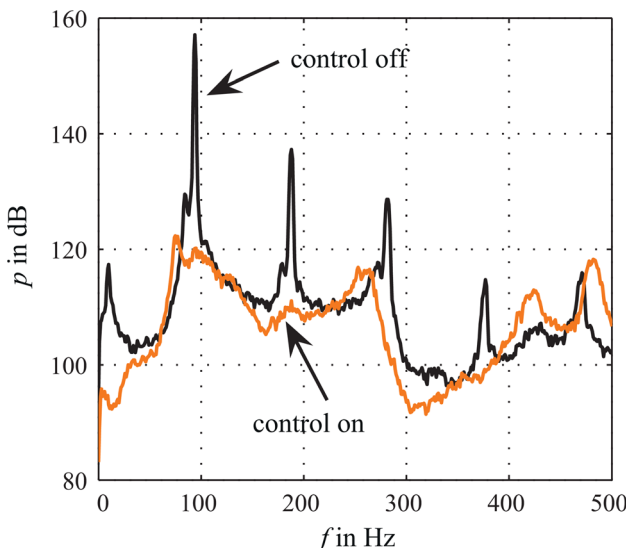


Fig. 23 Acoustic pressure reduction in combustor experiment with modified ESC algorithm. The main peak is reduced by about a factor of 60 when control is applied (Reproduced with permission from Gelbert et al. [288]. Copyright 2012 by Elsevier).

experience. The control structure is often chosen for a combination of flexibility and simplicity, as in the ubiquitous PID control

$$b(t) = k_P s(t) + k_I \int_{t_0}^t s(\tau) d\tau + k_D \frac{d}{dt} s(t)$$

The PID control above is *parameterized* by three constants, k_P , k_I , and k_D , the proportional, integral, and derivative gains. When the controller is parameterized, as in PID control, it is possible to tune the controller to improve performance and meet specifications (rise-time, bandwidth, overshoot, etc.) by identifying locally or globally optimal parameters. Without an underlying system model, there is tremendous freedom in choosing these parameters. This parameter tuning may be based on intuition, trial-and-error, or on a physical mechanism, as in the case of opposition control in Sec. 6.3.2.

6.3.2 Case Study: Opposition Control in Wall Turbulence. In 1994, Choi et al. introduced a method of active feedback control to reduce the drag in a fully developed turbulent boundary layer flow [43]. In DNS, a 20–30% reduction in drag was achieved by imposing a surface boundary condition (blowing/suction) to oppose the effect of vortices in the near wall region. This *opposition control* was an early model-free control approach based on intuition about flow physics and drag mechanisms, rather than a mathematical model. References [10,27,40,208,293] provide reviews of opposition control. One of the earliest experimental demonstrations of active feedback suppression was Liepmann and Nosenchuck [18], where they canceled T-S waves using a downstream heating element and a phase-shifted measurement feedback. This may be seen as a predecessor of the popular opposition control, and the experiments were quite successful, resulting in a significant increase in the transitional Reynolds number for a flat plate experiment.

There are many extensions to opposition control. The best performance of skin-friction reduction [43] was achieved when sensors were located at $y^+ = 10$, which is not nearly as practical as measurements at the wall. This led to the development of a neural network architecture to optimize the mapping from surface measurements to opposition control [22], as shown in Fig. 24. A drag reduction of about 20% was achieved in a low Reynolds number turbulent channel flow. Some studies suggest that opposition control does not scale favorably with increasing Reynolds number [294], although there are studies suggesting significant potential drag reduction, even at high Reynolds numbers, assuming perfect damping of near-wall fluctuations [295]. The method of opposition control is also strongly dependent on the amplitude and phase of the actuation response [296].

Opposition control has also been generalized to utilize piston actuation [297] and has been used to reduce drag in a DNS of turbulent channel flow using wall deformation [298]. Drag reduction has also been achieved in DNS of pipe flow using opposition control [299,300] and suboptimal control [301]. Opposition control has also been investigated in the context of stochastically forced non-normal dynamical systems [302].

Recently, opposition control has been explained in the context of resolvent analysis, whereby the Fourier transformed Navier–Stokes equations are viewed as an input–output system [303]. In this approach, the convective terms are viewed as the input and the turbulent flow field is the output, and a SVD of the resolvent operator indicates the forcing that results in the largest gain in the response.

6.4 Neural Network Based Control. Many model-based open-loop controllers in fluid dynamics are based on the inversion of a model, as discussed in Sec. 4.2. When an input–output function is not well-approximated in a simple linear or quadratic framework, it is often necessary to employ more sophisticated methods, such as artificial neural networks (ANNs). ANNs are a

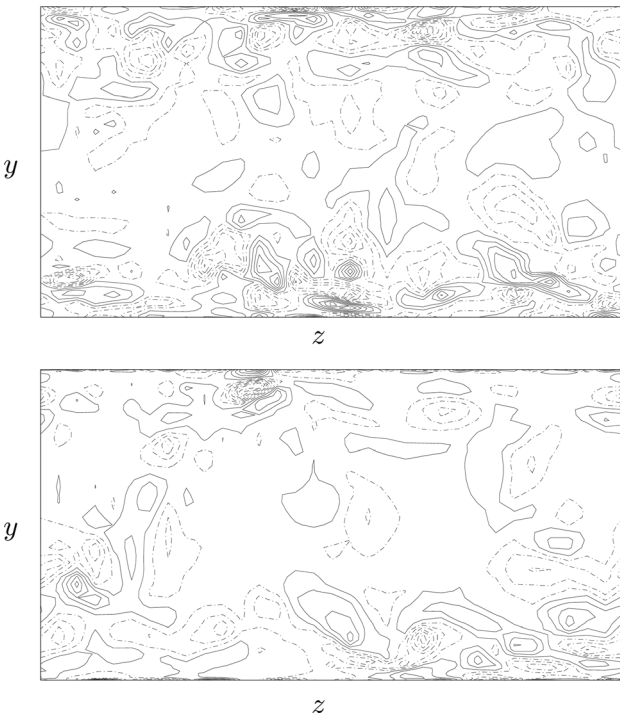


Fig. 24 Illustration of the benefits of opposition control (bottom) in contrast to the unforced system (top). Contours of streamwise vorticity are plotted in a cross-flow plane. Negative contours are indicated with dashed lines (Reproduced with permission from Lee et al. [22]. Copyright 1997 by AIP Publishing LLC).

construct in machine learning that attempts to mimic the computational flexibility observed in the brains of animals. In particular, a number of individual computational components, or *neurons*, may be connected in a graph structure with inputs and outputs. By exposing this network to example stimulus, it is possible to train the network to perform complex tasks, though either supervised or unsupervised reinforcement learning. There is a tendency to use a gradient search to determine network weights, although there are many variations in the literature [304,305].

In turbulence, there are examples where neural networks have been used for both modeling and control [249,306,307]. As mentioned earlier, neural networks have also been used to optimize opposition control [22]. Interestingly, the POD, also known as PCA, may be trained in a neural network [308]. The neural network framing of PCA also allows for powerful nonlinear generalizations [309,310]. Recent work has demonstrated the application of network-theoretic tools more generally to fluid modeling [311], resulting in a graph theoretic model of the vortex dynamics in a flow.

In general, neural networks are adaptable and may approximate any input–output function to arbitrary precision with enough layers and enough training. However, they are often susceptible to local minima and may result in overfit models when trained on too much data. In recent years, SVMs [158–160] have begun to replace neural networks for a number of reasons. First, SVMs result in global solutions that have simple geometric interpretation. SVMs also scale favorably for systems with very large input spaces. However, multilayer neural networks have seen a recent resurgence in activity with the associated field of deep learning [312–314]. The fact that these algorithms have been developed to scale to extremely large data sets (i.e., by Google, etc.) is promising for the mining of high-Reynolds number turbulence data.

6.5 GA-Based Control. An important class of machine learning algorithms is based on evolutionary algorithms that mimic the

process of optimization by natural selection, whereby a population of individuals compete in a given task and rules exist to propagate successful strategies to future generations. Evolutionary algorithms are typically employed to find near globally optimal solutions when there are multiple extrema and gradient searches would not work. They may also provide an alternative to the extremely expensive Monte Carlo search algorithm, which does not scale well with high-dimensional parameter spaces. In this section, evolutionary algorithms are employed for parameter identification of controllers in the GA [315–317]. In Sec. 6.6, evolutionary algorithms are employed for both parameter and structure identification of controllers in GP [318,319]. The implementation of evolutionary algorithms for engineering control is relatively recent [278].

In both GAs and GP, an initial generation of candidate parameters or controllers, called individuals, is randomly populated and the performance of each individual is quantified by some cost function for that particular simulation or experiment. The cost function balances various design goals and constraints, and it should be minimized by an effective individual. In the case of GAs, the individuals correspond to parameter values to be identified in a parameterized model, as shown in Fig. 25. In GP, the individual corresponds to both the structure of the control law and the specific parameters, as shown in Fig. 26 (see Sec. 6.6).

After an initial generation is populated with individuals, the performance of each individual is assessed based on their performance on the relevant cost function. Individuals resulting in a lower cost function have a higher probability of being selected for

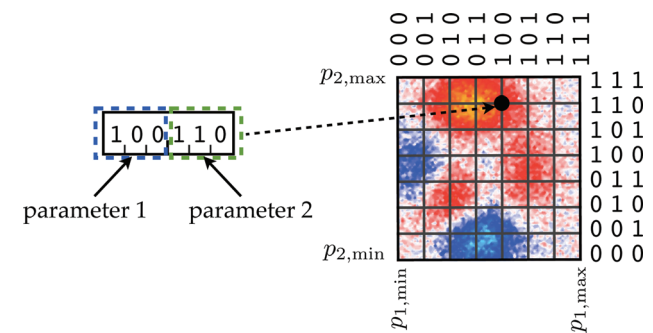


Fig. 25 Illustration of a possible binary representation of parameters used in GAs. This example has two parameters, each represented with a 3-bit binary number.

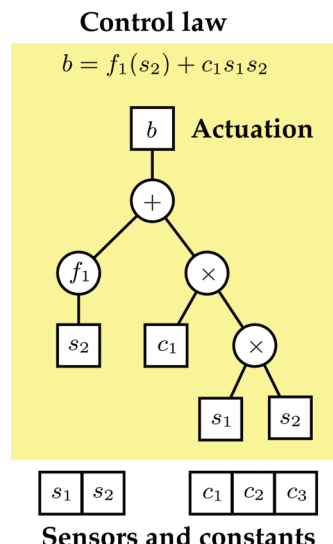


Fig. 26 Illustration of function tree representation used in GP

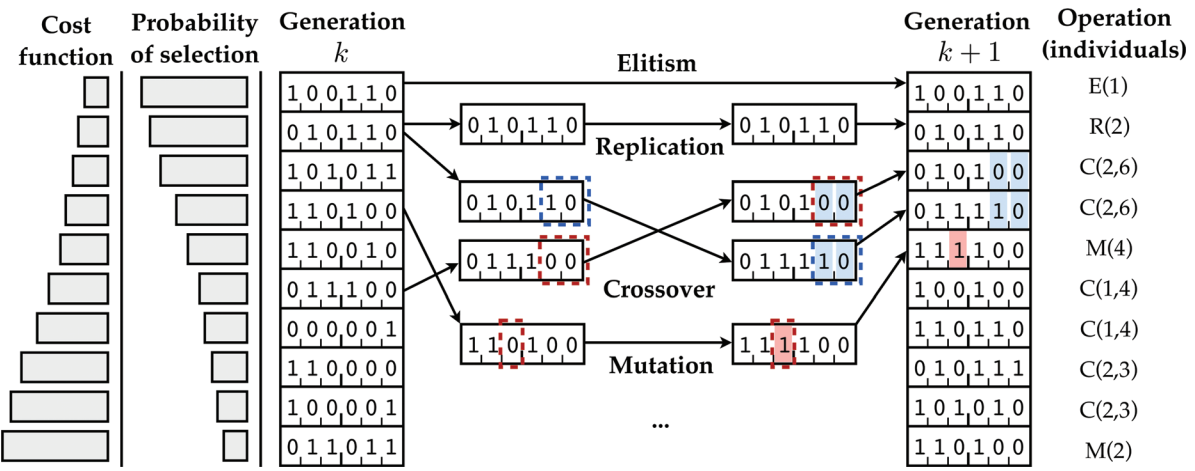


Fig. 27 Genetic operations are used to advance generations of individuals in GAs. Operations are elitism (E), replication (R), crossover (C), and mutation (M). For each individual of generation $k+1$, after the elitism step, a genetic operation is chosen randomly according to a predetermined probability distribution. The individuals participating in this operation are selected from generation k with probability related to their fitness (e.g., inversely proportional to the cost function).

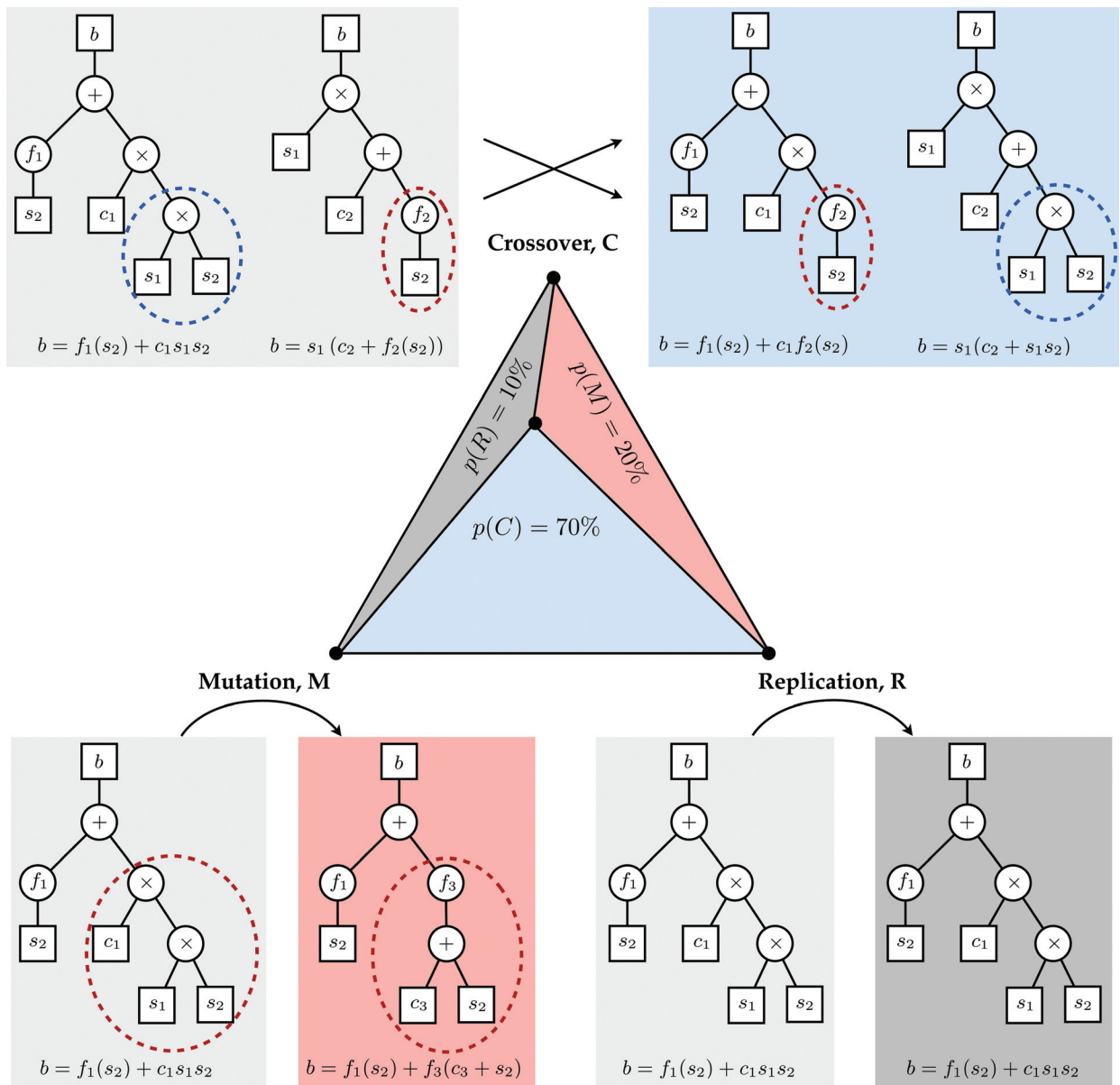


Fig. 28 Genetic operations are used to advance generations of functions in GP

the next generation. Successful individuals advance to the next generation according to a handful of rules or genetic operations:

- Elitism (optional)—a given number of top-performing individuals are copied directly to the next generation. Elitism guarantees that the best individuals of the next generation will not perform worse in a noise-free environment.
- Replication—a statistically selected individual is copied directly to the next generation. Replication, also called (asexual) reproduction in GP, has a positive memory function.
- Crossover—two statistically selected individuals exchange randomly selected values or structures and then advance to the next generation. Crossover has an exploitation purpose and tends to breed better individuals.
- Mutation—some portion of a statistically selected individual is modified with new values or structures. Mutation has an explorative function as it can discover better minima of the cost function.

The top-performing individuals from each generation are advanced to the next generation using these four genetic operations, and a handful of new random individuals are added for variety. This is illustrated conceptually for the GA in Fig. 27. These generations are evolved until the algorithm converges or performance is within a desired range.

There are no guarantees that the evolutionary algorithms will converge, although they have been successful in a wide range of applications and may converge to a nearly globally optimal solution. There are a number of choices that can improve the performance and convergence time of these algorithms. For example, the number of individuals in a generation, the number of generations, the rate of each genetic operation, and the schedule for advancing top-performers all determine the quality of solution and speed of convergence.

GAs generally involve a large-scale parameter identification in a possibly high-dimensional space. Thus, these methods are typically applied to tune control laws with predetermined structure. Early efforts in using machine learning for flow control involved the application of GAs for parameter optimization in open-loop control [306]. Applications included jet mixing [320], optimization of noisy combustion processes [321], wake control and drag reduction [322,323], and drag reduction of linked bodies [324]. These early GAs optimized cost functions by specifying input forcing parameters without taking into account sensor feedback. However, the method was also applied to tune the parameters of H_∞ controllers in a combustion experiment [325].

6.6 GP Control. GP [318,319] achieves both structure and parameter identification of input–output maps using evolutionary algorithms. In genetic programming control (GPC), GP is used to iteratively learn and refine a nonlinear mapping from the sensors to the actuators to achieve some control objective. The resulting control law is determined by sequential mathematical operations on combinations of sensors and constants, which may be represented in a recursive tree structure where each branch is a signal and the merging points denote a mathematical operation, as illustrated in Fig. 26. The sensors and constants are the “leaves,” and each subsequent merging of branches results in a more finely tuned mapping. The “root,” where all branches eventually merge, is the signal that is fed into the actuation.

The same evolutionary operations of elitism, replication, crossover, and mutation, described in Sec. 6.5, are used to advance individuals across generations in GP. These operations are shown in Fig. 28 for GP function trees. The probability of each operation is chosen to balance exploration with exploitation.

Recently, GPC has been applied on a set of benchmark turbulence control experiments that exhibit various levels of complexity [263,265,326–329]. The interaction of the GPC paradigm with a dynamical system is illustrated in Fig. 29. It is important to reiterate that the methods are based on GP so that both control structure and parameters are identified, as opposed to GAs, which are useful for parameter optimization only. These examples demonstrate the ability of machine-learning control using GP to produce desired macroscopic behavior (e.g., drag reduction, mixing enhancement, etc.) for a variety of flow configurations. These flow configurations include a generalized mean-field model [329], the mixing layer with pulsed actuation jets on the splitter plate [263,265,327,329], the backward facing step controlled by a slotted jet [265,328], and a turbulent separated boundary layer [265].

The first experimental demonstration of machine-learning control employing GP was performed in a mixing-layer with a velocity ratio of approximately 1:3—both for laminar and turbulent boundary layers [263]. The flow was actuated with 96 equidistantly spaced streamwise facing jets and sensed with a rake of 24 equidistantly spaced hot-wire sensors downstream. Machine learning control (MLC) yields a control law which increases the mixing-layer width by 67%. Thus, MLC performs 20% better as compared to the best periodic forcing while simultaneously reducing the volume flux by over 46% (see Fig. 30) [265]. In addition, the MLC performance has been shown to be robust against large changes of oncoming velocities implying a transition from laminar to turbulent boundary layers. Also other experimental studies

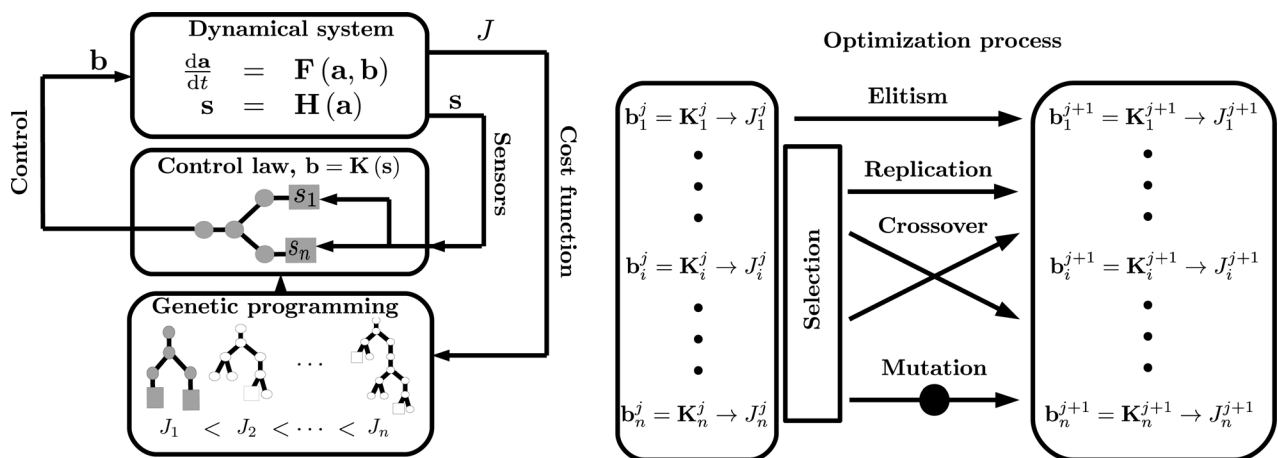


Fig. 29 Schematic of closed-loop feedback control using GP for optimization. Various controllers in a population compete to minimize a cost function J , and the best performing individual controllers may advance to the next generation according to the optimization procedure on the right (Reproduced with permission from Fig. 4 of Duriez et al. [265]. Copyright 2014 by T. Duriez, V. Parezanovic, J.-C. Laurentie, C. Fourment, J. Delville, J.P. Bonnet, L. Cordier, B.R. Noack, M. Segond, M. Abel, N. Gautier, J.L. Aider, C. Raibaudo, C. Cuvier, M. Stanislas, S.L. Brunton).

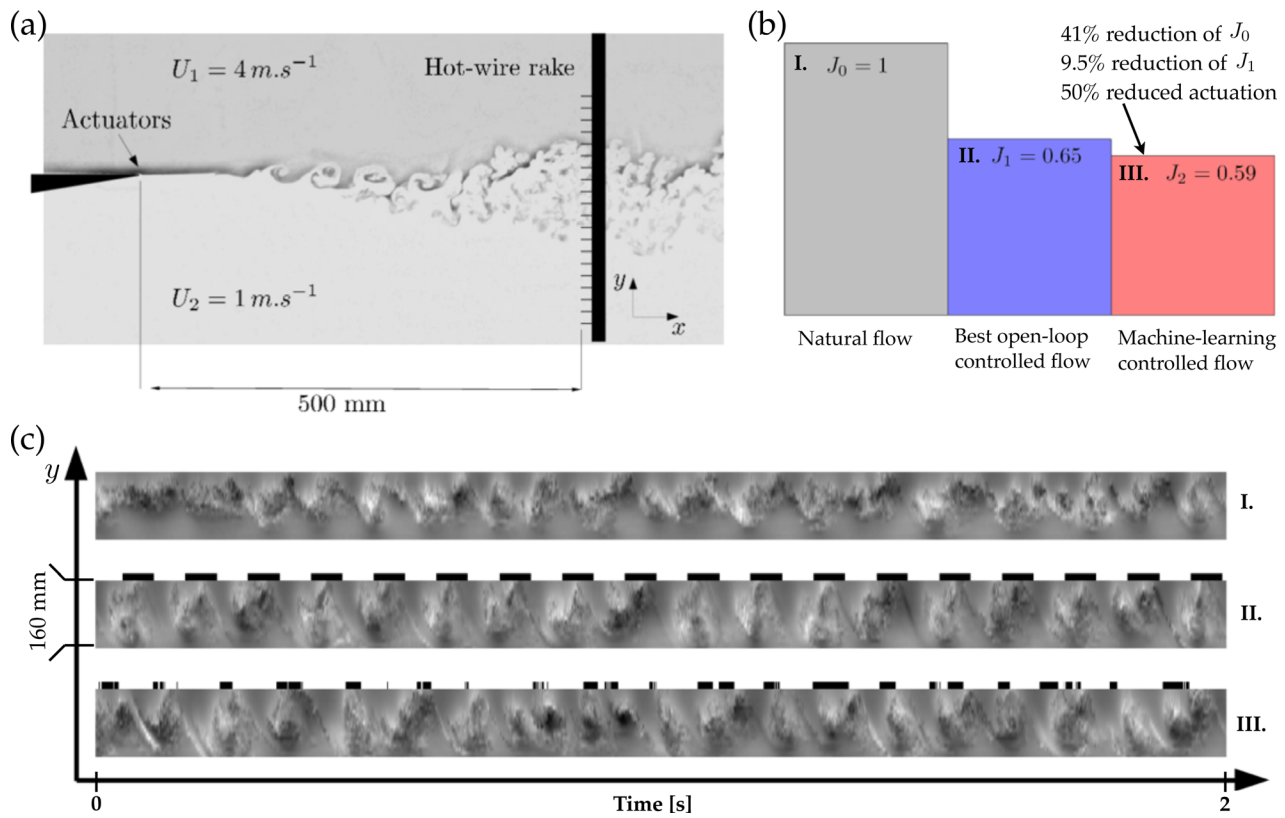


Fig. 30 “Pseudovisualizations of the TUCOROM experimental mixing layer demonstrator for three cases: (I) unforced baseline (width $W=100\%$), (II) the best open-loop benchmark (width $W=155\%$), and (III) MLC closed-loop control (width $W=167\%$). The velocity fluctuations recorded by 24 hot-wires probes are shown as contour-plot over the time t (abscissa) and the sensor position y (ordinate). The black stripes above the controlled cases indicate when the actuator is active (taking into account the convective time). The average actuation frequency achieved by the MLC control is comparable to the open-loop benchmark.” The relative mixing cost function of the natural flow, open-loop forcing, and machine-learning control is shown in (b), and the mixing layer is shown in (a) (Reproduced with permission from Parezanovic et al. [263]. Copyright 2015 by Springer). A lower cost function J indicates improved mixing (Reproduced with permission from Duriez et al. [265]. Copyright 2014 by T. Duriez, V. Parezanovic, J.-C. Laurentie, C. Fourment, J. Delville, J.P. Bonnet, L. Cordier, B.R. Noack, M. Segond, M. Abel, N. Gautier, J.L. Aider, C. Raibaudo, C. Cuvier, M. Stanislask, S.L. Brunton).

with laminar and turbulent wall-bounded shear flows have shown that MLC can significantly outperform the best open-loop control and increase robustness against varying operating conditions [265,328,330].

The performance of GP for turbulence control is striking, providing robust performance in extremely nonlinear regimes that are not amenable to traditional model-based or model-free control design. Yet, there are a number of unexplored extensions of GP for the control of complex dynamical systems. First, in addition to sensor measurements and constants, a modified GP algorithm could create nonlinear mappings on time-delayed sensor measurements or measurements that have been passed through LTI filters. Second, the inputs of a control law may consist of suitable time-periodic functions. Thus, open-loop actuation may be optimized. Third, the control law arguments may comprise sensors and periodic functions so that GPC can choose between open- and closed-loop control or combine them. Finally, it will also be interesting to augment the machine-learning control to include reference tracking and disturbance rejection, among other classical control methods.

7 Conclusions

Understanding turbulence has been a central engineering challenge of the past century, with the clear goal of passively manipulating and eventually actively controlling turbulence. Many advances in improved turbulence models have resulted in devices that enable passive manipulation. The focus has rapidly shifted from passive control of turbulence to actively controlling it, and

this will surely be a central focus of engineering efforts during the present century. Put simply, our ability to control and manipulate turbulence will be a deciding factor in our ability to advance key technologies, addressing challenges in energy, security, transportation, medicine, and many other endeavors.

Our goal throughout this review has been to explore the possibilities associated with turbulence control in various contexts and for different problems. We have emphasized aspects of model complexity and resolution as well as control logic and design objectives. In this section, we summarize this review from three perspectives: historical, practical, and industrial. In Sec. 8, we point toward exciting future directions that we believe will be particularly impactful for closed-loop turbulence control.

As discussed throughout this review, there is not one single method of turbulence control, just as there is not a single type of turbulence. Fortunately, as difficult as it has been to develop improved models of turbulence, control strategies may be quite robust to model imperfections and uncertainties. It was pointed out in Ref. [20] that models suitable for control may not be suitable for accurate prediction. Hopefully, controlling turbulence will prove to be a more manageable task than understanding it.

7.1 Historical Perspective. Progress and challenges in turbulence control may be understood more clearly in a historical context. The story of turbulence control is one of the oldest and richest chapters in humans’ engineering history, marking great technological and theoretical strides along with ongoing struggles.

An in-depth treatment of this fascinating history is beyond the scope of this review; there are other excellent sources [331,332].

The first chapter of quantitative research in flow control can be considered to be shape optimization. While Lilienthal optimized the wings of his gliders purely based on careful experiments in the 1880s, airfoil design has profited immensely from potential flow theory around 1900. Joukowski formulated his famous lift theorem for two-dimensional airfoils in 1906 after visiting Lilienthal and observing his experiments. Prandtl generalized the lift theory for finite wings with his famous lifting line theory in 1923. Further progress in quantitative shape optimization using potential theory is associated with the names of Betz, von Kármán, and Theodorsen, to name a few. More recently, these achievements have been generalized for use in adjoint-based shape optimization using the full Navier-Stokes equations.

The discovery of boundary-layer theory by Prandtl in 1904 has stimulated active control, as suction and blowing were rapidly realized to change important boundary-layer properties. The first experimental demonstrations included stabilization of boundary layers with steady suction. These efforts have enjoyed a thorough mathematical treatment entering Schlichting's famous book on boundary-layer theory [333]. In the past century, many other forms of actuators have been invented with continually increasing authority and dynamic bandwidth [36]. Destabilizing control using unsteady periodic forcing was considered later for mixing enhancements of shear flows [334].

In the 1940s, the foundations of modern turbulence theory were laid by Kolmogorov, Landau, Millionshtchikov, Monin, von Neumann, Obukhov, and Yaglom, to name only a few (see, e.g., Refs. [335,336]). Neither the energy cascade nor the mathematical closure approaches have entered main-stream flow control methodologies until now. Yet, the need for closures in nonlinear control design is increasingly realized as an important grand challenge problem.

Around 1950, passive actuators were explored and optimized. The vortex generator [337] for separation mitigation is one prominent example. These developments are continued—hydrophobe surfaces for ships, riblets for airplanes, and spoilers on cars serving as prominent examples.

In the 1980s, chaos theory has stimulated fluid mechanics toward the search for universal transition scenarios, for low-dimensional strange attractors [338], and for chaos control [339,340]. The success of quantitative nonlinear dynamics methods for turbulent flows has been limited. Yet, nonlinear dynamics has entered fluid dynamics thinking with the qualitative notions of strange attractors, domains of attraction, edge states, and bifurcations, just to name a few.

In the same period, the first closed-loop control experiments were performed for the suppression of boundary layer instabilities [18], for wake stabilization [19], for skin friction reduction of turbulent boundary layers [43], etc. The first control designs were based on heuristic considerations, like superposition of traveling waves and opposition control. Rapidly, control theory has entered fluid mechanics [27,212] and is providing a solid foundation for model identification and control design. Even the nomenclature, like “plant” for actuated flow and “order” for the model dimension, is largely borrowed from control theory.

In the late 1980s, the foundation of many current reduced-order models for flow control has been laid by the pioneering POD model of wall turbulence [341], the snapshot method for POD [86,188,187], and other early work on coherent structures [342–344]. This development of control-oriented reduced-order models is attracting increasingly many researchers with numerical and experimental control demonstrations. At the same time, the challenges of POD models are becoming more obvious. A minimum requirement and challenge for model-based control design is that the model describes unactuated and actuated states as well as the transients between both. A more comprehensive presentation is provided in Ref. [271].

Starting around 2000, the technological development of MEMS with actuators and sensors of increasing performance [69] has

stimulated the development of more complex hierarchical control laws, based on globally coupled local sensing and control units. This area is undergoing rapid development. The complexity of turbulent dynamics has been partially addressed by a novel form of model-free control design. The control laws have been cast in the form of ANNs with the pioneering computational demonstrations in wall turbulence [22]. Currently, many other machine-learning methods are entering fluid mechanics for an increasing number of analysis, modeling, and control tasks.

There are two common and recurring themes in this historical perspective on turbulence control. First, advances in theory drive progress in control design. These theoretical advances may involve first-principles understanding of instabilities and turbulence itself. Additionally, theoretical advances in external fields, such as linear systems, control theory, and dynamical systems, have all had a transformative impact on the direction and progress of flow control efforts.

The next general rule is that whatever is possible on the existing hardware will be fully exploited by the software. Physical demonstrations of flow control have been necessarily tied to advances in sensor and actuator hardware and to growth in computational capabilities. With recent developments in micromanufacturing techniques, including MEMS, many industrial applications of closed-loop flow control are becoming increasingly feasible.

7.2 Current Practices.

Here, we attempt to summarize some of the current “best practices” gathered from success stories in the literature (Fig. 31). Because of the mercurial nature of the field, this discussion may be viewed as a work in progress. The specific control strategy will vary depending on whether the goal is to minimize or maximize a cost function, track a reference value of some quantity, or stabilize an unstable steady state and reject disturbances.

It is reasonable to start by assessing whether or not superposition holds. If so, then it is possible to develop balanced linear input-output models, either gray-box or black-box, and then design optimal linear feedback controllers. These controllers may be optimal in the sense of minimizing the control expenditure, attenuating sensor noise, and rejecting disturbances while minimizing the error of the state to some reference value. Alternatively, if model uncertainty is large and stability margins are critical; then, it is possible to optimize the controller for robust performance. Linear control has been especially successful in delaying the transition to turbulence, which involves stabilizing an unstable steady state.

If superposition does not hold, then the flow may be dominated by oscillatory components. If there are a few dominant frequencies in the flow, then it is possible to develop a mean-field model and resulting nonlinear control law. This strategy has been proven effective in suppressing shedding behind bluff bodies.

If there are not strong, isolated oscillatory components, but rather there is broadband frequency cross-talk, then open-loop control may be able to modify the spectrum toward desirable specifications. It may be necessary to explore the input parameter space to identify the most effective combination of inputs for open-loop actuation. Once these input directions are identified, an adaptive control algorithm, such as extremum-seeking, may be applied to find a locally optimal open-loop forcing. Effective open-loop strategies may then be emulated in closed-loop with added robustness.

A very general approach, including open- and closed-loop control, is enabled by machine-learning methods. Machine-learning control can be configured to yield either open-loop or closed-loop control, depending on the choice of inputs. Although the resulting controllers may approach globally minimizing values of the cost function, there is no guaranteed convergence, and depending on the dimension of the input space, convergence may be slow. More work is needed to extend MLC to include two-degrees-of-freedom reference tracking control to suppress disturbances via feedback.

The progress in turbulence control, both passive and active, has been significant, as evidenced by the ability to relaminarize flows and reduce drag, to control separation, and to modulate mixing. However, each of these three canonical flow control problems presents unique challenges to large-scale industrial implementation, which in turn motivate new opportunities for research. Note that the association of the following three flows with corresponding control methodologies is not inclusive, but instead covers a large portion of the cases in the literature.

7.2.1 Linear Control and Transition. Linear feedback flow control benefits from the most well-developed theoretical foundations and a set of clear goals. For instance, it is often used to stabilize unstable laminar steady states and delay the transition to turbulence, reducing drag. These techniques amount to a systematic approach to identify and suppress unstable structures and disturbances in the flow utilizing sensors and actuators. Many feedforward techniques in the optimal linear control of turbulent boundary layers closely resemble opposition control, except that future model predictions of disturbances are used to cancel flow structures after they have been deformed and convected with the flow. Feedback control offers better robustness to unmodeled dynamics and disturbances, although it is sensitive to time-delays which are inevitable in convective flows, as it takes time for the effect of actuation to reach downstream sensors. The limitations imposed by time delays motivate the need for a denser array of sensors and actuators for more complex convective flows, which in turn motivate bio-inspired sensing and actuation along with local computations.

7.2.2 Nonlinear Control and Separation. Nonlinear control presents a significant opportunity to manipulate flows that are not close enough to a fixed point for linear flow control. For example, massively separated flows are in a fully nonlinear regime, and manipulation of coherent structures requires an understanding of their nonlinear coupling. In contrast to linear control, which involved suppressing structures, nonlinear control involves redirecting some flow structures, possibly to suppress others. The biggest issue for nonlinear flow regimes is the lack of theoretical understanding of nonlinear turbulence models and closures. Moreover, many tools from control theory are developed for linear systems and do not generalize to nonlinear problems. The need for improved nonlinear reduced-order models and turbulence closures will be an important area of turbulence research, facilitating advances in turbulence control.

7.2.3 Model-Free Control and Mixing. Effective linear control will suppress disturbances and bring the flow state closer to the fixed point where a model was developed. However, applying control to a nonlinear flow that is on an unsteady attractor, rather than a fixed point, may significantly distort the attractor, rendering models invalid. It may be prohibitively difficult to develop models that are sufficiently general to predict control responses. Instead of developing detailed models that will then be rendered invalid by control, model-free approaches are promising when it is desirable to change the nature of an attractor, for example, to increase mixing. The most challenging nonlinear problems are excellent candidates for advanced model-free techniques. Data-driven methods, including compressive sensing, machine learning, and uncertainty quantification (UQ), may be increasingly effective in the development of control strategies for highly complex, fully turbulent problems.

7.3 Industrial Applications. There are many industrial research programs centered around turbulence control, but it is not always clear how control results will scale to high Reynolds number flows. For instance, how does the actuation velocity, energy input, etc., scale with the Reynolds number of the problem? In cases where we do understand the scaling, such as the spatial and temporal scales of flow perturbations for disturbance rejection through linear feedback control, the scaling is not favorable.

Results suggest that at industrial Reynolds numbers, a finer mesh of sensors and actuators with improved bandwidth and more powerful computational capabilities will be required for similar transition delay and drag reduction.

As a consequence of the large Reynolds numbers, industrial flows are often exceedingly complex, with broadband frequency cross-talk and many orders of magnitude scale separation in space and time. It is entirely possible that data-driven techniques, such as machine-learning control methodologies, will enable turbulence control in these situations before we are fully able to understand the mechanisms. However complex the flow, the multitude of industrial and defense applications will continue to drive research developments in turbulence control for decades to come.

8 Future Developments Beyond Control Theory

In the past, control theory has shaped flow control and significantly influenced the path from open-loop to closed-loop control. Flow control and control theory were both mature disciplines with little synergy before the 1990s. After techniques from mathematical control theory were embedded in flow control, dramatic progress has been made. The luminary words of N. Wiener are apt in this situation: “*The most fruitful areas for the growth of the sciences were those which had been neglected as a no-man’s land between the various established fields*” [76]. In the following, we sketch three mature disciplines which have not fully integrated into mainstream fluid mechanics, but which are likely to dramatically improve the complexity and performance of flow control in the future.

The first area includes advances in sensor and actuator hardware, as well as principled or heuristic placement of sensors and actuators in the flow. Recent developments in biologically inspired sensing and actuation are motivated by the extreme performance observed in biological turbulence control, and they remain promising for engineering flow control. Next, advances in data-driven modeling and control are poised to leverage the growing movement in data science. These new techniques include machine learning, compressive sensing, and UQ, all of which have direct relevance for in-time closed-loop flow control. Finally, developments in first-principles modeling and control of turbulence will remain a critical backbone of efforts in flow control. These developments may include a common control-theoretic framework generalizing linear systems theory to handle various classes of flow nonlinearity, as well as developments in turbulence closures. Combining bottom-up (theoretical) advances in turbulence models and control theory with top-down (data-driven) approaches will enable hybrid controllers with greater flexibility and robustness (see Fig. 32). These directions are necessarily a product of the authors’ experiences and biases, and there are certainly many more fruitful directions that remain unlisted in this review.

8.1 Bio-Inspired Sensing and Actuation. Sensors and actuators are the workhorses of active flow control. Advances in hardware will be a critical determining factor in the ultimate success and adoption of turbulence control in industry. These advances include smaller, higher-bandwidth, cheaper, and more reliable devices that may be integrated directly into existing hardware, such as wings. There have been many advances in actuator hardware, as reviewed in Ref. [36] and discussed in Sec. 2.4. These have included plasma actuators, MEMS, fluidic oscillators [345,346], synthetic jets, and zero-net-mass-flux actuators, such as piezoelectric actuators. Advances in sensors, such as the nano-scale thermal anemometry probe [347–349], are facilitating ever finer measurements of turbulent systems. We expect that continued developments in sensing and actuation hardware will continue to drive advances in turbulence control. In addition, we predict significant progress in the effective placement of sensors and actuators for a given control objective. This progress should be marked by theoretical breakthroughs in the first-principles optimal

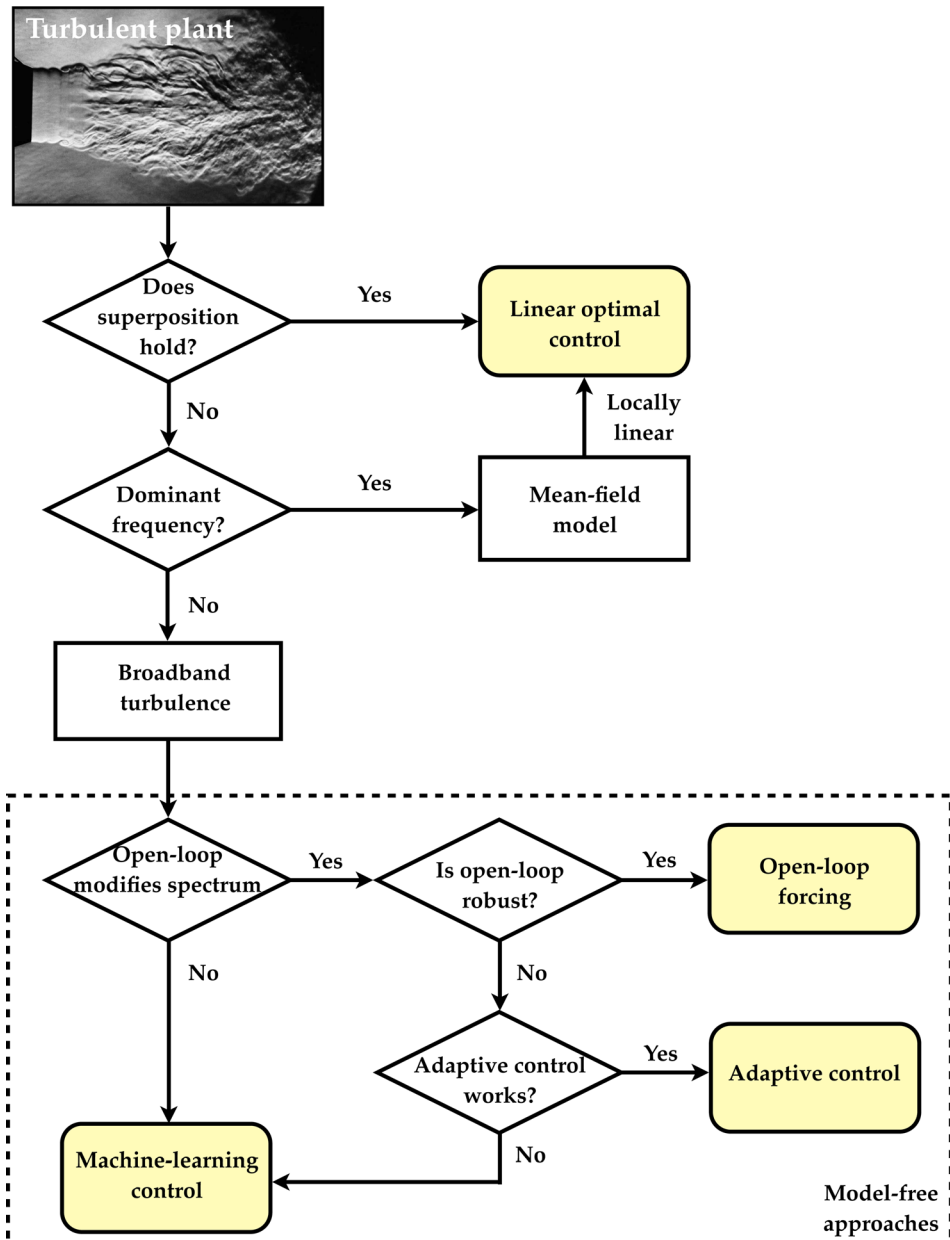


Fig. 31 Flow chart illustrating the hierarchy of active control approaches. This diagram is conservative in giving preference to the most established techniques. If the task is optimization or minimization of measurement time, machine-learning control may be an earlier branch. Top panel depicts a turbulent jet from Bradshaw et al. [38].

placement as well as improved heuristics for key engineering flows.

8.1.1 Cheap Hardware and Local Computations. Active separation control has not been adopted in the automobile industry, in part because of low fuel prices and the perception among automakers that drivers are unwilling to pay the upfront cost for hardware upgrades. Reducing the cost of control hardware, either through manufacturing advances or economies of scale, will be important to gain traction in the consumer automobile market.

Other markets, such as air travel or commercial shipping, may be willing to bear upgrade costs for significant improvements to fuel economy or improved range of operability. However, modifying the design and manufacture of an airplane wing is extremely costly and will likely require advances in the manufacture of embedded or surface-laminated sensors and actuators. Because the smallest eddies become smaller with increased flow velocity,

transition delay on a modern aircraft may involve a fine web of integrated sensors and actuators. Moreover, time-scales also shrink with faster flows, and it may be necessary to perform local computations in a neighborhood of the sensors and actuators. This will have a twofold benefit: first, local computations will greatly reduce the transfer of data associated with a fine mesh of sensors, and second, local computations will reduce the latency in a control decision.

These ideas are already being explored in the context of bio-inspired engineering [350–369] and biomanipulation [370–376]. It is observed that birds, bats, insects, fish, and swimming mammals routinely harness unsteady and turbulent fluid phenomena to improve their propulsive efficiency, maximize lift and thrust, and enhance maneuverability [364,377–388]. They achieve this performance with robustness to external factors and disturbances, rapid changes in flight conditions, such as gusts, and even significant changes to body geometry.

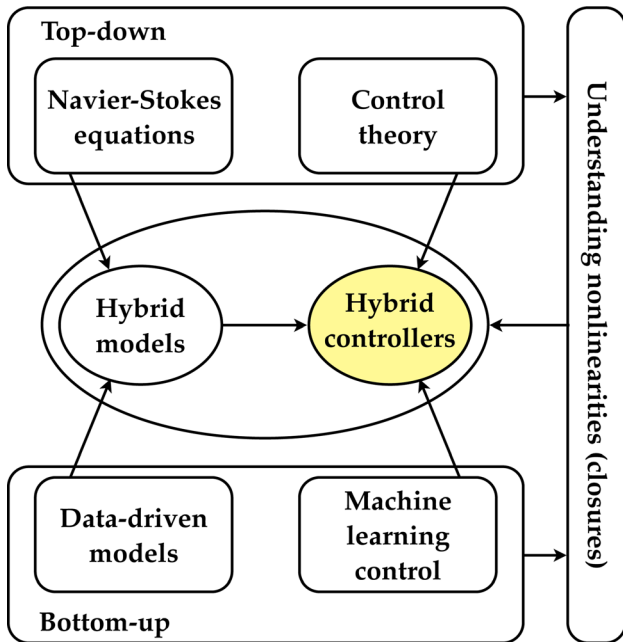


Fig. 32 Schematic illustrating a roadmap for future development. We envision the synthesis of classical control theory with data-driven methods for the development of hybrid controllers. Both top-down and bottom-up approaches will contribute to a better understanding of nonlinearities, which will in turn contribute to the development of more effective controllers.

Insect flight is particularly remarkable, since aerodynamic time-scales are faster than the time it takes for signal transduction from the visual system to the central nervous system [389]. In addition to centralized computations, local computations are being performed in the shoulder muscles and these decisions are fed directly to motor neuron outputs. Thus, the insect's neural flight control system is largely centered around the mechanosensory system, comprised of sparsely distributed sensors that act on the fastest time scales and provide the lowest latency [390,391]. Nearly, all flying insects contain microscopic-embedded strain sensors in their wings, called campaniform sensilla, along with other mechanosensors, such as antennas and halter, which are small passive wings that serve as gyroscopes [392]. Moths, for example, have up to hundreds of these campaniform sensors, more densely spaced at the wing base. Similarly, birds sense flow disturbances with their feathers [393], and bats with tiny hairs on the surfaces of their wings [394–396].

Biological systems suggest a strategy for sensing turbulence based on a large number of relatively inaccurate or noisy sensors, as opposed to a few accurate, reliable sensors. In the correct estimation framework, utilizing the law of large numbers, it is possible that many low-fidelity sensors may be more accurate and robust in the aggregate than a few accurate sensors. This strategy has already been employed in a number of diverse settings, ranging from finance to optical detection with cameras [397] to distributed sensor networks.

8.1.2 Sensor and Actuator Placement. As discussed above, sensor and actuator placement is of central importance in turbulent flow control. This is especially clear in the context of linear control, where the matrix C is determined entirely by the sensor placement and type, and the matrix B is similarly determined by the actuators. These matrices, in conjunction with the dynamics A , determine to what extent flow states are observable and controllable.

The optimal locations of a small number of actuators and sensors were recently determined for the H_2 optimal control of the complex Ginzburg–Landau equation in Ref. [37]. In Ref. [398],

sensor/actuator placement was investigated in the context of the cylinder wake, and both direct and adjoint modes were used to determine regions of high sensitivity to disturbances. Optimal actuation is also explored in the form of small upstream jets to delay the transition to turbulence in a pipe flow [399–401]. As mentioned previously, sensor and actuator placement was also investigated for a transitional boundary layer [250].

Determining optimal sensor and actuator placement in general, even for linear feedback control, is an important unsolved problem. Currently, optimal placement can only be determined using a brute-force combinatorial search, at least with existing mathematical machinery. This combinatorial search does not scale well to larger problems, and even with Moore's law, exponentially increasing computer power does not grow quickly enough to help. Advances in compressive sensing, however, may provide convex algorithms to *almost certainly* find optimal sensor/actuator placement, under certain conditions. Ideas from compressive sensing have recently been used to determine the optimal sensor locations for categorical decision making based on high-dimensional data [402] with applications in dynamic processes [403].

8.2 Data-Driven Modeling and Control. As researchers strive to make more complete measurements and simulations of increasingly complex flows, we as a community find ourselves in a deluge of data. This burden of data will only become more acute as sensor arrays are manufactured with finer spatial and temporal resolution. Some of the foundational techniques used in the analysis of big data [404], such as dimensionality reduction and parallel computation, were developed extensively in the fluids community. However, many of the most promising recent techniques have been largely applied to static data problems in artificial intelligence and computer vision. There is a tremendous opportunity ahead to embrace and innovate new techniques in compressive sensing, machine learning, and other data-driven methods applied to the rich *dynamical* system of turbulence; data-driven methods are also being applied more broadly in the aerospace industry [405]. For an overview of data techniques applied to dynamical systems, see Refs. [403,406].

8.2.1 Compressive Sensing. Compressive sensing [407–411] has the potential to be a disruptive technology in turbulence control, marking one of the most important breakthroughs in computational mathematics since the FFT. Compressive sensing allows complex, high-dimensional signals and states to be reconstructed from surprisingly few measurements, as long as the high-dimensional signal is sparse in some basis; most natural signals are. Sparsity means that the vector, written in a transformed basis, contains mostly zeros. For instance, image and audio signals are sparse in Fourier or wavelet bases, as evidenced by their high degree of compressibility (e.g., JPEG and MP3 compression).

In fluid dynamics, signals of interest may represent flow field snapshots with many degrees-of-freedom from PIV [412] or the time-history of hot-wire measurements in the wake of a turbulent flow. The first example is analogous to an image, and the second example is analogous to a multichannel audio signal.

The conventional wisdom in signal processing and data acquisition is that a signal must be sampled at twice the rate of the highest frequency present, the so-called Shannon–Nyquist sampling rate [413,414], for perfect signal reconstruction. However, when a signal is sparse in some basis, meaning that its vector representation in those coordinates contains mostly zeros, it is possible to relax this sampling rate restriction. A reduction in the sampling rate may have a dramatic effect in bandwidth-limited control applications.

A vector $\mathbf{a} \in \mathbb{R}^{N_a}$ is K -sparse in a transformation basis $\Phi \in \mathbb{R}^{N_a \times N_a}$ if $\mathbf{a} = \Phi \xi$ and $\xi \in \mathbb{R}^{N_a}$ has exactly K nonzero elements; this means that \mathbf{a} may be represented in a low-dimensional subspace of Φ . Compressive sensing provides a framework to determine the K nonzero coefficients in ξ , and therefore to determine \mathbf{a} , from the measurements $s \in \mathbb{R}^{N_s}$.

$$s = \mathbf{C}\mathbf{a} = \mathbf{C}\Phi\xi \quad (61)$$

The measurements (i.e., rows of \mathbf{C}) must be incoherent with respect to the columns of Φ , meaning that they are not strongly correlated, and there must be $N_s \geq \mathcal{O}(K \log(N_a/K))$ measurements. Note that this is a significant reduction in measurements when $K \ll N_a$. For a signal \mathbf{a} that is sparse in the Fourier domain, Φ is an inverse discrete Fourier transform, and spatial or temporal point measurements are incoherent, since they are broadband in frequency. This is very convenient, since many signals of interest are sparse in the frequency domain and point measurements are realistic in many engineering applications.

Compressive sensing has recently been applied to reduce the data acquisition required in PIV systems [102,415–418]. Time-resolved PIV may be prohibitively expensive for high-speed, high-Reynolds number flows because of the multiscale nature of turbulence. PIV systems are often limited by the bandwidth of data transfer. Reducing the spatial or temporal sampling rate using compressive sensing may open up orders of magnitude more complex flows to PIV analysis. Other advances in time-resolved PIV involve using a Kalman smoother to combine a time-resolved point measurement with nontime-resolved PIV data [135].

Before the advent of compressive sensing, finding the K -sparse solution ξ to Eq. (61) involved a combinatorial brute force search among all possible vectors. This is a nonpolynomial (NP) hard problem, meaning that the computational complexity does not scale as a polynomial of the size of the problem N_a . With compressive sensing, it is possible to find the K -sparse vector in polynomial time with high probability using techniques in convex minimization [419–422]. The ability to solve these problems in polynomial time means that we will be able to solve proportionally more challenging problems with the continued progress of Moore's law of exponential growth in computing power. Recently, compressive sensing techniques have been applied to the (previously) NP hard problem of sensor placement for categorical discrimination in high-dimensional data [402].

Although compressive sensing has been extremely successful in image processing, it has not been widely applied to *dynamical* systems, with some notable exceptions [423–427]. In fact, fluid dynamics is one of the first fields in dynamical systems to adopt compressive sensing techniques. Compressive sensing and other sparsity-based ideas have been used recently in the computation of the DMD [102,428–430]. In addition, POD modes have been used as a data-driven sparsifying basis [102,417,431,432]. Indeed, the application of dimensionality reduction and compressive sensing to dynamical systems is synergistic, since low-rank attractors facilitate sparse measurements. Other applications of compressive sensing in fluids are provided in Refs. [433–435].

8.2.2 Machine Learning. ML comprises a set of tools that extend classic dimensionality reduction techniques to automatically generate models that both learn from and improve with more data [275–277,406]. In fluid dynamics, dimensionality reduction techniques, such as POD or DMD, may be thought of as *library* building. In ML, these low-rank libraries are stored for each dynamic regime, and they may be used to rapidly characterize a system. These models are used for categorical decision, pattern recognition, high-dimensional regression, occlusion inference in data with incorrect or missing values, and outlier rejection. Moreover, these methods improve as more data are collected, and they may either be trained by expert supervision or used in an unsupervised context to elucidate underlying patterns that may not have been readily apparent to a human investigator. ML offers a paradigm shift in modeling and control based on engineering data, leveraging both human expertise and the statistical power of a large sample size for quantifiably improved decisions and diagnostics based on features mined from high-dimensional data.

Turbulence control may be characterized by many different attractors in a small region of parameter space. With classification protocols, it is possible to characterize underlying bifurcation

parameters from relatively few measurements of a complex system [431–437]. Once the system is characterized, the high-level control system may jump to a previously determined control strategy, which may be good but suboptimal for the particular instantaneous parameters. Then, feedback may be applied to reduce errors. If a new region is found that is not amenable to previous controllers, it is characterized and incorporated into the library.

System identification may be thought of as a form of machine learning, where training data are used to generate a model based on observed patterns. It is hoped that the model is valid on new inputs that were not used for training, providing a so-called cross-validation. Decreasing the amount of data required for the training and execution of the model is often important when a prediction or decision is required quickly, as in turbulence control. Compressive sensing and machine learning have already begun to be combined for *sparse decision making* [402,403,406,432,438], which may dramatically reduce the latency in a control decision. Many of these methods involve clustering techniques, which are a cornerstone of machine learning. Cluster-based reduced-order models are especially promising and have recently been developed in fluids [439], building on cluster analysis [440], and transition matrix models [441].

Turbulence control based on GP has had a number of recent successes in canonically challenging flow control problems [263,265,326–329]. These advances motivate renewed effort to integrate aspects of machine learning and control theory. For instance, adding reference tracking and robust performance to machine-learning control may provide the best of both strategies.

8.2.3 UQ and Equation-Free Methods. Although many engineering phenomena satisfy governing equations, it is often the case that the high-level questions of interest are far removed from first-principles analysis. Moreover, initial conditions, parameters, and even the equations of motion may only be known with some certainty. As an alternative to classical equation-based approaches, model-free methods have emerged in the past decade and have the potential to transform the control of complex systems. Equation-free analysis [442–445] and UQ [446–448] are two crucial fields that have direct relevance for turbulence modeling and control.

For instance, in fluid dynamics, DMD has been useful for identifying important spatial-temporal coherent structures that are spatially correlated and share the same time dynamics (i.e., growth, decay, oscillation, etc.) [98–101]. This method is purely data-driven, making it equally useful for data from simulations and experiments. Moreover, a low-order dynamical system is identified, which may be used for short-time predictions and closed-loop feedback control to shape the system dynamics toward a desired outcome. Recently, DMD has been extended to disambiguate the internal dynamics from externally applied control [195]. Other extensions to DMD include video analysis [449], streaming data sets [450], and data with noise [451].

Two of the defining characteristics of turbulent flows are that they are chaotic and that it is difficult or impossible to measure every scale simultaneously with arbitrary precision. The inherent *uncertainty* in the measured flow state may dramatically affect future predictions as the uncertainty propagates through the dynamical system. This is especially challenging when the dynamics are chaotic, as probabilistic descriptions of the uncertainty will become stretched and folded by the nonlinearity [452]. The field of UQ has arisen to characterize such systems. Generalized polynomial chaos (gPC) provides a modern perspective on an old technique [453], approximating the evolution of stochastic dynamical systems through a Galerkin projection using a set of orthogonal polynomials. These polynomials are chosen to describe the probability distribution of uncertain quantities [446–448]. gPC can become quite expensive for long-time evaluation of uncertain quantities, because of the significant distortion of trajectories and probability densities. To address this, various extensions have been developed, such as multi-element gPC [454], time-dependent

gPC [455], and gPC based on short-time flow-map composition [456]. There has been a recent explosion of interesting methods for UQ [457] and stochastic dynamics [458,459].

In addition, the finite-time Lyapunov exponent (FTLE) has been a rapidly developing data-driven technique in the analysis of time-varying fluid fields [460–467]. Like DMD, this method only relies on velocity field measurements, either from simulations or experiments. FTLE analysis identifies time-varying coherent structures in fluids that are analogous to stable and unstable manifolds. Thus, FTLE provides a quantitative technique to visualize flows and identify regions of separation, recirculation, dispersion, material attraction, and high sensitivity to perturbations. This method has been used to analyze aortic blood flows for predictions involving recirculation regions, separation, and stenosis [468]. FTLE has also been used to study biopropulsion [469–471], fluid mixing in large bodies of water [472–474], and to understand turbulent structure [463,464,467,475]. FTLE provides a measure of sensitivity, which is essential in the quantification and management of uncertainty. Sensitivity and coherence are closely related to the calculation of almost invariant sets [476–478], using set-oriented methods [479,480], and to eigenvectors of the Perron Frobenius operator.

8.2.4 Design of Experiments. Many of the data-driven techniques discussed above suggest innovations in experimental design. Understanding what measurements must be acquired to design models and controllers from experimental data is an important part of turbulence control. UQ and sensitivity analysis can offer some guidance about what design factors have the most impact on measurement quality, and where the flow is most sensitive to actuation. Compressive sensing may allow for improved bandwidth through a principled reduction in the spatial and temporal resolution of measurements required for signal reconstruction. ML provides an exploratory protocol for actuating the system into new and beneficial dynamic regimes.

8.3 Advanced Nonlinear Models, Controllers, and Closures. As discussed above, there may be serious limitations to physics-based modeling of flows with strongly nonlinear dynamics. Consequently, model-based control will be challenged by the accuracy of the model. In addition, control design methods generally assume either a working linearized model or a well-understood nonlinearity. At the same time, dramatic advances in data-driven methods, such as system identification and machine learning, have produced powerful new tools in turbulence control. This trend is accelerated by the tremendous global resource investment in machine learning across all physical sciences. However promising these new methods are, there will continue to be many compelling reasons to develop improved nonlinear models, controllers, and closures. First, physics-based models are interpretable and allow for the inclusion of expert human knowledge. Second, understanding the fundamental reasons *why* a given controller works is central in developing this human intuition. Such intuition is critical when deciding on what control strategy (hardware, logic, etc.) to employ in a new situation. Third, a physically interpretable model might lead to a simple control law with one or a few easily tunable parameters. These first-principles models can be expected to develop more slowly as the mathematical challenges are enormous. Yet, they will undoubtedly remain a critical part of engineering turbulence control. Hence, understanding of the physical mechanisms underlying effective turbulence control will remain a critical enabler—regardless of the control strategy, lest we lose mastery of the machinery we employ.

There are a host of advanced modeling techniques, including powerful generalizations of POD, which are useful for obtaining efficient parameterized models of complex turbulent flows using high-performance computation [481–484]. The gappy POD method provides the ability to sparsely sample a system and still evaluate the POD and terms in the Galerkin projection [485,486]. In addition, there are reduced-basis methods for PDEs [487] and

the associated discrete empirical interpolation method [488–490], which approximates nonlinear terms by evaluating the nonlinearity at a few specially determined points. There have also been powerful advances in the filtering of turbulent systems [434,491–493]. Finally, robust control has also been used as a method of understanding underlying nonlinear mechanisms in turbulence [494]. In addition, advanced measurement capabilities contribute to improving our understanding of high Reynolds number turbulent flows [495,496].

These advanced models are broken into three critical pieces—modeling, closure, and control design—although the true division may be more subtle. First, nonlinear model identification needs to be advanced comprising both structure and parameter identification. Significant progress has been made with 4D VAR methods [497,498]. Second, turbulence closures have always been a critical part of reduced-order turbulence models. Yet, eddy-viscosity based subscale models are too coarse to resolve critical frequency cross-talk mechanisms. Closure schemes based on a Gaussian approximation [273], on a maximum entropy principle [499–501], and on finite-time thermodynamics [502–504] hold corresponding promises. Finally, the nonlinear theory of control needs to be significantly advanced. It is currently unclear how nonlinear models and closures will be used by control theorists, motivating the need for a common framework, like the state-space and frequency domain framework in Sec. 4 for linear systems.

8.3.1 Graph-Theoretic Flow Control. Advances in network science have recently been applied with success in fluid systems [505], providing a new set of mathematical techniques for complex systems. The resulting graph models may be based on snapshot clusters [439], or on a sparsified graph model for the underlying vortex network [311]. The integration of methods from network science and network control theory in turbulence control is promising, especially since many network control techniques have been developed to handle nonlinear systems.

The past two decades have marked numerous advances in graph-theoretic control theory surrounding multi-agent systems, and network science has experienced significant recent attention [506–510]. Networks are often characterized by a large collection of individuals (represented by nodes) that each executes their own set of local protocols in response to external stimulus [511]. This analogy holds quite well for a number of large graph dynamical systems, including animals flocking [512,513], multirobotic cooperative control systems [514], sensor networks [515,516], biological regulatory networks [517,518], and the internet [519,520], to name a few. Similarly, in a fluid packets of vorticity may be viewed as nodes in a graph, which interact collectively according to global rules (i.e., governing equations) based on local rules (diffusion, etc.) as well as their external inputs summed across the entire network (i.e., convection due to induced velocity from the Biot–Savart law) [311].

In large multi-agent systems, it is often possible to manipulate the large-scale behavior with leader nodes that enact a larger supervisory control protocol to create a system-wide minima that is favorable [512,521–523]. The fact that birds and fish often act as local flows with large-scale coherence, and that leaders can strongly influence and manipulate the large-scale coherent motion [512,513], is promising when considering network-based fluid flow control. Based on the network-control methodology used to analyze schooling fish and flocking birds [512,513], there is an appealing goal of *schooling* turbulence by collecting and harnessing distributed multiscale eddies into a collective organization, or *community*, with favorable large-scale properties.

Recent work investigating the number of leader nodes required for structural controllability of a network [522] suggests that large, sparse networks with heterogeneous degree distributions,⁶

⁶The *degree distribution* of a network is the probability distribution of the number of connections each node has to other nodes. All scale-free networks are inherently sparse, with heterogeneous degree distribution [509].

such as scale-free turbulence networks, are especially difficult to control. In particular, the number of driver nodes may be quite large for these systems, as compared with a regular or random graph with more homogeneous degree distribution. However, full structural controllability of a turbulent vortex network is not necessarily a reasonable or desirable goal. In fact, these results are consistent with physical intuition that controlling every single turbulent eddy would require immense control authority with distributed actuation over a number of spatial locations.

In flow control, especially for turbulent fluids, the goal is not necessarily to control every minor eddy in the flow, but rather to manipulate the base flow and large-scale coherent structures that mediate quantities of interest (lift, drag, etc.). In addition, practically, we are more interested in the *degree of controllability* [524], rather than structural controllability, of large-scale vortical structures in order to manipulate the base flow. Even with the goal of increasing mixing, which involves increasing the level of turbulence, individual eddies need not be controlled, but rather control should manipulate the statistical distribution of eddies that determine dominant energy balances in the fluid.

8.3.2 Markov Model-Based Control. One elegant strategy comprising modeling, closures, and control design starts with the Liouville equation for the probability distribution [525]. The probability density $p(\mathbf{a}, t)$ of Eq. (2a) evolves according to the Liouville equation

$$\partial_t p(\mathbf{a}, t) + \nabla_{\mathbf{a}} \cdot [\mathbf{f}(\mathbf{a}, \mathbf{b}) p(\mathbf{a}, t)] = 0$$

where $\nabla_{\mathbf{a}}$ is the Nabla operator in the state space. The elegance lies in the fact that this evolution equation is a linear conservation equation for the probability distribution and thus allows to take advantage of the sophisticated *linear* control design methods for *nonlinear* dynamics. In addition, the probability distribution gives immediate access to engineering goals, like average drag, average lift, or level of fluctuation. Such averages are not provided by linearized models. However, the challenge is that the Liouville equation of the Navier-Stokes equation [526] is a functional equation and thus computationally far more demanding than the original equation. Yet, a suitable cluster-based phase-space discretization may reduce this Liouville equation down to a low-dimensional linear Markov model [439,440] providing easy access to linear control design. Intriguingly, the adjoint of the Liouville equation is related to the Koopman operator [439,527,528]. This deep relation still waits to be exploited in probability control. In summary, there are plenty of promising opportunities advancing nonlinear model-based control.

Acknowledgment

We have benefited tremendously from many fruitful discussions on machine learning, compressive sensing, and control of complex dynamical systems with Nathan Kutz, Josh Proctor, and Bing Brunton. We acknowledge highly stimulating discussions with the local TUCOROM team (Jean-Paul Bonnet, Laurent Cordier, Joël Delville, Thomas Duriez, Eurika Kaiser, Kai von Krbek, Jean-Charles Laurentie, Vladimir Parezanović, and Andreas Spohn), with the OpenLab PPRIME/PSA team (Diogo Barros, Cecile Li, Jacques Borée, and Tony Ruiz), with the SépaCoDe team managed by Azeddine Kourta, Andreas Spohn, and Michel Stanislas, with Ambrosys (Markus W. Abel and Marc Segond), with the SFB 880, in particular Rolf Radespiel, Peter Scholz, and Richard Semaan, with the ARC team (Robert Niven and Steven Waldrip), and with our close visitors and collaborators Jean-Luc Aider, Shervin Bagheri, Maciej Balajewicz, Zacharias Berger, Jason Bourgeois, Helmut Eckelmann, Nicolas Gautiers, Mark Glauser, Hans-Christian Hege, Jens Kasten, Siniša Krajanović, Jacques Lewalle, Kervin Low, Robert Martinuzzi, Marek Morzyński, Christian Nayeri, Jan Östh, Oliver Paschereit, Brian Polagye,

Bartosz Protas, Michael Schlegel, Tamir Shaqarin, Sam Taira, Jonathan Tu, and Dave Williams.

S.L.B. would also like to gratefully acknowledge and thank Clancy Rowley, Richard Murray, Rob Stengel, and Naomi Leonard, who each found unique ways to make control theory come to life. S.L.B. has also had the pleasure of learning about bio-inspired fluids from Tom Daniel and turbulence from Lex Smits, Jim Riley, and Gigi Martinelli. S.L.B. was generously supported by the Department of Mechanical Engineering, and as a Data Science Fellow in the eScience Institute (NSF, Moore-Sloan Foundation, and Washington Research Foundation) at the University of Washington, as well as by the Department of Energy and Boeing.

B.R.N. is deeply indebted to his turbulence control mentors Andrzej Banaszuk, Andreas Dillmann, Helmut Eckelmann, Rudibert King, and William K. George who shared and fueled the passion for the field. B.R.N. acknowledges generous funding from the French Agence Nationale de la Recherche (ANR) via the Senior Chair of Excellence TUCOROM and the SepaCoDe project, from the OpenLab PPRIME/PSA by Peugeot-Citroën, from the region Poitou-Charentes, from the German Science Foundation via the Collaborative Research Center SFB 880, from the Rector-Funded Visiting Professorship of the UNSW, Canberra, Australia, from the US National Research Foundation via the PIRE Grant No. OISE-0968313 from Ambrosys GmbH, Potsdam, Germany and from Bernd Noack Cybernetics Foundation.

We are deeply indebted to both anonymous referees for providing valuable suggestions regarding many technical aspects of the manuscript.

Nomenclature

\mathbf{a}	= model state
\mathbf{A}	= matrix function of the dynamics
$\hat{\mathbf{a}}$	= estimated model state
\mathbf{A}_i	= matrix of the quadratic nonlinearity
\mathbf{A}_0	= Jacobian of dynamics at \mathbf{a}^s
\mathbf{a}^s	= steady fixed point
$(\mathbf{A}, \mathbf{B}, \mathbf{C}, \mathbf{D})$	= linearized state-space system
$(\hat{\mathbf{A}}, \hat{\mathbf{B}}, \hat{\mathbf{C}}, \hat{\mathbf{D}})$	= controller state-space system
$(\mathbf{A}_d, \mathbf{B}_d, \mathbf{C}_d, \mathbf{D}_d)$	= discrete-time system
$(\mathbf{A}_r, \mathbf{B}_r, \mathbf{C}_r, \mathbf{D}_r)$	= reduced-order model
\mathbf{b}	= actuation input
\mathcal{B}	= balancing transformation
\mathbf{b}^*	= optimal actuation
\mathcal{C}	= controllability matrix
\mathbf{C}_d	= discrete-time controllability matrix
\mathcal{D}	= dissipation in TKE
\mathbb{D}	= discretization operator
\mathbf{e}	= error signal
E	= expectation value
\mathbf{f}	= dynamics
\mathbf{F}_k	= prefilter for mixed sensitivity synthesis
\mathbf{g}	= volume force
\mathcal{G}	= forcing in TKE
\mathbf{h}	= impulse response function
\mathbf{H}	= Hankel matrix
h_k	= Volterra kernels
\mathcal{H}_2	= hardy space with bounded two norm
\mathcal{H}_{∞}	= hardy space with bounded infinity norm
\mathbf{I}	= identity matrix
\mathbf{J}	= cost function
\mathbf{K}	= controller
\mathcal{K}	= turbulent kinetic energy (TKE)
k_D	= derivative control gain
k_i	= gain of the Galerkin system
k_I	= integral control gain
k_P	= proportional control gain
\mathbf{K}_d	= disturbance feed-forward control
\mathbf{K}_f	= Kalman filter

K_r	= regulator
K_{ref}	= reference feed-forward control
L	= loop transfer function ($L = PK$)
ℓ	= Laplace transform
l_{ij}	= coefficients of the linear term in the Galerkin system
m	= output function
M	= amplitude of ESC input
M_S	= maximum peak of sensitivity function
N_a	= number of states
N_b	= number of actuators
N_s	= number of sensors
N_r	= number of reduced-order states
N_a^f	= number of fast states
\mathcal{O}	= observability matrix
\mathcal{O}_d	= discrete-time observability matrix
P	= plant model
\mathcal{P}	= production in TKE
P_d	= disturbance model
P_r	= reduced-order plant model
P_{des}	= desired plant
Q	= LQR state weight
q_{ijk}	= coefficients of the quadratic term in the Galerkin system
R	= LQR actuation weight
Re	= Reynolds number
s	= sensor output
S	= sensitivity function
\hat{s}	= estimated sensor output
S_d	= sensitivity function to disturbance
S_{ref}	= sensitivity function to reference
t	= time
T	= complementary sensitivity
U	= left singular vectors from SVD
U_r	= first N_r columns of U
$u(\mathbf{x}, t)$	= fluid velocity field
$u'(\mathbf{x}, t)$	= velocity fluctuations
$u^a(\mathbf{x}, t)$	= actuation component
$u^s(\mathbf{x})$	= steady Navier-Stokes solution
$u^u(\mathbf{x}, t)$	= unsteady component
$u^\Delta(\mathbf{x}, t)$	= mean-flow deformation
V	= right singular vectors from SVD
V_d	= disturbance covariance
V_n	= noise covariance
V_r	= first N_r columns of V
w	= exogenous inputs
w_d	= disturbance
w_n	= sensor noise
w_r	= reference input
W_c	= controllability Gramian
W_o	= observability Gramian
\mathbf{x}	= position vector
X	= unknown variable in Riccati equation
Y	= unknown variable in dual Riccati equation
α^a	= manifold parameter associated with u^a
α^u	= manifold parameter associated with u^u
β^u	= nonlinear damping parameter
β^{aa}	= nonlinear damping parameter of u^a on u^a
β^{au}	= nonlinear damping parameter of u^u on u^a
β^{ua}	= nonlinear damping parameter of u^a on u^u
β^{uu}	= nonlinear damping parameter of u^u on u^u
γ^u	= nonlinear frequency parameter
γ^{**}	= nonlinear frequency parameter (superscripts have analogous meaning as in β)
Δt	= time step
$\delta(t)$	= Dirac delta function
ζ	= Laplace variable
μ	= bifurcation parameters
ξ	= sparse vector for compressive sensing

Σ	= singular values from SVD
Σ_r	= first $N_r \times N_r$ singular values
σ^a	= growth rate associated with u^a
σ^u	= growth rate associated with u^u
σ^c	= designed growth rate with control
τ	= time delay
ϕ	= phase variable
Φ	= direct BPOD modes
Φ_r	= first N_r direct BPOD modes
Ψ	= adjoint BPOD modes
Ψ_r	= first N_r adjoint BPOD modes
ω	= oscillation frequency
ω^a	= frequency associated with u^a
ω^u	= frequency associated with u^u

References

- [1] Fish, F. E., and Lauder, G. V., 2006, "Passive and Active Flow Control by Swimming Fishes and Mammals," *Annu. Rev. Fluid Mech.*, **38**, pp. 193–224.
- [2] Ahlbom, B. K., 2004, *Zoological Physics*, Springer-Verlag, Berlin.
- [3] Dean, B., and Bhushan, B., 2010, "Shark-Skin Surfaces for Fluid-Drag Reduction in Turbulent Flow: A Review," *Philos. Trans. R. Soc. A*, **368**(1929), pp. 4775–4806.
- [4] Bechert, D. W., Bruse, M., Hage, W., van der Hoeven, J. G. T., and Hoppe, G., 1997, "Experiments on Drag-Reducing Surfaces and Their Optimization With an Adjustable Geometry," *J. Fluid Mech.*, **338**, pp. 59–87.
- [5] Gilliéron, P., and Kourta, A., 2010, "Aerodynamic Drag Reduction by Vertical Splitter Plates," *Exp. Fluids*, **48**(1), pp. 1–16.
- [6] Grandemange, M., Ricot, D., Vartanian, C., Ruiz, T., and Cadot, O., 2014, "Characterisation of the Flow Past Real Road Vehicles With Blunt Afterbodies," *Int. J. Aerodyn.*, **4**(1), pp. 24–42.
- [7] Pfeiffer, J., and King, R., 2012, "Multivariable Closed-Loop Flow Control of Drag and Yaw Moment for a 3D Bluff Body," *AIAA Paper No. 2012-2802*.
- [8] Gad-el Hak, M., 1989, "Flow Control," *ASME Appl. Mech. Rev.*, **42**(10), pp. 261–293.
- [9] Gad-el Hak, M., and Tsai, H. M., 2006, *Transition and Turbulence Control*, Vol. 8, World Scientific, Singapore.
- [10] Kim, J., 2011, "Physics and Control of Wall Turbulence for Drag Reduction," *Philos. Trans. R. Soc. A*, **369**(1940), pp. 1396–1411.
- [11] Baker, C., Jones, J., Lopez-Calleja, F., and Munday, J., 2004, "Measurements of the Cross Wind Forces on Trains," *J. Wind Eng. Ind. Aerodyn.*, **92**(7), pp. 547–563.
- [12] Baker, C., 2010, "The Flow Around High Speed Trains," *J. Wind Eng. Ind. Aerodyn.*, **98**(6), pp. 277–298.
- [13] Schetzel, J. A., 2001, "Aerodynamics of High-Speed Trains," *Annu. Rev. Fluid Mech.*, **33**(1), pp. 371–414.
- [14] Gad-el Hak, M., 1996, "Modern Developments in Flow Control," *ASME Appl. Mech. Rev.*, **49**(7), pp. 365–379.
- [15] Barber, T. J., 1999, private communication.
- [16] King, R., 2007, "Active Flow Control," *Notes on Numerical Fluid Mechanics and Interdisciplinary Design*, Vol. 95, Springer, Berlin.
- [17] King, R., 2010, "Active Flow Control II," *Notes on Numerical Fluid Mechanics and Interdisciplinary Design*, Vol. 108, Springer, Berlin.
- [18] Liepmann, H., and Nosenchuck, D., 1982, "Active Control of Laminar-Turbulent Transition," *J. Fluid Mech.*, **118**, pp. 201–204.
- [19] Roussopoulos, K., 1993, "Feedback Control of Vortex Shedding at Low Reynolds Numbers," *J. Fluid Mech.*, **248**, pp. 267–296.
- [20] Kim, J., and Bewley, T., 2007, "A Linear Systems Approach to Flow Control," *Annu. Rev. Fluid Mech.*, **39**, pp. 383–417.
- [21] Sipp, D., Marquet, O., Meliga, P., and Barbagallo, A., 2010, "Dynamics and Control of Global Instabilities in Open-Flows—A Linearized Approach," *ASME Appl. Mech. Rev.*, **63**(3), p. 030801.
- [22] Lee, C., Kim, J., Babcock, D., and Goodman, R., 1997, "Application of Neural Networks to Turbulence Control for Drag Reduction," *Phys. Fluids*, **9**(6), pp. 1740–1747.
- [23] Medjo, T. T., Temam, R., and Ziane, M., 2008, "Optimal and Robust Control of Fluid Flows: Some Theoretical and Computational Aspects," *ASME Appl. Mech. Rev.*, **61**(1), p. 010802.
- [24] Bewley, T. R., 2001, "Flow Control: New Challenges for a New Renaissance," *Prog. Aerosp. Sci.*, **37**(1), pp. 21–58.
- [25] Greenblatt, D., and Wygnanski, I. J., 2000, "The Control of Flow Separation by Periodic Excitation," *Prog. Aerosp. Sci.*, **36**(7), pp. 487–545.
- [26] Bushnell, D. M., and McGinley, C. B., 1989, "Turbulence Control in Wall Flows," *Annu. Rev. Fluid Mech.*, **21**, pp. 1–20.
- [27] Moin, P., and Bewley, T., 1994, "Feedback Control of Turbulence," *ASME Appl. Mech. Rev.*, **47**(6S), pp. S3–S13.
- [28] Lumley, J., and Blossey, P., 1998, "Control of Turbulence," *Annu. Rev. Fluid Mech.*, **30**, pp. 311–327.
- [29] Gutmark, E. J., Schadow, K. C., and Yu, K. H., 1994, "Methods for Enhanced Turbulence Mixing in Supersonic Shear Flows," *ASME Appl. Mech. Rev.*, **47**(6S), pp. S188–S192.
- [30] Aamo, O. M., and Krstić, M., 2002, *Flow Control by Feedback: Stabilization and Mixing*, Springer-Verlag, London.

- [31] Dimotakis, P. E., 2005, "Turbulent Mixing," *Annu. Rev. Fluid Mech.*, **37**, pp. 329–356.
- [32] Mankbadi, R. R., 1992, "Dynamics and Control of Coherent Structures in Turbulent Jets," *ASME Appl. Mech. Rev.*, **45**(6), pp. 219–248.
- [33] Dowling, A. P., and Morgans, A. S., 2005, "Feedback Control of Combustion Oscillations," *Annu. Rev. Fluid Mech.*, **37**, pp. 151–182.
- [34] Rowley, C., and Williams, D., 2006, "Dynamics and Control of High-Reynolds Number Flows Over Open Cavities," *Annu. Rev. Fluid Mech.*, **38**, pp. 251–276.
- [35] Choi, H., Jeon, W.-P., and Kim, J., 2008, "Control of Flow Over a Bluff Body," *Annu. Rev. Fluid Mech.*, **40**, pp. 113–139.
- [36] Cattafesta, L., 2011, "Actuators for Active Flow Control," *Annu. Rev. Fluid Mech.*, **43**, pp. 247–272.
- [37] Chen, K. K., and Rowley, C. W., 2011, "H₂ Optimal Actuator and Sensor Placement in the Linearised Complex Ginzburg-Landau System," *J. Fluid Mech.*, **681**, pp. 241–260.
- [38] Bradshaw, P., Ferriss, D. H., and Johnson, R., 1964, "Turbulence in the Noise-Producing Region of a Circular Jet," *J. Fluid Mech.*, **19**(4), pp. 591–624.
- [39] Brown, G. L., and Roshko, A., 1974, "On Density Effects and Large Structure in Turbulent Mixing Layers," *J. Fluid Mech.*, **64**(4), pp. 775–816.
- [40] Kim, J., 2003, "Control of Turbulent Boundary Layers," *Phys. Fluids*, **15**(5), pp. 1093–1105.
- [41] Siauw, W., Bonnet, J.-P., Tensi, J., Cordier, L., Noack, B. R., and Cattafesta, L. I., 2010, "Transient Dynamics of the Flow Around a NACA0015 Airfoil Using Fluid Vortex Generators," *Int. J. Heat Fluid Flow*, **31**(3), pp. 450–459.
- [42] Shaqarin, T., 2014, private communication.
- [43] Choi, H., Moin, P., and Kim, J., 1994, "Active Turbulence Control for Drag Reduction in Wall-Bounded Flows," *J. Fluid Mech.*, **262**, pp. 75–110.
- [44] Gerhard, J., Pastoor, M., King, R., Noack, B. R., Dillmann, A., Morzyński, M., and Tadmor, G., 2003, "Model-Based Control of Vortex Shedding Using Low-Dimensional Galerkin Models," *AIAA Paper No. 2003-4262*.
- [45] Pastoor, M., Henning, L., Noack, B. R., King, R., and Tadmor, G., 2008, "Feedback Shear Layer Control for Bluff Body Drag Reduction," *J. Fluid Mech.*, **608**, pp. 161–196.
- [46] Samimy, M., Debiasi, M., Caraballo, E., Serrani, A., Yuan, X., Little, J., and Myatt, J., 2007, "Feedback Control of Subsonic Cavity Flows Using Reduced-Order Models," *J. Fluid Mech.*, **579**, pp. 315–346.
- [47] Vukasinovic, B., Rusak, Z., and Glezer, A., 2010, "Dissipative, Small-Scale Actuation of a Turbulent Shear Layer," *J. Fluid Mech.*, **656**, pp. 51–81.
- [48] Luchtenburg, D. M., Günter, B., Noack, B. R., King, R., and Tadmor, G. A., 2009, "Generalized Mean-Field Model of the Natural and Actuated Flows Around a High-Lift Configuration," *J. Fluid Mech.*, **623**, pp. 283–316.
- [49] Aider, J.-L., 2014, private communication.
- [50] Gordon, M., and Soria, J., 2002, "PIV Measurements of a Zero-Net-Mass-Flux Jet in Cross Flow," *Exp. Fluids*, **33**(6), pp. 863–872.
- [51] Cater, J. E., and Soria, J., 2002, "The Evolution of Round Zero-Net-Mass-Flux Jets," *J. Fluid Mech.*, **472**, pp. 167–200.
- [52] Zhang, P., Wang, J., and Feng, L., 2008, "Review of Zero-Net-Mass-Flux Jet and Its Application in Separation Flow Control," *Sci. China Ser. E, Technol. Sci.*, **51**(9), pp. 1315–1344.
- [53] Cattafesta, L. N., Garg, S., and Shukla, D., 2001, "Development of Piezoelectric Actuators for Active Flow Control," *AIAA J.*, **39**(8), pp. 1562–1568.
- [54] Gallas, Q., Holman, R., Nishida, T., Carroll, B., Sheplak, M., and Cattafesta, L., 2003, "Lumped Element Modeling of Piezoelectric-Driven Synthetic Jet Actuators," *AIAA J.*, **41**(2), pp. 240–247.
- [55] Glezer, A., and Amitay, M., 2002, "Synthetic Jets," *Annu. Rev. Fluid Mech.*, **34**, pp. 503–529.
- [56] Smith, B. L., and Glezer, A., 1998, "The Formation and Evolution of Synthetic Jets," *Phys. Fluids*, **10**(9), pp. 2281–2297.
- [57] Holman, R., Uturkar, Y., Mittal, R., Smith, B. L., and Cattafesta, L., 2005, "Formation Criterion for Synthetic Jets," *AIAA J.*, **43**(10), pp. 2110–2116.
- [58] You, D., and Moin, P., 2008, "Active Control of Flow Separation Over an Airfoil Using Synthetic Jets," *J. Fluids Struct.*, **24**(8), pp. 1349–1357.
- [59] Moreau, E., 2007, "Airflow Control by Non-Thermal Plasma Actuators," *J. Phys. D: Appl. Phys.*, **40**(3), p. 605.
- [60] Hanson, R. E., Lavoie, P., and Naguib, A. M., 2010, "Effect of Plasma Actuator Excitation for Controlling Bypass Transition in Boundary Layers," *AIAA Paper No. 2010-1091*.
- [61] Hanson, R. E., Bade, K. M., Belson, B. A., Lavoie, P., Naguib, A. M., and Rowley, C. W., 2014, "Feedback Control of Slowly-Varying Transient Growth by an Array of Plasma Actuators," *Phys. Fluids*, **26**(2), p. 024102.
- [62] Huang, J., Corke, T. C., and Thomas, F. O., 2006, "Plasma Actuators for Separation Control of Low-Pressure Turbine Blades," *AIAA J.*, **44**(1), pp. 51–57.
- [63] Roth, J. R., Sherman, D. M., and Wilkinson, S. P., 2000, "Electrohydrodynamic Flow Control With a Glow-Discharge Surface Plasma," *AIAA J.*, **38**(7), pp. 1166–1172.
- [64] Post, M. L., and Corke, T. C., 2004, "Separation Control on High Angle of Attack Airfoil Using Plasma Actuators," *AIAA J.*, **42**(11), pp. 2177–2184.
- [65] Hanson, R. E., Lavoie, P., Naguib, A. M., and Morrison, J. F., 2010, "Transient Growth Instability Cancellation by a Plasma Actuator Array," *Exp. Fluids*, **49**(6), pp. 1339–1348.
- [66] Ho, C.-M., and Tai, Y.-C., 1996, "Review: MEMS and Its Applications for Flow Control," *ASME J. Fluids Eng.*, **118**(3), pp. 437–447.
- [67] Ho, C.-M., and Tai, Y.-C., 1998, "Micro-Electro-Mechanical Systems (MEMS) and Fluid Flows," *Annu. Rev. Fluid Mech.*, **30**, pp. 579–612.
- [68] Naguib, A., Christopoulou, C., Alnajjar, E., Nagib, H., Huang, C., and Najafi, K., 1997, "Arrays of MEMS-Based Actuators for Control of Supersonic Jet Screech," *AIAA Paper No. 1997-1963*.
- [69] Löfdahl, L., and Gad-el-Hak, M., 1999, "MEMS Applications in Turbulence and Flow Control," *Prog. Aeronaut. Sci.*, **35**(2), pp. 101–203.
- [70] Huang, C., Christopoulou, C., Najafi, K., Naguib, A., and Nagib, H. M., 2002, "An Electrostatic Microactuator System for Application in High-Speed Jets," *Microelectromech. Syst.*, **11**(3), pp. 222–235.
- [71] Suzuki, H., Kasagi, N., and Suzuki, Y., 2004, "Active Control of an Axisymmetric Jet With Distributed Electromagnetic Flap Actuators," *Exp. Fluids*, **36**(3), pp. 498–509.
- [72] Kasagi, N., Suzuki, Y., and Fukagata, K., 2009, "Microelectromechanical Systems-Based Feedback Control of Turbulence for Skin Friction Reduction," *Annu. Rev. Fluid Mech.*, **41**, pp. 231–251.
- [73] Wu, J., Wang, L., and Tadmor, J., 2007, "Suppression of the Von Karman Vortex Street Behind a Circular Cylinder by a Traveling Wave Generated by a Flexible Surface," *J. Fluid Mech.*, **574**, pp. 365–391.
- [74] Thiria, B., Goujon-Durand, S., and Wesfreid, J. E., 2006, "The Wake of a Cylinder Performing Rotary Oscillations," *J. Fluid Mech.*, **560**, pp. 123–147.
- [75] Bergmann, M., Cordier, L., and Brancher, J.-P., 2005, "Optimal Rotary Control of the Cylinder Wake Using Proper Orthogonal Decomposition Reduced Order Model," *Phys. Fluids*, **17**(9), p. 097101.
- [76] Wiener, N., 1948, *Cybernetics or Control and Communication in the Animal and the Machine*, 1st ed., MIT Press, Boston.
- [77] Kolmogorov, A., 1941, "The Local Structure of Turbulence in Incompressible Viscous Fluid for Very Large Reynolds Number," *Dokl. Akad. Nauk. SSSR*, **30**, pp. 9–13.
- [78] Kolmogorov, A., 1941, "On Degeneration (Decay) of Isotropic Turbulence," *Dokl. Akad. Nauk SSSR*, **31**, pp. 538–540.
- [79] Landau, L. D., and Lifshitz, E. M., 1987, "Fluid Mechanics," *Course of Theoretical Physics*, 2nd ed., Vol. 6, Pergamon Press, Oxford, UK.
- [80] Pope, S., 2000, *Turbulent Flows*, 1st ed., Cambridge University Press, Cambridge, UK.
- [81] Lee, M., Malaya, N., and Moser, R. D., 2013, "Petascale Direct Numerical Simulation of Turbulent Channel Flow on Up to 786 k Cores," International Conference on High Performance Computing, Networking, Storage and Analysis (SC'13), Denver, CO, Nov. 17–21, p. 61.
- [82] Kaneda, Y., Ishihara, T., Yokokawa, M., Itakura, K., and Uno, A., 2003, "Energy Dissipation Rate and Energy Spectrum in High Resolution Direct Numerical Simulations of Turbulence in a Periodic Box," *Phys. Fluids*, **15**(2), pp. L21–L24.
- [83] Moore, G. E., 1965, "Cramming More Components Onto Integrated Circuits," *Electronics*, **38**(8), pp. 114–117.
- [84] Lumley, J., 1970, *Stochastic Tools in Turbulence*, Academic Press, New York.
- [85] Holmes, P., Lumley, J. L., Berkooz, G., and Rowley, C. W., 2012, *Turbulence, Coherent Structures, Dynamical Systems and Symmetry*, 2nd ed., Cambridge University Press, Cambridge, UK.
- [86] Sirovich, L., 1987, "Turbulence and the Dynamics of Coherent Structures, Part I—Coherent Structures," *Q. Appl. Math.*, **XLV**(3), pp. 561–571.
- [87] Golub, G. H., and Reinsch, C., 1970, "Singular Value Decomposition and Least Squares Solutions," *Numer. Math.*, **14**(5), pp. 403–420.
- [88] Golub, G., and Kahan, W., 1965, "Calculating the Singular Values and Pseudo-Inverse of a Matrix," *J. Soc. Ind. Appl. Math. Ser. B: Numer. Anal.*, **2**(2), pp. 205–224.
- [89] Trefethen, L. N., and Bau, D., III, 1997, *Numerical Linear Algebra*, Vol. 50, SIAM, Philadelphia.
- [90] Antoulas, A. C., 2005, *Approximation of Large-Scale Dynamical Systems*, SIAM, Philadelphia.
- [91] Pearson, K., 1901, "On Lines and Planes of Closest Fit to Systems of Points in Space," *Philos. Mag.*, **2**(7–12), pp. 559–572.
- [92] Hotelling, H., 1933, "Analysis of a Complex of Statistical Variables Into Principal Components," *J. Educ. Psychol.*, **24**(6), pp. 417–441.
- [93] Karhunen, K., 1946, "Zur Spektraltheorie Stochastischer Prozesse," *Ann. Acad. Sci. Fennicae, Ser. A I, Math.-Phys.*, **37**, pp. 1–79.
- [94] Lorenz, E., 1956, "Empirical Orthogonal Functions and Statistical Weather Prediction," Department of Meteorology, Statistical Forecasting Project, MIT, Cambridge, MA, Scientific Report No. 1.
- [95] Andino, M. Y., Wallace, R. D., Glauser, M. N., Camphouse, R. C., Schmit, R. F., and Myatt, J. H., 2011, "Boundary Feedback Flow Control: Proportional Control With Potential Application to Aero-Optics," *AIAA J.*, **49**(1), pp. 32–40.
- [96] Willcox, K., and Peraire, J., 2002, "Balanced Model Reduction Via the Proper Orthogonal Decomposition," *AIAA J.*, **40**(11), pp. 2323–2330.
- [97] Rowley, C., 2005, "Model Reduction for Fluids Using Balanced Proper Orthogonal Decomposition," *Int. J. Bifurcation Chaos*, **15**(3), pp. 997–1013.
- [98] Schmid, P. J., and Sesterhenn, J., 2008, "Dynamic Mode Decomposition of Numerical and Experimental Data," 61st Annual Meeting of the APS Division of Fluid Dynamics, San Antonio, TX, Nov. 23–25, American Physical Society, College Park, MD, pp. 208.
- [99] Schmid, P. J., 2010, "Dynamic Mode Decomposition for Numerical and Experimental Data," *J. Fluid Mech.*, **656**, pp. 5–28.
- [100] Rowley, C. W., Mezić, I., Bagheri, S., Schlatter, P., and Henningson, D., 2009, "Spectral Analysis of Nonlinear Flows," *J. Fluid Mech.*, **645**, pp. 115–127.
- [101] Tu, J. H., Rowley, C. W., Luchtenburg, D. M., Brunton, S. L., and Kutz, J. N., 2014, "On Dynamic Mode Decomposition: Theory and Applications," *J. Comput. Dyn.*, **1**(2), pp. 391–421.

- [102] Tu, J. H., Rowley, C. W., Kutz, J. N., and Shang, J. K., 2014, "Spectral Analysis of Fluid Flows Using Sub-Nyquist-Rate PIV Data," *Exp. Fluids*, **55**(9), p. 1805.
- [103] Koopman, B. O., 1931, "Hamiltonian Systems and Transformation in Hilbert Space," *Proc. Natl. Acad. Sci.*, **17**(5), pp. 315–318.
- [104] Mezić, I., and Banaszuk, A., 2004, "Comparison of Systems With Complex Behavior," *Phys. D: Nonlinear Phenom.*, **197**(1), pp. 101–133.
- [105] Mezić, I., 2005, "Spectral Properties of Dynamical Systems, Model Reduction and Decompositions," *Nonlinear Dyn.*, **41**(1–3), pp. 309–325.
- [106] Budinić, M., Mohr, R., and Mezić, I., 2012, "Applied Koopmanism," *Chaos: Interdiscip. J. Nonlinear Sci.*, **22**(4), p. 047510.
- [107] Mezić, I., 2013, "Analysis of Fluid Flows Via Spectral Properties of the Koopman Operator," *Annu. Rev. Fluid Mech.*, **45**, pp. 357–378.
- [108] Schmid, P. J., and Hennigson, D. S., 2001, *Stability and Transition in Shear Flows*, Springer, New York.
- [109] Schmid, P. J., 2007, "Nonmodal Stability Theory," *Annu. Rev. Fluid Mech.*, **39**, pp. 129–162.
- [110] Theofilis, V., 2011, "Global Linear Instability," *Annu. Rev. Fluid Mech.*, **43**, pp. 319–352.
- [111] Schmid, P. J., and Brandt, L., 2014, "Analysis of Fluid Systems: Stability, Receptivity, Sensitivity," *ASME Appl. Mech. Rev.*, **66**(2), p. 024803.
- [112] Gorsch, C. E., and Salwen, H., 1978, "The Continuous Spectrum of the Orr-Sommerfeld Equation Part I—The Spectrum and the Eigenfunctions," *J. Fluid Mech.*, **87**, pp. 33–54.
- [113] Salwen, H., and Gorsch, C. E., 1981, "The Continuous Spectrum of the Orr-Sommerfeld Equation. Part 2—Eigenfunction Expansions," *J. Fluid Mech.*, **104**, pp. 445–465.
- [114] Joseph, D. D., 1976, "Stability of Fluid Motions I & II," *Springer Tracts in Natural Philosophy*, Vols. 26 and 27, Springer, New York.
- [115] Boberg, L., and Brosa, U., 1988, "Onset of Turbulence in a Pipe," *Z. Naturforsch.*, **43a**, pp. 697–726.
- [116] Trefethen, L. N., Trefethen, A. E., Reddy, S. C., and Driscoll, T. A., 1993, "Hydrodynamic Stability Without Eigenvalues," *Science*, **261**(5121), pp. 578–584.
- [117] Belson, B. A., Tu, J. H., and Rowley, C. W., 2014, "Algorithm 945: MODRED—A Parallelized Model Reduction Library," *ACM Trans. Math. Software*, **40**(4), p. 30.
- [118] von Karman, T., 1912, "Über Den Mechanismus des Widerstands, den Ein Bewegter Körper in Einer Flüssigkeit Erfährt," *Göttinger Nachrichten, Math. Phys. Kl.*, **1912**, pp. 547–556.
- [119] Föppl, L., 1913, "Wirbelbewegung hinter einem Kreiszylinder," *Sitzb. d. k. Bayer. Akad. d. Wiss.*, **1**, pp. 1.
- [120] Suh, Y., 1993, "Periodic Motion of a Point Vortex in a Corner Subject to a Potential Flow," *J. Phys. Soc. Jpn.*, **62**, pp. 3441–3445.
- [121] Noack, B. R., Mezić, I., Tadmor, G., and Banaszuk, A., 2004, "Optimal Mixing in Recirculation Zones," *Phys. Fluids*, **16**(4), pp. 867–888.
- [122] Lugt, H., 1996, *Introduction to Vortex Theory*, Vortex Flow Press, Potomac, MA.
- [123] Cottet, G. H., and Koumoutsakos, P., 2000, *Vortex Methods—Theory and Practice*, Cambridge University Press, Cambridge, UK.
- [124] Wu, J.-Z., Ma, H.-Y., and Zhou, M.-D., 2006, *Vorticity and Vortex Dynamics*, 1st ed., Springer, Berlin.
- [125] Adrian, R., and Moin, P., 1988, "Stochastic Estimation of Organized Turbulent Structure: Homogeneous Shear Flow," *J. Fluid Mech.*, **190**, pp. 531–559.
- [126] Nicoud, F., Baggett, J., Moin, P., and Cabot, W., 2001, "Large Eddy Simulation Wall-Modeling Based on Suboptimal Control Theory and Linear Stochastic Estimation," *Phys. Fluids*, **13**(10), pp. 2968–2984.
- [127] Bonnet, J.-P., Cole, D., Delville, J., Glauser, M. N., and Ukeiley, L. S., 1998, "Stochastic Estimation and Proper Orthogonal Decomposition—Complementary Techniques for Identifying Structure," *Exp. Fluids*, **17**(5), pp. 307–314.
- [128] Glauser, M. N., Higuchi, H., Ausseur, J., and Pinier, J., 2004, "Feedback Control of Separated Flows," *AIAA Paper No. 2004-2521*.
- [129] Ausseur, J. M., Pinier, J. T., Glauser, M. N., Higuchi, H., and Carlson, H., 2006, "Experimental Development of a Reduced-Order Model for Flow Separation Control," *AIAA Paper No. 2006-1251*.
- [130] Tinney, C., Coiffet, F., Delville, J., Hall, A., Jordan, P., and Glauser, M., 2006, "On Spectral Linear Stochastic Estimation," *Exp. Fluids*, **41**(5), pp. 763–775.
- [131] Hudy, L. M., Naguib, A., and Humphreys, W. M., 2007, "Stochastic Estimation of a Separated-Flow Field Using Wall-Pressure-Array Measurements," *Phys. Fluids*, **19**(2), p. 024103.
- [132] Pinier, J. T., Ausseur, J. M., Glauser, M. N., and Higuchi, H., 2007, "Proportional Closed-Loop Feedback Control of Flow Separation," *AIAA J.*, **45**(1), pp. 181–190.
- [133] Farrell, B. F., and Ioannou, P. J., 2001, "State Estimation Using a Reduced-Order Kalman Filter," *J. Atmos. Sci.*, **58**(23), pp. 3666–3680.
- [134] King, R., and Gilles, E., 1985, "Multiple Kalman Filters for Early Detection of Hazardous States," International Conference Industrial Process Modelling and Control, Hangzhou, China, June 6–9, pp. 130–138.
- [135] Tu, J. H., Griffin, J., Hart, A., Rowley, C. W., III, L. N. C., and Ukeiley, L. S., 2013, "Integration of Non-Time-Resolved PIV and Time-Resolved Velocity Point Sensors for Dynamic Estimation of Velocity Fields," *Exp. Fluids*, **54**(2), p. 1429.
- [136] Welch, G., and Bishop, G., 1995, "An Introduction to the Kalman Filter," University of North Carolina, Chapel Hill, NC, Technical Report 95-041.
- [137] Busse, F. H., 1991, "Numerical Analysis of Secondary and Tertiary States of Fluid Flow and Their Stability Properties," *Appl. Sci. Res.*, **48**(3–4), pp. 341–351.
- [138] Noack, B. R., and Eckelmann, H., 1994, "A Global Stability Analysis of the Steady and Periodic Cylinder Wake," *J. Fluid Mech.*, **270**, pp. 297–330.
- [139] Fletcher, C. A. J., 1984, *Computational Galerkin Methods*, 1st ed., Springer, New York.
- [140] Holmes, P., Lumley, J. L., and Berkooz, G., 1998, *Turbulence, Coherent Structures, Dynamical Systems and Symmetry*, 1st ed., Cambridge University Press, Cambridge, UK.
- [141] Juang, J. N., and Pappa, R. S., 1985, "An Eigensystem Realization Algorithm for Modal Parameter Identification and Model Reduction," *J. Guid., Control, Dyn.*, **8**(5), pp. 620–627.
- [142] Juang, J. N., 1994, *Applied System Identification*, Prentice-Hall, Upper Saddle River, NJ.
- [143] Ljung, L., 2001, "Black-Box Models From Input–Output Measurements," 18th IEEE Instrumentation and Measurement Technology Conference (IMTC 2001), Budapest, May 21–23, pp. 138–146.
- [144] Ljung, L., 1999, *System Identification: Theory for the User*, Prentice-Hall, Upper Saddle River, NJ.
- [145] Crouch, P., 1981, "Dynamical Realizations of Finite Volterra Series," *SIAM J. Control Optim.*, **19**(2), pp. 177–202.
- [146] Boyd, S., Chua, L. O., and Desoer, C. A., 1984, "Analytical Foundations of Volterra Series," *IMA J. Math. Control Inf.*, **1**(3), pp. 243–282.
- [147] Boyd, S., and Chua, L. O., 1985, "Fading Memory and the Problem of Approximating Nonlinear Operators With Volterra Series," *IEEE Trans. Circuits Syst.*, **32**(11), pp. 1150–1161.
- [148] Lesjak, C., and Krener, A. J., 1978, "The Existence and Uniqueness of Volterra Series for Nonlinear Systems," *IEEE Trans. Autom. Control*, **23**(6), pp. 1090–1095.
- [149] Brockett, R. W., 1976, "Volterra Series and Geometric Control Theory," *Automatica*, **12**(2), pp. 167–176.
- [150] Krstić, M., Smyshlyaev, A., and Vazquez, R., 2006, "Boundary Control of PDEs and Applications to Turbulent Flows and Flexible Structures," IEEE Chinese Control Conference (CCC 2006), Harbin, China, Aug. 7–11, pp. PL-4-PL-16.
- [151] Floriani, E., de Wit, T. D., and Le Gal, P., 2000, "Nonlinear Interactions in a Rotating Disk Flow: From a Volterra Model to the Ginzburg–Landau Equation," *Chaos: Interdiscip. J. Nonlinear Sci.*, **10**(4), pp. 834–847.
- [152] Tromp, J. C., and Jenkins, J. E. A., 1990, "Volterra Kernel Identification Scheme Applied to Aerodynamic Reactions," *AIAA Paper No. 90-2803*.
- [153] Prazenica, R. J., Reisenthel, P. H., Kurdila, A. J., and Breinier, M. J., 2007, "Volterra Kernel Extrapolation for Modeling Nonlinear Aeroelastic Systems at Novel Flight Conditions," *J. Aircr.*, **44**(1), pp. 149–162.
- [154] Balajewicz, M., and Dowell, E., 2012, "Reduced-Order Modeling of Flutter and Limit-Cycle Oscillations Using the Sparse Volterra Series," *J. Aircr.*, **49**(6), pp. 1803–1812.
- [155] Balikhin, M., Bates, I., and Walker, S., 2001, "Identification of Linear and Nonlinear Processes in Space Plasma Turbulence Data," *Adv. Space Res.*, **28**(5), pp. 787–800.
- [156] Vazquez, R., and Krstić, M., 2007, *Control of Turbulent and Magnetohydrodynamic Channel Flows: Boundary Stabilization and State Estimation*, Springer, New York.
- [157] Estrada, T., Happel, T., Hidalgo, C., Ascasibar, E., and Blanco, E., 2010, "Experimental Observation of Coupling Between Turbulence and Sheared Flows During LH Transitions in a Toroidal Plasma," *Europhys. Lett.*, **92**(3), p. 35001.
- [158] Smola, A. J., and Schölkopf, B., 2004, "A Tutorial on Support Vector Regression," *Stat. Comput.*, **14**(3), pp. 199–222.
- [159] Schölkopf, B., and Smola, A. J., 2002, *Learning With Kernels: Support Vector Machines, Regularization, Optimization, and Beyond*, MIT Press, Cambridge, MA.
- [160] Suykens, J. A., and Vandewalle, J., 1999, "Least Squares Support Vector Machine Classifiers," *Neural Process. Lett.*, **9**(3), pp. 293–300.
- [161] Doyle, J. C., 1978, "Guaranteed Margins for LQG Regulators," *IEEE Trans. Autom. Control*, **23**(4), pp. 756–757.
- [162] Doyle, J. C., and Stein, G., 1981, "Multivariable Feedback Design: Concepts for a Classical/Modern Synthesis," *IEEE Trans. Autom. Control*, **26**(1), pp. 4–16.
- [163] Glover, K., and Doyle, J. C., 1988, "State-Space Formulae for All Stabilizing Controllers That Satisfy an H_∞ -Norm Bound and Relations to Risk Sensitivity," *Syst. Control Lett.*, **11**(3), pp. 167–172.
- [164] Doyle, J. C., Glover, K., Khargonekar, P. P., and Francis, B. A., 1989, "State-Space Solutions to Standard H_2 and H_∞ Control Problems," *IEEE Trans. Autom. Control*, **34**(8), pp. 831–847.
- [165] Schlinker, R., Simonich, J., Shannon, D., Reba, R., Colonius, T., Gudmundsson, K., and Laendeine, F., 2009, "Supersonic Jet Noise From Round and Chevron Nozzles: Experimental Studies," *AIAA Paper No. 2009-3257*.
- [166] Skogestad, S., and Postlethwaite, I., 1996, *Multivariable Feedback Control*, Wiley, Chichester, UK.
- [167] Dullerud, G. E., and Paganini, F., 2000, "A Course in Robust Control Theory: A Convex Approach," *Texts in Applied Mathematics*, Springer, Berlin.
- [168] Scott Collis, S., Joslin, R. D., Seifert, A., and Theofilis, V., 2004, "Issues in Active Flow Control: Theory, Control, Simulation, and Experiment," *Prog. Aerosp. Sci.*, **40**(4), pp. 237–289.
- [169] Rowley, C. W., and Batten, B. A., 2008, "Dynamic and Closed-Loop Control," *Fundamentals and Applications of Modern Flow Control* (Progress in Astronautics and Aeronautics, Vol. 231), American Institute of Aeronautics and Astronautics, Reston, VA, pp. 115–148.
- [170] Bagheri, S., Hoepffner, J., Schmid, P. J., and Henningson, D. S., 2009, "Input–Output Analysis and Control Design Applied to a Linear Model of Spatially Developing Flows," *ASME Appl. Mech. Rev.*, **62**(2), p. 020803.
- [171] Fabbiane, N., Semeraro, O., Bagheri, S., and Henningson, D. S., 2014, "Adaptive and Model-Based Control Theory Applied to Convectively Unstable Flows," *ASME Appl. Mech. Rev.*, **66**(6), p. 060801.

- [172] Devasia, S., Chen, D., and Paden, B., 1996, "Nonlinear Inversion-Based Output Tracking," *IEEE Trans. Autom. Control*, **41**(7), pp. 930–942.
- [173] Krstić, M., and Banaszuk, A., 2006, "Multivariable Adaptive Control of Instabilities Arising in Jet Engines," *Control Eng. Pract.*, **14**(7), pp. 833–842.
- [174] Bewley, T. R., Temam, R., and Ziane, M., 2000, "A General Framework for Robust Control in Fluid Mechanics," *Phys. D*, **138**(3–4), pp. 360–392.
- [175] King, R., *Active Flow and Combustion Control*, Vol. 127, Springer International Publishing, Cham, Switzerland.
- [176] Kerstens, W., Pfeiffer, J., Williams, D., King, R., and Colonius, T., 2011, "Closed-Loop Control of Lift for Longitudinal Gust Suppression at Low Reynolds Numbers," *AIAA J.*, **49**(8), pp. 1721–1728.
- [177] Devasia, S., 2002, "Should Model-Based Inverse Inputs be Used as Feedforward Under Plant Uncertainty?" *IEEE Trans. Autom. Control*, **47**(11), pp. 1865–1871.
- [178] Chen, K. K., and Rowley, C. W., 2013, "Normalized Coprime Robust Stability and Performance Guarantees for Reduced-Order Controllers," *IEEE Trans. Autom. Control*, **58**(4), pp. 1068–1073.
- [179] Businger, P. A., and Golub, G. H., 1969, "Algorithm 358: Singular Value Decomposition of a Complex Matrix [F1, 4, 5]," *Commun. ACM*, **12**(10), pp. 564–565.
- [180] Ho, B. L., and Kalman, R. E., 1965, "Effective Construction of Linear State-Variable Models From Input/Output Data," 3rd Annual Allerton Conference on Circuit and System Theory, Monticello, IL, Oct. 20–22, pp. 449–459.
- [181] Moore, B. C., 1981, "Principal Component Analysis in Linear Systems: Controllability, Observability, and Model Reduction," *IEEE Trans. Autom. Control*, **26**(1), pp. 17–32.
- [182] Berkooz, G., Holmes, P., and Lumley, J., 1993, "The Proper Orthogonal Decomposition in the Analysis of Turbulent Flows," *Annu. Rev. Fluid Mech.*, **25**, pp. 539–575.
- [183] Ilak, M., and Rowley, C. W., 2008, "Modeling of Transitional Channel Flow Using Balanced Proper Orthogonal Decomposition," *Phys. Fluids*, **20**(3), p. 034103.
- [184] Lall, S., Marsden, J. E., and Glavaški, S., 1999, "Empirical Model Reduction of Controlled Nonlinear Systems," International Federation of Automatic Control (IFAC) World Congress, Beijing, July 5–9, pp. 473–478.
- [185] Lall, S., Marsden, J. E., and Glavaški, S., 2002, "A Subspace Approach to Balanced Truncation for Model Reduction of Nonlinear Control Systems," *Int. J. Rob. Nonlinear Control*, **12**(6), pp. 519–535.
- [186] Laub, A. J., Heath, M. T., Paige, C., and Ward, R., 1987, "Computation of System Balancing Transformations and Other Applications of Simultaneous Diagonalization Algorithms," *IEEE Trans. Autom. Control*, **32**(2), pp. 115–122.
- [187] Sirovich, L., 1987, "Turbulence and the Dynamics of Coherent Structures, Part III—Dynamics and Scaling," *Q. Appl. Math.*, **XLV**, pp. 583–590.
- [188] Sirovich, L., 1987, "Turbulence and the Dynamics of Coherent Structures, Part II—Symmetries and Transformations," *Q. Appl. Math.*, **XLV**, pp. 573–582.
- [189] Ma, Z., Ahuja, S., and Rowley, C. W., 2011, "Reduced Order Models for Control of Fluids Using the Eigensystem Realization Algorithm," *Theor. Comput. Fluid Dyn.*, **25**(1), pp. 233–247.
- [190] Luchtenburg, D. M., and Rowley, C. W., 2011, "Model Reduction Using Snapshot-Based Realizations," *Bull. Am. Phys. Soc.*, **56**, p. BAPS.2011.DFD.H19.4.
- [191] Tu, J. H., and Rowley, C. W., 2012, "An Improved Algorithm for Balanced POD Through an Analytic Treatment of Impulse Response Tails," *J. Comput. Phys.*, **231**(16), pp. 5317–5333.
- [192] Juang, J. N., Phan, M., Horta, L. G., and Longman, R. W., 1991, "Identification of Observer/Kalman Filter Markov Parameters: Theory and Experiments," NASA Langley Research Center, Hampton, VA, *NASA Technical Memorandum No. 104069*.
- [193] Phan, M., Juang, J. N., and Longman, R. W., 1992, "Identification of Linear-Multivariable Systems by Identification of Observers With Assigned Real Eigenvalues," *J. Astronaut. Sci.*, **40**(2), pp. 261–279.
- [194] Phan, M., Horta, L. G., Juang, J. N., and Longman, R. W., 1993, "Linear System Identification Via an Asymptotically Stable Observer," *J. Optim. Theory Appl.*, **79**(1), pp. 59–86.
- [195] Proctor, J. L., Brunton, S. L., and Kutz, J. N., 2014, "Dynamic Mode Decomposition With Control: Using State and Input Snapshots to Discover Dynamics," *arXiv:1409.6358*.
- [196] Barkley, D., and Tuckerman, L. S., 1999, "Stability Analysis of Perturbed Planar Couette Flow," *Phys. Fluids*, **11**(5), pp. 1187–1195.
- [197] Bayly, B. J., Orszag, S. A., and Herbert, T., 1988, "Instability Mechanisms in Shear-Flow Transition," *Annu. Rev. Fluid Mech.*, **20**(1), pp. 359–391.
- [198] Orszag, S. A., and Patera, A. T., 1983, "Secondary Instability of Wall-Bounded Shear Flows," *J. Fluid Mech.*, **128**, pp. 347–385.
- [199] Ruelle, D., and Takens, F., 1971, "On the Nature of Turbulence," *Commun. Math. Phys.*, **20**(3), pp. 167–192.
- [200] Aamo, O. M., Krstić, M., and Bewley, T. R., 2003, "Control of Mixing by Boundary Feedback in 2D Channel Flow," *Automatica*, **39**(9), pp. 1597–1606.
- [201] Bagheri, S., and Henningson, D. S., 2011, "Transition Delay Using Control Theory," *Philos. Trans. R. Soc. A*, **369**(1940), pp. 1365–1381.
- [202] Abergel, F., and Temam, R., 1990, "On Some Control Problems in Fluid Mechanics," *Theor. Comput. Fluid Dyn.*, **1**(6), pp. 303–325.
- [203] Jameson, A., 2003, "Aerodynamic Shape Optimization Using the Adjoint Method" (VKI Lecture Series on Aerodynamic Drag Prediction and Reduction), von Karman Institute of Fluid Dynamics, Rhode-St-Genèse, Belgium.
- [204] Reuther, J. J., Jameson, A., Alonso, J. J., Rimlinger, M. J., and Saunders, D., 1999, "Constrained Multipoint Aerodynamic Shape Optimization Using an Adjoint Formulation and Parallel Computers, Part 1," *J. Aircr.*, **36**(1), pp. 51–60.
- [205] Jameson, A., Martinelli, L., and Pierce, N., 1998, "Optimum Aerodynamic Design Using the Navier-Stokes Equations," *Theor. Comput. Fluid Dyn.*, **10**(1–4), pp. 213–237.
- [206] Reuther, J. J., Jameson, A., Farmer, J., Martinelli, L., and Saunders, D., 1996, "Aerodynamic Shape Optimization of Complex Aircraft Configurations Via an Adjoint Formulation," Research Institute for Advanced Computer Science, NASA Ames Research Center, Mountain View, CA, Report No. NASA-CR-203275.
- [207] Choi, H., Temam, R., Moin, P., and Kim, J., 1993, "Feedback Control for Unsteady Flow and Its Application to the Stochastic Burgers Equation," *J. Fluid Mech.*, **253**, pp. 509–543.
- [208] Bewley, T., and Moin, P., 1994, "Optimal Control of Turbulent Channel Flows," *Act. Control Vib. Noise*, ASME DE-Vol. 75, pp. 221–227.
- [209] Lee, C., Kim, J., and Choi, H., 1998, "Suboptimal Control of Turbulent Channel Flow for Drag Reduction," *J. Fluid Mech.*, **358**, pp. 245–258.
- [210] Bewley, T. R., Moin, P., and Temam, R., 2001, "DNS-Based Predictive Control of Turbulence: An Optimal Benchmark for Feedback Algorithms," *J. Fluid Mech.*, **447**, pp. 179–225.
- [211] Collis, S. S., Chang, Y., Kellogg, S., and Prabhu, R., 2000, "Large Eddy Simulation and Turbulence Control," *AIAA Paper No. 2000-2564*.
- [212] Bewley, T., and Liu, S., 1998, "Optimal and Robust Control and Estimation of Linear Paths to Transition," *J. Fluid Mech.*, **365**, pp. 305–349.
- [213] Baramov, L., Tutty, O. R., and Rogers, E., 2000, "Robust Control of Plane Poiseuille Flow," *AIAA Paper No. 2000-2684*.
- [214] Höglberg, M., Bewley, T. R., and Henningson, D. S., 2003, "Linear Feedback Control and Estimation of Transition in Plane Channel Flow," *J. Fluid Mech.*, **481**, pp. 149–175.
- [215] Höglberg, M., and Henningson, D. S., 2002, "Linear Optimal Control Applied to Instabilities in Spatially Developing Boundary Layers," *J. Fluid Mech.*, **470**, pp. 151–179.
- [216] Chevalier, M., Heepffner, J., Åkerkvist, E., and Henningson, D., 2007, "Linear Feedback Control and Estimation Applied to Instabilities in Spatially Developing Boundary Layers," *J. Fluid Mech.*, **588**, pp. 163–187.
- [217] Åkerkvist, E., Heepffner, J., Ehrenstein, U., and Henningson, D. S., 2007, "Optimal Growth, Model Reduction and Control in Separated Boundary-Layer Flow Using Global Eigenmodes," *J. Fluid Mech.*, **579**, pp. 305–314.
- [218] Ahuja, S., Rowley, C. W., Kevrekidis, I. G., Wei, M., Colonius, T., and Tadmor, G., 2007, "Low-Dimensional Models for Control of Leading-Edge Vortices: Equilibria and Linearized Models," *AIAA Paper No. 2007-709*.
- [219] Colonius, T., and Taira, K., 2008, "A Fast Immersed Boundary Method Using a Nullspace Approach and Multi-Domain Far-Field Boundary Conditions," *Comput. Methods Appl. Mech. Eng.*, **197**(25–28), pp. 2131–2146.
- [220] Taira, K., and Colonius, T., 2007, "The Immersed Boundary Method: A Projection Approach," *J. Comput. Phys.*, **225**(2), pp. 2118–2137.
- [221] Bagheri, S., Brandt, L., and Henningson, D., 2009, "Input–Output Analysis, Model Reduction and Control of the Flat-Plate Boundary Layer," *J. Fluid Mech.*, **620**, pp. 263–298.
- [222] Semeraro, O., Bagheri, S., Brandt, L., and Henningson, D. S., 2011, "Feedback Control of Three-Dimensional Optimal Disturbances Using Reduced-Order Models," *J. Fluid Mech.*, **677**, pp. 63–102.
- [223] Illingworth, S. J., Morgans, A. S., and Rowley, C. W., 2010, "Feedback Control of Flow Resonances Using Balanced Reduced-Order Models," *J. Sound Vib.*, **330**(8), pp. 1567–1581.
- [224] Illingworth, S. J., Morgans, A. S., and Rowley, C. W., 2012, "Feedback Control of Cavity Flow Oscillations Using Simple Linear Models," *J. Fluid Mech.*, **709**, pp. 223–248.
- [225] Semeraro, O., Bagheri, S., Brandt, L., and Henningson, D. S., 2013, "Transition Delay in a Boundary Layer Flow Using Active Control," *J. Fluid Mech.*, **731**, pp. 288–311.
- [226] Moarref, R., and Jovanović, M. R., 2012, "Model-Based Design of Transverse Wall Oscillations for Turbulent Drag Reduction," *J. Fluid Mech.*, **707**, pp. 205–240.
- [227] Cortelezzi, L., Lee, K., Kim, J., and Speyer, J., 1998, "Skin-Friction Drag Reduction Via Robust Reduced-Order Linear Feedback Control," *Int. J. Comput. Fluid Dyn.*, **11**(1–2), pp. 79–92.
- [228] Cortelezzi, L., and Speyer, J., 1998, "Robust Reduced-Order Controller of Laminar Boundary Layer Transitions," *Phys. Rev. E*, **58**(2), pp. 1906–1910.
- [229] Lee, K. H., Cortelezzi, L., Kim, J., and Speyer, J., 2001, "Application of Reduced-Order Controller to Turbulent Flows for Drag Reduction," *Phys. Fluids*, **13**(5), pp. 1321–1330.
- [230] Kasagi, N., Hasegawa, Y., and Fukagata, K., 2009, "Toward Cost-Effective Control of Wall Turbulence for Skin Friction Drag Reduction," *Advances in Turbulence XII*, Springer, Berlin, pp. 189–200.
- [231] Fukagata, K., Kobayashi, M., and Kasagi, N., 2010, "On the Friction Drag Reduction Effect by a Control of Large-Scale Turbulent Structures," *J. Fluid Sci. Technol.*, **5**(3), pp. 574–584.
- [232] Mamori, H., Fukagata, K., and Hoepffner, J., 2010, "Phase Relationship in Laminar Channel Flow Controlled by Traveling-Wave-Like Blowing or Suction," *Phys. Rev. E*, **81**(4), p. 046304.
- [233] Kametani, Y., and Fukagata, K., 2011, "Direct Numerical Simulation of Spatially Developing Turbulent Boundary Layers With Uniform Blowing or Suction," *J. Fluid Mech.*, **681**, pp. 154–172.
- [234] Nakanishi, R., Mamori, H., and Fukagata, K., 2012, "Relaminarization of Turbulent Channel Flow Using Traveling Wave-Like Wall Deformation," *Int. J. Heat Fluid Flow*, **35**, pp. 152–159.

- [235] Kasagi, N., Hasegawa, Y., Fukagata, K., and Iwamoto, K., 2012, "Control of Turbulent Transport: Less Friction and More Heat Transfer," *ASME J. Heat Transfer*, **134**(3), p. 031009.
- [236] Rathnasingham, R., and Breuer, K. S., 1997, "System Identification and Control of a Turbulent Boundary Layer," *Phys. Fluids*, **9**(7), pp. 1867–1869.
- [237] Rathnasingham, R., and Breuer, K. S., 2003, "Active Control of Turbulent Boundary Layers," *J. Fluid Mech.*, **495**, pp. 209–233.
- [238] Rowley, C. W., 2002, "Modeling, Simulation, and Control of Cavity Flow Oscillations," Ph.D. thesis, California Institute of Technology, Pasadena, CA.
- [239] Cattafesta, L., Shukla, D., Garg, S., and Ross, J., 1999, "Development of an Adaptive Weapons-Bay Suppression System," *AIAA Paper No. 1999-1901*.
- [240] Cattafesta, L., Williams, D., Rowley, C., and Alvi, F., 2003, "Review of Active Control of Flow-Induced Cavity Resonance," *AIAA Paper No. 2003-3567*.
- [241] Cattafesta, L. N., III, Song, Q., Williams, D. R., Rowley, C. W., and Alvi, F. S., 2008, "Active Control of Flow-Induced Cavity Oscillations," *Prog. Aerosp. Sci.*, **44**(7), pp. 479–502.
- [242] Rowley, C. W., Colonius, T., and Basu, A. J., 2002, "On Self-Sustained Oscillations in Two-Dimensional Compressible Flow Over Rectangular Cavities," *J. Fluid Mech.*, **455**, pp. 315–346.
- [243] Rowley, C. W., Colonius, T., and Murray, R. M., 2000, "POD Based Models of Self-Sustained Oscillations in the Flow Past an Open Cavity," *AIAA Paper No. 2000-1969*.
- [244] Rowley, C., Colonius, T., and Murray, R., 2004, "Model Reduction for Compressible Flows Using POD and Galerkin Projection," *Physica D*, **189**(1–2), pp. 115–129.
- [245] Rowley, C. W., Williams, D. R., Colonius, T., Murray, R. M., MacMartin, D. G., and Fabris, D., 2002, "Model-Based Control of Cavity Oscillations. Part II: System Identification and Analysis," *AIAA Paper No. 2002-0972*.
- [246] Samimy, M., Debiasi, M., Caraballo, E., Malone, J., Little, J., Özbay, H., Efe, M., Yan, X., Yuan, X., DeBonis, J., Myatt, J., and Camphouse, R., 2004, "Exploring Strategies for Closed-Loop Cavity Flow Control," *AIAA Paper No. 2004-0576*.
- [247] Rowley, C. W., Williams, D. R., Colonius, T., Murray, R. M., and Macmynowski, D. G., 2006, "Linear Models for Control of Cavity Flow Oscillations," *J. Fluid Mech.*, **547**, pp. 317–330.
- [248] Samimy, M., Debiasi, M., Caraballo, E., Serrani, A., Yuan, X., and Little, J., 2007, "Reduced-Order Model-Based Feedback Control of Subsonic Cavity Flows—An Experimental Approach," *Notes on Numerical Fluid Mechanics and Multidisciplinary Design (NNFM)*, Vol. 25, Springer, Berlin, pp. 211–230.
- [249] Efe, M., Debiasi, M., Yan, P., Özbay, H., and Samimy, M., 2005, "Control of Subsonic Cavity Flows by Neural Networks—Analytical Models and Experimental Validation," *AIAA Paper No. 2005-294*.
- [250] Belson, B. A., Semeraro, O., Rowley, C. W., and Henningson, D. S., 2013, "Feedback Control of Instabilities in the Two-Dimensional Blasius Boundary Layer: The Role of Sensors and Actuators," *Phys. Fluids*, **25**(5), p. 054106.
- [251] Hervé, A., Sipp, D., Schmid, P. J., and Samuelides, M., 2012, "A Physics-Based Approach to Flow Control Using System Identification," *J. Fluid Mech.*, **702**, pp. 26–58.
- [252] Semeraro, O., Pralits, J. O., Rowley, C. W., and Henningson, D. S., 2013, "Riccati-Less Approach for Optimal Control and Estimation: An Application to Two-Dimensional Boundary Layers," *J. Fluid Mech.*, **731**, pp. 394–417.
- [253] Weller, J., Camarri, S., and Iollo, A., 2009, "Feedback Control by Low-Order Modelling of the Laminar Flow Past a Bluff Body," *J. Fluid Mech.*, **634**, pp. 405–418.
- [254] Stuart, J., 1958, "On the Non-Linear Mechanics of Hydrodynamic Stability," *J. Fluid Mech.*, **4**(1), pp. 1–21.
- [255] Stuart, J., 1971, "Nonlinear Stability Theory," *Annu. Rev. Fluid Mech.*, **3**, pp. 347–370.
- [256] Schumm, M., Berger, E., and Monkewitz, P., 1994, "Self-Excited Oscillations in the Wake of Two-Dimensional Bluff Bodies and Their Control," *J. Fluid Mech.*, **271**, pp. 17–53.
- [257] Dusek, J., Le Gal, P., and Fraunié, P., 1994, "A Numerical and Theoretical Study of the First Hopf Bifurcation in a Cylinder Wake," *J. Fluid Mech.*, **264**, pp. 59–80.
- [258] Bourgeois, J. A., Martinuzzi, R. J., and Noack, B. R., 2013, "Generalised Phase Average With Applications to Sensor-Based Flow Estimation of the Wall-Mounted Square Cylinder Wake," *J. Fluid Mech.*, **736**, pp. 316–350.
- [259] Luchtenburg, M., Tadmor, G., Lehmann, O., Noack, B. R., King, R., and Morzyński, M., 2006, "Tuned POD Galerkin Models for Transient Feedback Regulation of the Cylinder Wake," 44th AIAA Aerospace Sciences Meeting, Reno, NV, Jan. 9–12, *AIAA Paper 2006-1407*.
- [260] Tadmor, G., Lehmann, O., Noack, B. R., Cordier, L., Delville, J., Bonnet, J.-P., and Morzyński, M., 2011, "Reduced Order Models for Closed-Loop Wake Control," *Philos. Trans. R. Soc. A*, **369**(1940), pp. 1513–1523.
- [261] King, R., Seibold, M., Lehmann, O., Noack, B. R., Morzyński, M., and Tadmor, G., 2005, "Nonlinear Flow Control Based on a Low Dimensional Model of Fluid Flow," *Control and Observer Design for Nonlinear Finite and Infinite Dimensional Systems* (Lecture Notes in Control and Information Sciences, Vol. 322), T. Meurer, K. Graichen, and E. Gilles, eds., Springer, Berlin, pp. 369–386.
- [262] Bergmann, M., and Cordier, L., 2008, "Optimal Control of the Cylinder Wake in the Laminar Regime by Trust-Region Methods and POD Reduced Order Models," *J. Comput. Phys.*, **227**(16), pp. 7813–7840.
- [263] Parezanovic, V., Laurentie, J.-C., Duriez, T., Fourment, C., Delville, J., Bonnet, J.-P., Cordier, L., Noack, B. R., Segond, M., Abel, M., Shaqarin, T., and Brunton, S. L., 2015, "Mixing Layer Manipulation Experiment—From Periodic Forcing to Machine Learning Closed-Loop Control," *J. Flow Turbul. Combust.*, **94**(1), pp. 155–173.
- [264] Aleksić, K., Luchtenburg, D. M., King, R., Noack, B. R., and Pfeiffer, J., 2010, "Robust Nonlinear Control Versus Linear Model Predictive Control of a Bluff Body Wake," *AIAA Paper No. 2010-4833*.
- [265] Duriez, T., Parezanovic, V., Laurentie, J.-C., Fourment, C., Delville, J., Bonnet, J.-P., Cordier, L., Noack, B. R., Segond, M., Abel, M., Gautier, N., Aider, J.-L., Raibaudo, C., Cuvier, C., Stanislas, M., and Brunton, S. L., 2014, "Closed-Loop Control of Experimental Shear Flows Using Machine Learning," *AIAA Paper No. 2014-2219*.
- [266] Luchtenburg, D. M., Schlegel, M., Noack, B. R., Aleksić, K., King, R., Tadmor, G., and Günther, B., 2010, "Turbulence Control Based on Reduced-Order Models and Nonlinear Control Design," *Active Flow Control II* (Notes on Numerical Fluid Mechanics and Multidisciplinary Design, Vol. 108), R. King, ed., Springer-Verlag, Berlin, pp. 341–356.
- [267] Farazmand, M. M., Kevlahan, N. K.-R., and Protas, B., 2011, "Controlling the Dual Cascade of Two-Dimensional Turbulence," *J. Fluid Mech.*, **668**, pp. 202–222.
- [268] Schlegel, M., Noack, B. R., Comte, P., Kolomenskiy, D., Schneider, K., Farge, M., Scoulet, J., Luchtenburg, D. M., and Tadmor, G., 2009, "Reduced-Order Modelling of Turbulent Jets for Noise Control," *Numerical Simulation of Turbulent Flows and Noise Generation: Results of the DFG/CNRS Research Groups FOR 507 and FOR 508* (Notes on Numerical Fluid Mechanics and Multidisciplinary Design (NNFM)), Springer-Verlag, Berlin, pp. 3–27.
- [269] John, C., Noack, B. R., Schlegel, M., Tröltzsch, F., and Wachsmuth, D., 2010, "Optimal Boundary Control Problems Related to High-Lift Configurations," *Active Flow Control II* (Notes on Numerical Fluid Mechanics and Multidisciplinary Design), R. King, ed., Springer-Verlag, Berlin.
- [270] Cordier, L., Noack, B. R., Daviller, G., Delville, J., Lehnasch, G., Tissot, G., Balajewicz, M., and Niven, R., 2013, "Control-Oriented Model Identification Strategy," *Exp. Fluids*, **54**, p. 1580.
- [271] Noack, B. R., Morzyński, M., and Tadmor, G. E., 2011, *Reduced-Order Modelling for Flow Control* (CISM Courses and Lectures, Vol. 528), Springer-Verlag, Berlin.
- [272] Morzyński, M., Stankiewicz, W., Noack, B. R., Thiele, F., and Tadmor, G., 2006, "Generalized Mean-Field Model for Flow Control Using Continuous Mode Interpolation," *AIAA Paper No. 2006-3488*.
- [273] Sapsis, T. P., and Majda, A., 2013, "Statistically Accurate Low-Order Models for Uncertainty Quantification in Turbulent Dynamical Systems," *Proc. Natl. Acad. Sci.*, **110**(34), pp. 13705–13710.
- [274] Mitchell, T. M., 1997, *Machine Learning*, McGraw-Hill, Maidenhead, UK.
- [275] Duda, R. O., Hart, P. E., and Stork, D. G., 2000, *Pattern Classification*, Wiley-Interscience, New York.
- [276] Bishop, C. M., 2006, *Pattern Recognition and Machine Learning*, Vol. 1, Springer, New York.
- [277] Murphy, K. P., 2012, *Machine Learning: A Probabilistic Perspective*, MIT Press, Cambridge, MA.
- [278] Fleming, P. J., and Purshouse, R. C., 2002, "Evolutionary Algorithms in Control Systems Engineering: A Survey," *Control Eng. Pract.*, **10**(11), pp. 1223–1241.
- [279] Krstić, M., and Wang, H., 2000, "Stability of Extremum Seeking Feedback for General Nonlinear Dynamic Systems," *Automatica*, **36**(4), pp. 595–601.
- [280] Ariyur, K. B., and Krstić, M., 2003, *Real-Time Optimization by Extremum-Seeking Control*, Wiley, Hoboken, NJ.
- [281] Beaudoin, J., Cadot, O., Aider, J., and Wesfreid, J. E., 2006, "Bluff-Body Drag Reduction by Extremum-Seeking Control," *J. Fluids Struct.*, **22**(6), pp. 973–978.
- [282] Beaudoin, J.-F., Cadot, O., Aider, J.-L., and Wesfreid, J.-E., 2006, "Drag Reduction of a Bluff Body Using Adaptive Control Methods," *Phys. Fluids*, **18**(8), p. 085107.
- [283] Becker, R., King, R., Petz, R., and Nitsche, W., 2007, "Adaptive Closed-Loop Control on a High-Lift Configuration Using Extremum Seeking," *AIAA J.*, **45**(6), pp. 1382–1392.
- [284] Banaszuk, A., Zhang, Y., and Jacobson, C. A., 2000, "Adaptive Control of Combustion Instability Using Extremum-Seeking," American Control Conference (ACC), Chicago, June 28–30, Vol. 1, pp. 416–422.
- [285] Banaszuk, A., Ariyur, K. B., Krstić, M., and Jacobson, C. A., 2004, "An Adaptive Algorithm for Control of Combustion Instability," *Automatica*, **40**(11), pp. 1965–1972.
- [286] Banaszuk, A., Narayanan, S., and Zhang, Y., 2003, "Adaptive Control of Flow Separation in a Planar Diffuser," *AIAA Paper No. 2003-617*.
- [287] Maury, R., Keonig, M., Cattafesta, L., Jordan, P., and Delville, J., 2012, "Extremum-Seeking Control of Jet Noise," *Aeroacoustics*, **11**(3–4), pp. 459–474.
- [288] Gelbert, G., Moeck, J. P., Paschereit, C. O., and King, R., 2012, "Advanced Algorithms for Gradient Estimation in One- and Two-Parameter Extremum Seeking Controllers," *J. Process Control*, **22**(4), pp. 700–709.
- [289] Wiederhold, O., King, R., Noack, B. R., Neuhaus, L., Neise, W., Enghard, L., and Swoboda, M., 2009, "Extensions of Extremum-Seeking Control to Improve the Aerodynamic Performance of Axial Turbomachines," *AIAA Paper No. 092407*.
- [290] Krieger, J. P., and Krstić, M., 2011, "Extremum Seeking Based on Atmospheric Turbulence for Aircraft Endurance," *J. Guid. Control Dyn.*, **34**(6), pp. 1876–1885.
- [291] Killingsworth, N. J., and Krstić, M., 2006, "PID Tuning Using Extremum Seeking: Online, Model-Free Performance Optimization," *IEEE Control Syst. Mag.*, **26**(1), pp. 70–79.

- [292] Krstić, M., Krupadanam, A., and Jacobson, C., 1999, "Self-Tuning Control of a Nonlinear Model of Combustion Instabilities," *IEEE Trans. Control Syst. Technol.*, **7**(4), pp. 424–436.
- [293] Koumoutsakos, P., 1997, "Active Control of Turbulent Channel Flow," *Center for Turbulence Research*, Stanford University, Stanford, CA, Annual Research Briefs, C, pp. 289–297.
- [294] Pamiès, M., Garnier, E., Merlen, A., and Sagaut, P., 2007, "Response of a Spatially Developing Turbulent Boundary Layer to Active Control Strategies in the Framework of Opposition Control," *Phys. Fluids*, **19**(10), p. 108102.
- [295] Iwamoto, K., Fukagata, K., Kasagi, N., and Suzuki, Y., 2005, "Friction Drag Reduction Achievable by Near-Wall Turbulence Manipulation at High Reynolds Numbers," *Phys. Fluids*, **17**(1), p. 011702.
- [296] Chung, Y. M., and Talha, T., 2011, "Effectiveness of Active Flow Control for Turbulent Skin Friction Drag Reduction," *Phys. Fluids*, **23**(2), p. 025102.
- [297] Rebecek, H., and Choi, K.-S., 2001, "Opposition Control of Near-Wall Turbulence With a Piston-Type Actuator," *Phys. Fluids*, **13**(8), pp. 2142–2145.
- [298] Endo, T., Kasagi, N., and Suzuki, Y., 2000, "Feedback Control of Wall Turbulence With Wall Deformation," *Int. J. Heat Fluid Flow*, **21**(5), pp. 568–575.
- [299] Fukagata, K., and Kasagi, N., 2002, "Active Control for Drag Reduction in Turbulent Pipe Flow," *Engineering Turbulence Modelling and Experiments 5*, W. Rodi and N. Fueyo, eds., Elsevier Science, Oxford, UK, pp. 607–616.
- [300] Fukagata, K., and Kasagi, N., 2003, "Drag Reduction in Turbulent Pipe Flow With Feedback Control Applied Partially to Wall," *Int. J. Heat Fluid Flow*, **24**(4), pp. 480–490.
- [301] Fukagata, K., and Kasagi, N., 2004, "Suboptimal Control for Drag Reduction Via Suppression of Near-Wall Reynolds Shear Stress," *Int. J. Heat Fluid Flow*, **25**(3), pp. 341–350.
- [302] Farrell, B. F., and Ioannou, P. J., 1996, "Turbulence Suppression by Active Control," *Phys. Fluids*, **8**(5), pp. 1257–1268.
- [303] Luhar, M., Sharma, A. S., and McKeon, B. J., 2014, "Opposition Control Within the Resolvent Analysis Framework," *J. Fluid Mech.*, **749**, pp. 597–626.
- [304] Cheng, B., and Titterington, D. M., 1994, "Neural Networks: A Review From a Statistical Perspective," *Statistical Science*, **9**(1), pp. 2–30.
- [305] Haykin, S., 2004, *Neural Networks: A Comprehensive Foundation*, Prentice Hall, Upper Saddle River, NJ.
- [306] Müller, S., Milano, M., and Koumoutsakos, P., 1999, "Application of Machine Learning Algorithms to Flow Modeling and Optimization," *Center for Turbulence Research Annual Research Briefs*, Stanford University, Stanford, CA, pp. 169–178.
- [307] Milano, M., and Koumoutsakos, P., 2002, "Neural Network Modeling for Near Wall Turbulent Flow," *J. Comput. Phys.*, **182**(1), pp. 1–26.
- [308] Oja, E., 1992, "Principal Components, Minor Components, and Linear Neural Networks," *Neural Networks*, **5**(6), pp. 927–935.
- [309] Oja, E., 1997, "The Nonlinear PCA Learning Rule in Independent Component Analysis," *Neurocomputing*, **17**(1), pp. 25–45.
- [310] Karhunen, J., and Joutsensalo, J., 1994, "Representation and Separation of Signals Using Nonlinear PCA Type Learning," *Neural Networks*, **7**(1), pp. 113–127.
- [311] Nair, A. G., and Taira, K., 2015, "Network-Theoretic Approach to Sparsified Discrete Vortex Dynamics," *J. Fluid Mech.*, **768**, pp. 549–571.
- [312] Ciresan, D., Meier, U., and Schmidhuber, J., 2012, "Multi-Column Deep Neural Networks for Image Classification," IEEE Conference on Computer Vision and Pattern Recognition (*CVPR*), Providence, RI, June 16–21, pp. 3642–3649.
- [313] Dean, J., Corrado, G., Monga, R., Chen, K., Devin, M., Mao, M., Senior, A., Tucker, P., Yang, K., Le, Q. V., and Ng, A. Y., 2012, "Large Scale Distributed Deep Networks," *Advances in Neural Information Processing Systems 25*, F. Pereira, C. J. C. Burges, L. Bottou, and K. Q. Weinberger, eds., Curran Associates, Inc., Red Hook, NY, pp. 1223–1231.
- [314] Hinton, G., Deng, L., Yu, D., Dahl, G. E., Mohamed, A.-R., Jaitly, N., Senior, A., Vanhoucke, V., Nguyen, P., Sainath, T. N., and Kingsbury, B., 2012, "Deep Neural Networks for Acoustic Modeling in Speech Recognition: The Shared Views of Four Research Groups," *Signal Process. Mag.*, **29**(6), pp. 82–97.
- [315] Holland, J. H., 1975, *Adaptation in Natural and Artificial Systems: An Introductory Analysis With Applications to Biology, Control, and Artificial Intelligence*, University of Michigan Press, Ann Arbor, MI.
- [316] Davis, L., 1991, *Handbook of Genetic Algorithms*, Vol. 115, Van Nostrand Reinhold, New York.
- [317] Goldberg, D. E., 2006, *Genetic Algorithms*, Pearson Education India, Delhi, India.
- [318] Koza, J. R., 1992, *Genetic Programming: On the Programming of Computers by Means of Natural Selection*, Vol. 1, MIT Press, Cambridge, MA.
- [319] Koza, J. R., Bennet, F. H., III, and Stiffelman, O., 1999, "Genetic Programming as a Darwinian Invention Machine," *Genetic Programming*, Springer, Berlin, pp. 93–108.
- [320] Koumoutsakos, P., Freund, J., and Parekh, D., 2001, "Evolution Strategies for Automatic Optimization of Jet Mixing," *AIAA J.*, **39**(5), pp. 967–969.
- [321] Buche, D., Stoll, P., Dornberger, R., and Koumoutsakos, P., 2002, "Multiobjective Evolutionary Algorithm for the Optimization of Noisy Combustion Processes," *IEEE Trans. Systems, Man, and Cybernet., Part C*, **32**(4), pp. 460–473.
- [322] Poncet, P., Cottet, G.-H., and Koumoutsakos, P., 2005, "Control of Three-Dimensional Wakes Using Evolution Strategies," *C. R. Mec.*, **333**(1), pp. 65–77.
- [323] Fukagata, K., Kern, S., Chatelain, P., Koumoutsakos, P., and Kasagi, N., 2008, "Evolutionary Optimization of an Anisotropic Compliant Surface for Turbulent Friction Drag Reduction," *J. Turbul.*, **9**(35), pp. 1–17.
- [324] Gazzola, M., Vasilyev, O. V., and Koumoutsakos, P., 2011, "Shape Optimization for Drag Reduction in Linked Bodies Using Evolution Strategies," *Comput. Struct.*, **89**(11), pp. 1224–1231.
- [325] Hansen, N., Niederberger, A. S., Guzzella, L., and Koumoutsakos, P., 2009, "A Method for Handling Uncertainty in Evolutionary Optimization With an Application to Feedback Control of Combustion," *IEEE Trans. Evol. Comput.*, **13**(1), pp. 180–197.
- [326] Noack, B. R., Duriez, T., Cordier, L., Segond, M., Abel, M., Brunton, S. L., Morzyński, M., Laurentie, J.-C., Parezanovic, V., and Bonnet, J.-P., 2013, "Closed-Loop Turbulence Control With Machine Learning Methods," *Bull. Am. Phys. Soc.*, **58**(18), p. 418.
- [327] Parezanović, V., Duriez, T., Cordier, L., Noack, B. R., Delville, J., Bonnet, J.-P., Segond, M., Abel, M., and Brunton, S. L., 2014, "Closed-Loop Control of an Experimental Mixing Layer Using Machine Learning Control," preprint [arXiv:1404.3259](https://arxiv.org/abs/1404.3259).
- [328] Gautier, N., Aider, J.-L., Duriez, T., Noack, B. R., Segond, M., and Abel, M., 2015, "Closed-Loop Separation Control Using Machine Learning," *J. Fluid Mech.*, **770**, pp. 442–457.
- [329] Duriez, T., Parezanović, V., Cordier, L., Noack, B. R., Delville, J., Bonnet, J.-P., Segond, M., and Abel, M., 2014, "Closed-Loop Turbulence Control Using Machine Learning," preprint [arXiv:1404.4589](https://arxiv.org/abs/1404.4589).
- [330] Gautier, N., 2014, "Flow Control Using Optical Sensors," Ph.D. thesis, Ecole Doctorale: Sciences Mécaniques, Acoustique, Électronique & Robotique (UPMC), ESPCI, Laboratoire PMMH, Paris.
- [331] Gunzburger, M. D., 2003, *Perspectives in Flow Control and Optimization*, Vol. 5, SIAM, Philadelphia.
- [332] Williams, D., and MacMynowski, D., "Brief History of Flow Control," *Fundamentals and Applications of Modern Flow Control*, Vol. 231, R. Joslin and D. Miller, eds., American Institute of Aeronautics and Astronautics, Reston, VA, pp. 1–20.
- [333] Schlichting, H., 1979, *Boundary-Layer Theory*, 7th ed., McGraw-Hill, New York.
- [334] Fiedler, H., and Fernholz, H.-H., 1990, "On the Management and Control of Turbulent Shear Flows," *Prog. Aeronaut. Sci.*, **27**(4), pp. 305–387.
- [335] McComb, D., 1991, *The Physics of Fluid Turbulence*, 1st ed., Clarendon Press, Oxford, UK.
- [336] Frisch, U., 1995, *Turbulence*, 1st ed., Cambridge University Press, Cambridge, UK.
- [337] Taylor, H., 1947, "The Elimination of Diffuser Separation by Vortex Generators," United Aircraft Corporation, East Hartford, CT, Technical Report No. R.4012-3.
- [338] Lorenz, E. N., 1963, "Deterministic Nonperiodic Flow," *J. Atmos. Sci.*, **20**(2), pp. 130–141.
- [339] Ott, E., Grebogi, C., and Yorke, J. A., 1990, "Controlling Chaos," *Phys. Rev. Lett.*, **64**(23), p. 2837.
- [340] Schöll, E., and Schuster, H. G., 2007, *Handbook of Chaos Control*, Wiley-VCH, Weinheim, Germany.
- [341] Aubry, N., Holmes, P., Lumley, J. L., and Stone, E., 1988, "The Dynamics of Coherent Structures in the Wall Region of a Turbulent Boundary Layer," *J. Fluid Mech.*, **192**, pp. 115–173.
- [342] Glauser, M. N., Leib, S. J., and George, W. K., 1987, *Coherent Structures in the Axisymmetric Turbulent Jet Mixing Layer*, Springer, Berlin.
- [343] George, W. K., 1988, "Insight Into the Dynamics of Coherent Structures From a Proper Orthogonal Decomposition," Symposium on Near Wall Turbulence, Dubrovnik, Yugoslavia, May 16–20.
- [344] Glauser, M. N., and George, W. K., 1992, "Application of Multipoint Measurements for Flow Characterization," *Exp. Therm. Fluid Sci.*, **5**(5), pp. 617–632.
- [345] Guyot, D., Paschereit, C. O., and Raghu, S., 2009, "Active Combustion Control Using a Fluidic Oscillator for Asymmetric Fuel Flow Modulation," *Int. J. Flow Control*, **1**(2), pp. 155–166.
- [346] Bobusch, B. C., Woszidlo, R., Bergada, J., Nayeri, C. N., and Paschereit, C. O., 2013, "Experimental Study of the Internal Flow Structures Inside a Fluidic Oscillator," *Exp. Fluids*, **54**(6), p. 1559.
- [347] Vallikivi, M., Hultmark, M., Bailey, S., and Smits, A., 2011, "Turbulence Measurements in Pipe Flow Using a Nano-Scale Thermal Anemometry Probe," *Exp. Fluids*, **51**(6), pp. 1521–1527.
- [348] Bailey, S. C., Kunkel, G. J., Hultmark, M., Vallikivi, M., Hill, J. P., Meyer, K. A., Tsay, C., Arnold, C. B., and Smits, A. J., 2010, "Turbulence Measurements Using a Nanoscale Thermal Anemometry Probe," *J. Fluid Mech.*, **663**, pp. 160–179.
- [349] Hultmark, M., Vallikivi, M., Bailey, S., and Smits, A., 2012, "Turbulent Pipe Flow at Extreme Reynolds Numbers," *Phys. Rev. Lett.*, **108**(9), p. 094501.
- [350] Daniel, T. L., 1988, "Forward Flapping Flight From Flexible Fins," *Can. J. Zool.*, **66**(3), pp. 630–638.
- [351] Anderson, J. M., Streitlien, K., Barrett, D. S., and Triantafyllou, M. S., 1998, "Oscillating Foils of High Propulsive Efficiency," *J. Fluid Mech.*, **360**, pp. 41–72.
- [352] Triantafyllou, M. S., and Triantafyllou, G. S., 1995, "An Efficient Swimming Machine," *Sci. Am.*, **272**(3), pp. 64–71.
- [353] Allen, J. J., and Smits, A. J., "Energy Harvesting Eel," *J. Fluids Struct.*, **15**(3–4), pp. 629–640.
- [354] Combes, S. A., and Daniel, T. L., 2001, "Shape, Flapping and Flexion: Wing and Fin Design for Forward Flight," *J. Exp. Biol.*, **204**(12), pp. 2073–2085.
- [355] Clark, R. P., and Smits, A. J., 2006, "Thrust Production and Wake Structure of a Batoid-Inspired Oscillating Fin," *J. Fluid Mech.*, **562**, pp. 415–429.
- [356] Buchholz, J. H., and Smits, A. J., 2008, "The Wake Structure and Thrust Performance of a Rigid Low-Aspect-Ratio Pitching Panel," *J. Fluid Mech.*, **603**(May), pp. 331–365.
- [357] Song, A., Tian, X., Israeli, E., Galvao, R., Bishop, K., Swartz, S., and Breuer, K., 2008, "Aeromechanics of Membrane Wings With Implications for Animal Flight," *AIAA J.*, **46**(8), pp. 2096–2106.

- [358] Taira, K., and Colonius, T., 2008, "Effect of Tip Vortices in Low-Reynolds-Number Poststall Flow Control," *AIAA J.*, **47**(3), pp. 749–756.
- [359] Taira, K., and Colonius, T., 2009, "Three-Dimensional Flows Around Low-Aspect-Ratio Flat-Plate Wings at Low Reynolds Numbers," *J. Fluid Mech.*, **623**, pp. 187–207.
- [360] Whittlesey, R. W., Liska, S. C., and Dabiri, J. O., 2010, "Fish Schooling as a Basis for Vertical-Axis Wind Turbine Farm Design," *Bioinspiration Biomimetics*, **5**(3), p. 035005.
- [361] Faruque, I., and Humbert, J. S., 2010, "Dipteran Insect Flight Dynamics. Part 1: Longitudinal Motion About Hover," *J. Theor. Biol.*, **264**(2), pp. 538–552.
- [362] Faruque, I., and Humbert, J. S., 2010, "Dipteran Insect Flight Dynamics. Part 2: Lateral-Directional Motion About Hover," *J. Theor. Biol.*, **265**(3), pp. 306–313.
- [363] Humbert, J. S., and Hyslop, A. M., 2010, "Bioinspired Visuomotor Convergence," *IEEE Trans. Rob.*, **26**(1), pp. 121–130.
- [364] Shelley, M. J., and Zhang, J., 2011, "Flapping and Bending Bodies Interacting With Fluid Flows," *Annu. Rev. Fluid Mech.*, **43**, pp. 449–465.
- [365] Leftwich, M. C., Tytell, E. D., Cohen, A. H., and Smits, A. J., 2012, "Wake Structures Behind a Swimming Robotic Lamprey With a Passively Flexible Tail," *J. Exp. Biol.*, **215**(3), pp. 416–425.
- [366] Dewey, P. A., Carriou, A., and Smits, A. J., 2012, "On the Relationship Between Efficiency and Wake Structure of a Batoid-Inspired Oscillating Fin," *J. Fluid Mech.*, **691**, pp. 245–266.
- [367] Nawroth, J. C., Lee, H., Feinberg, A. W., Ripplinger, C. M., McCain, M. L., Grosberg, A., Dabiri, J. O., and Parker, K. K., 2012, "A Tissue-Engineered Jellyfish With Biomimetic Propulsion," *Nat. Biotechnol.*, **30**, pp. 792–797.
- [368] Roth, E., Sponberg, S., and Cowan, N., 2014, "A Comparative Approach to Closed-Loop Computation," *Curr. Opin. Neurobiol.*, **25**, pp. 54–62.
- [369] Cowan, N. J., Ankarali, M. M., Dyhr, J. P., Madhav, M. S., Roth, E., Sefati, S., Sponberg, S., Stamper, S. A., Fortune, E. S., and Daniel, T. L., 2014, "Feedback Control as a Framework for Understanding Tradeoffs in Biology," *Integr. Comp. Biol.*, **54**(2), pp. 223–237.
- [370] Dickinson, M. H., and Gotz, K. G., 1996, "The Wake Dynamics and Flight Forces of the Fruit Fly *Drosophila melanogaster*," *J. Exp. Biol.*, **199**(9), pp. 2085–2104.
- [371] Sane, S. P., and Dickinson, M. H., 2001, "The Control of Flight Force by a Flapping Wing: Lift and Drag Production," *J. Exp. Biol.*, **204**(15), pp. 2607–2626.
- [372] Frye, M. A., and Dickinson, M. H., 2001, "Fly Flight: A Model for the Neural Control of Complex Behavior," *Neuron*, **32**(3), pp. 385–388.
- [373] Ghose, K., Horuchi, T. K., Krishnaprasad, P. S., and Moss, C. F., 2006, "Echolocating Bats Use a Nearly Time-Optimal Strategy to Intercept Prey," *PLoS Biol.*, **4**(5), p. e108.
- [374] Hedenstrom, A., Johansson, L., Wolf, M., Von Busse, R., Winter, Y., and Spedding, G., 2007, "Bat Flight Generates Complex Aerodynamic Tracks," *Science*, **316**(5826), pp. 894–897.
- [375] Riskin, D. K., Willis, D. J., Iriarte-Díaz, J., Hedrick, T. L., Kostandov, M., Chen, J., Laidlaw, D. H., Breuer, K. S., and Swartz, S. M., 2008, "Quantifying the Complexity of Bat Wing Kinematics," *J. Theor. Biol.*, **254**(3), pp. 604–615.
- [376] Hubel, T. Y., Hristov, N. I., Swartz, S. M., and Breuer, K. S., 2009, "Time-Resolved Wake Structure and Kinematics of Bat Flight," *Exp. Fluids*, **46**(5), pp. 933–943.
- [377] Fish, F. E., and Hui, C. A., 1991, "Dolphin Swimming—A Review," *Mamm. Rev.*, **21**(4), pp. 181–195.
- [378] Fish, F. E., 1996, "Transitions From Drag-Based to Lift-Based Propulsion in Mammalian Swimming," *Am. Zool.*, **36**(6), pp. 628–641.
- [379] Dickinson, M. H., Lehmann, F. O., and Sane, S. P., 1999, "Wing Rotation and the Aerodynamic Basis of Insect Flight," *Science*, **284**(5422), pp. 1954–1960.
- [380] Birch, J., and Dickinson, M., 2001, "Spanwise Flow and the Attachment of the Leading-Edge Vortex on Insect Wings," *Nature*, **412**(6848), pp. 729–733.
- [381] Sane, S. P., 2003, "The Aerodynamics of Insect Flight," *J. Exp. Biol.*, **206**(23), pp. 4191–4208.
- [382] Liao, J. C., Beal, D. N., Lauder, G. V., and Triantafyllou, M. S., 2003, "Fish Exploiting Vortices Decrease Muscle Activity," *Science*, **302**(5650), pp. 1566–1569.
- [383] Tytell, E. D., and Lauder, G. V., 2004, "The Hydrodynamics of Eel Swimming. I. Wake Structure," *J. Exp. Biol.*, **207**(11), pp. 1825–1841.
- [384] Lauder, G. V., and Tytell, E. D., 2005, "Hydrodynamics of Undulatory Propulsion," *Fish Physiol.*, **23**, pp. 425–468.
- [385] Videler, J. J., Samhuis, E. J., and Povel, G. D. E., 2004, "Leading-Edge Vortex Lifts Swifts," *Science*, **306**(5703), pp. 1960–1962.
- [386] Wang, Z. J., 2005, "Dissecting Insect Flight," *Annu. Rev. Fluid Mech.*, **37**, pp. 183–210.
- [387] Dabiri, J. O., 2009, "Optimal Vortex Formation as a Unifying Principle in Biological Propulsion," *Annu. Rev. Fluid Mech.*, **41**, pp. 17–33.
- [388] Wu, T. Y., 2011, "Fish Swimming and Bird/Insect Flight," *Annu. Rev. Fluid Mech.*, **43**, pp. 25–58.
- [389] Collett, T. S., and Land, M. F., 1975, "Visual Control of Flight Behaviour in the Hoverfly *Syrphus pipiens* L.," *J. Comp. Physiol. A*, **99**(1), pp. 1–66.
- [390] Fayyazuddin, A., and Dickinson, M. H., 1996, "Halteres Afferents Provide Direct, Electronic Input to a Steering Motor Neuron in the Blowfly, *Calliphora*," *J. Neurosci.*, **16**(16), pp. 5225–5232.
- [391] Fox, J. L., and Daniel, T. L., 2008, "A Neural Basis for Gyroscopic Force Measurement in the Halteres of *Holorusia*," *J. Comp. Physiol. A*, **194**(10), pp. 887–897.
- [392] Sane, S. P., Dieudonne, A., Willis, M. A., and Daniel, T. L., 2007, "Antennal Mechanosensors Mediate Flight Control in Moths," *Science*, **315**(5813), pp. 863–866.
- [393] Brown, R. E., and Fedde, M. R., 1993, "Airflow Sensors in the Avian Wing," *J. Exp. Biol.*, **179**(1), pp. 13–30.
- [394] Sterbing-D'Angelo, S. J., and Moss, C. F., 2014, "Air Flow Sensing in Bats," *Flow Sensing in Air and Water*, Springer, Berlin, pp. 197–213.
- [395] Sterbing-D'Angelo, S., Chadha, M., Chiu, C., Falk, B., Xian, W., Barcelo, J., Zook, J. M., and Moss, C. F., 2011, "Bat Wing Sensors Support Flight Control," *Proc. Natl. Acad. Sci.*, **108**(27), pp. 11291–11296.
- [396] Dickinson, B., 2010, "Hair Receptor Sensitivity to Changes in Laminar Boundary Layer Shape," *Bioinspiration Biomimetics*, **5**(1), p. 016002.
- [397] Massey, T., Kapur, R., Dabiri, F., Vu, L. N., and Sarrafzadeh, M., 2007, "Localization Using Low-Resolution Optical Sensors," *IEEE International Conference on Mobile Adhoc and Sensor Systems (MASS 2007)*, Pisa, Italy, Oct. 8–11.
- [398] Giannetti, F., and Luchini, P., 2007, "Structural Sensitivity of the First Instability of the Cylinder Wake," *J. Fluid Mech.*, **581**, pp. 167–197.
- [399] Hof, B., de Lozar, A., Avila, M., Tu, X., and Schneider, T. M., 2010, "Eliminating Turbulence in Spatially Intermittent Flows," *Science*, **327**(5972), pp. 1491–1494.
- [400] McKeon, B. J., 2010, "Controlling Turbulence," *Science*, **327**(5927), pp. 1462–1463.
- [401] Avila, K., Moxey, D., de Lozar, A., Avila, M., Barkley, D., and Hof, B., 2011, "The Onset of Turbulence in Pipe Flow," *Science*, **333**(6039), pp. 192–196.
- [402] Brunton, B. W., Brunton, S. L., Proctor, J. L., and Kutz, J. N., 2013, "Optimal Sensor Placement and Enhanced Sparsity for Classification," preprint arXiv:1310.4217.
- [403] Proctor, J. L., Brunton, S. L., Brunton, B. W., and Kutz, J. N., 2014, "Exploiting Sparsity and Equation-Free Architectures in Complex Systems (Invited Review)," *Eur. Phys. J. Spec. Top.*, **223**(13), pp. 2665–2684.
- [404] Hey, A. J., Tansley, S., and Tolle, K. M., 2009, *The Fourth Paradigm: Data-Intensive Scientific Discovery*, Microsoft Research, Redmond, WA.
- [405] Allaire, D., Biros, G., Chambers, J., Ghattas, O., Kordonowy, D., and Willcox, K., 2012, "Dynamic Data Driven Methods for Self-Aware Aerospace Vehicles," *Proc. Comput. Sci.*, **9**, pp. 1206–1210.
- [406] Kutz, J. N., 2013, *Data-Driven Modeling & Scientific Computation: Methods for Complex Systems & Big Data*, Oxford University Press, Oxford, UK.
- [407] Candès, E. J., 2006, "Compressive Sampling," *International Congress of Mathematics*, Madrid, Aug. 22–30, Vol. 3, pp. 1433–1452.
- [408] Donoho, D. L., 2006, "Compressed Sensing," *IEEE Trans. Inf. Theory*, **52**(4), pp. 1289–1306.
- [409] Baraniuk, R. G., 2007, "Compressive Sensing," *IEEE Signal Process. Mag.*, **24**(4), pp. 118–120.
- [410] Tropp, J. A., and Gilbert, A. C., 2007, "Signal Recovery From Random Measurements Via Orthogonal Matching Pursuit," *IEEE Trans. Inf. Theory*, **53**(12), pp. 4655–4666.
- [411] Candès, E. J., and Wakin, M. B., 2008, "An Introduction to Compressive Sampling," *IEEE Signal Process. Mag.*, **25**(2), pp. 21–30.
- [412] Willert, C. E., and Gharib, M., 1991, "Digital Particle Image Velocimetry," *Exp. Fluids*, **10**(4), pp. 181–193.
- [413] Nyquist, H., 1928, "Certain Topics in Telegraph Transmission Theory," *Trans. AIEE*, **47**(2), pp. 617–644.
- [414] Shannon, C. E., 1948, "A Mathematical Theory of Communication," *Bell Syst. Tech. J.*, **27**(3), pp. 379–423.
- [415] Petra, S., and Schnörr, C., 2009, "TomoPIV Meets Compressed Sensing," *Pure Math. Appl.*, **20**(1–2), pp. 49–76.
- [416] Becker, F., Wieneke, B., Petra, S., Schröder, A., and Schnörr, C., 2012, "Variational Adaptive Correlation Method for Flow Estimation," *IEEE Trans. Image Process.*, **21**(6), pp. 3053–3065.
- [417] Bai, Z., Wimalajeewa, T., Berger, Z., Wang, G., Glauser, M., and Varshney, P. K., 2013, "Physics Based Compressive Sensing Approach Applied to Airfoil Data Collection and Analysis," *AIAA Paper No. 2013-0772*.
- [418] Bai, Z., Wimalajeewa, T., Berger, Z., Wang, G., Glauser, M., and Varshney, P. K., 2014, "Low-Dimensional Approach for Reconstruction of Airfoil Data Via Compressive Sensing," *AIAA J.*, **53**(4), pp. 920–933.
- [419] Candès, E. J., Romberg, J., and Tao, T., 2006, "Robust Uncertainty Principles: Exact Signal Reconstruction From Highly Incomplete Frequency Information," *IEEE Trans. Inf. Theory*, **52**(2), pp. 489–509.
- [420] Candès, E. J., Romberg, J., and Tao, T., 2006, "Stable Signal Recovery From Incomplete and Inaccurate Measurements," *Commun. Pure Appl. Math.*, **59**(8), pp. 1207–1223.
- [421] Candès, E. J., and Tao, T., 2006, "Near Optimal Signal Recovery From Random Projections: Universal Encoding Strategies?" *IEEE Trans. Inf. Theory*, **52**(12), pp. 5406–5425.
- [422] Boyd, S., and Vandenberghe, L., 2009, *Convex Optimization*, Cambridge University Press, Cambridge, UK.
- [423] Mathelin, L., and Gallivan, K. A., 2012, "A Compressed Sensing Approach for Partial Differential Equations With Random Input Data," *Commun. Comput. Phys.*, **12**(4), pp. 1–36.
- [424] Schaeffer, H., Caflisch, R., Hauck, C. D., and Osher, S., 2013, "Sparse Dynamics for Partial Differential Equations," *Proc. Natl. Acad. Sci. U.S.A.*, **110**(17), pp. 6634–6639.
- [425] Mackey, A., Schaeffer, H., and Osher, S., "On the Compressive Spectral Method," *Multiscale Model. & Simul.*, **12**(4), pp. 1800–1827.
- [426] Tran, G., Schaeffer, H., Feldman, W. M., and Osher, S. J., 2014, "An L1 Penalty Method for General Obstacle Problems," preprint arXiv:1404.1370.

- [427] Shi, J. V., Yin, W., Sankaranarayanan, A. C., and Baraniuk, R. G., "Video Compressive Sensing for Dynamic MRI," *BMC Neurosci.*, **13**(Suppl 1), p. 183.
- [428] Jovanović, M. R., Schmid, P. J., and Nichols, J. W., 2014, "Sparsity-Promoting Dynamical Mode Decomposition," *Phys. Fluids*, **26**(2), p. 024103.
- [429] Brunton, S. L., Proctor, J. L., and Kutz, J. N., "Compressive Sampling and Dynamic Mode Decomposition," *arXiv:1312.5186*.
- [430] Gueniat, F., Mathelin, L., and Pastur, L., 2015, "A Dynamic Mode Decomposition Approach for Large and Arbitrarily Sampled Systems," *Phys. Fluids*, **27**(2), p. 025113.
- [431] Bright, I., Lin, G., and Kutz, J. N., 2013, "Compressive Sensing and Machine Learning Strategies for Characterizing the Flow Around a Cylinder With Limited Pressure Measurements," *Phys. Fluids*, **25**(12), p. 127102.
- [432] Brunton, S. L., Tu, J. H., Bright, I., and Kutz, J. N., 2014, "Compressive Sensing and Low-Rank Libraries for Classification of Bifurcation Regimes in Nonlinear Dynamical Systems," *SIAM J. Appl. Dyn. Syst.*, **13**(4), pp. 1716–1732.
- [433] Tayler, A. B., Holland, D. J., Sederman, A. J., and Gladden, L. F., 2012, "Exploring the Origins of Turbulence in Multiphase Flow Using Compressed Sensing MRI," *Phys. Rev. Lett.*, **108**(26), p. 264505.
- [434] Branicki, M., and Majda, A. J., 2014, "Quantifying Bayesian Filter Performance for Turbulent Dynamical Systems Through Information Theory," *Commun. Math. Sci.*, **12**(5), pp. 901–978.
- [435] Bourguignon, J.-L., Tropp, J., Sharma, A., and McKeon, B., 2014, "Compact Representation of Wall-Bounded Turbulence Using Compressive Sampling," *Phys. Fluids*, **26**(1), p. 015109.
- [436] Fu, X., Brunton, S. L., and Kutz, J. N., 2014, "Classification of Birefringence in Mode-Locked Fiber Lasers Using Machine Learning and Sparse Representation," *Opt. Express*, **22**(7), pp. 8585–8597.
- [437] Brunton, S. L., Fu, X., and Kutz, J. N., 2014, "Self-Tuning Fiber Lasers," *IEEE J. Sel. Top. Quantum Electron.*, **20**(5), p. 1101408.
- [438] Wright, J., Yang, A., Ganesh, A., Sastry, S., and Ma, Y., 2009, "Robust Face Recognition Via Sparse Representation," *IEEE Trans. Pattern Anal. Mach. Intell. (PAMI)*, **31**(2), pp. 210–227.
- [439] Kaiser, E., Noack, B. R., Cordier, L., Spohn, A., Segond, M., Abel, M., Daviller, G., and Niven, R. K., 2014, "Cluster-Based Reduced-Order Modelling of a Mixing Layer," *J. Fluid Mech.*, **754**, pp. 365–414.
- [440] Burkardt, J., Gunzburger, M., and Lee, H.-C., 2004, "Centroidal Voronoi Tessellation-Based Reduced-Order Modeling of Complex Systems," *SIAM J. Sci. Comput.*, **28**(2), pp. 459–484.
- [441] Schneider, T. M., Eckhardt, B., and Vollmer, J., 2007, "Statistical Analysis of Coherent Structures in Transitional Pipe Flow," *Phys. Rev. E*, **75**(6), pp. 66–313.
- [442] Gear, C. W., Kevrekidis, I. G., and Theodoropoulos, C., "Coarse" Integration/Bifurcation Analysis Via Microscopic Simulators: Micro-Galerkin Methods," *Comput. Chem. Eng.*, **26**(7–8), pp. 941–963.
- [443] Gorban, A., Kazantzis, N. K., Kevrekidis, I. G., Öttinger, H., and Theodoropoulos, C., eds., 2006, *Model Reduction and Coarse-Graining Approaches for Multiscale Phenomena*, Springer-Verlag, Berlin.
- [444] Kevrekidis, I. G., Gear, C. W., Hyman, J. M., Kevrekidis, P. G., Runborg, O., and Theodoropoulos, C., 2003, "Equation-Free, Coarse-Grained Multiscale Computation: Enabling Microscopic Simulators to Perform System-Level Analysis," *Commun. Math. Sci.*, **1**(4), pp. 715–762.
- [445] Sirisup, S., Karniadakis, G. E., Xiu, D., and Kevrekidis, I. G., 2005, "Equation-Free/Galerkin-POD-Assisted Computation of Incompressible Flows," *J. Comput. Phys.*, **207**(2), pp. 568–587.
- [446] Xiu, D., and Karniadakis, G. E., 2002, "The Wiener–Askey Polynomial Chaos for Stochastic Differential Equations," *SIAM J. Sci. Comput.*, **24**(2), pp. 619–644.
- [447] Xiu, D., and Karniadakis, G. E., 2003, "Modeling Uncertainty in Flow Simulations Via Generalized Polynomial Chaos," *J. Comput. Phys.*, **187**(1), pp. 137–167.
- [448] Xiu, D., 2010, *Numerical Methods for Stochastic Computations: A Spectral Method Approach*, Princeton University Press, Princeton, NJ.
- [449] Grosek, J., and Kutz, J. N., 2014, "Dynamic Mode Decomposition for Real-Time Background/Foreground Separation in Video," preprint *arXiv:1404.7592*.
- [450] Hemati, M. S., Williams, M. O., and Rowley, C. W., 2014, "Dynamic Mode Decomposition for Large and Streaming Datasets," preprint *arXiv:1406.7187*.
- [451] Dawson, S., Hemati, M., Williams, M., and Rowley, C., 2014, "Characterizing and Correcting for the Effect of Sensor Noise in the Dynamic Mode Decomposition," *Bull. Am. Phys. Soc.*, **59**(20), p. 428.
- [452] Aref, H., 1984, "Stirring by Chaotic Advection," *J. Fluid Mech.*, **143**, pp. 1–21.
- [453] Wiener, N., 1938, "The Homogeneous Chaos," *Am. J. Math.*, **60**(4), pp. 897–936.
- [454] Wan, X., and Karniadakis, G. E., 2005, "An Adaptive Multi-Element Generalized Polynomial Chaos Method for Stochastic Differential Equations," *J. Comput. Phys.*, **209**(2), pp. 617–642.
- [455] Gerritsma, M., van der Steen, J.-B., Vos, P. E. J., and Karniadakis, G. E., 2010, "Time-Dependent Generalized Polynomial Chaos," *J. Comput. Phys.*, **229**(22), pp. 8333–8363.
- [456] Luchtenburg, D. M., Brunton, S. L., and Rowley, C. W., 2014, "Long-Time Uncertainty Propagation Using Generalized Polynomial Chaos and Flow Map Composition," *J. Comput. Phys.*, **274**, pp. 783–802.
- [457] Le Maître, O. P., and Knio, O. M., 2010, *Spectral Methods for Uncertainty Quantification*, Springer, Dordrecht.
- [458] Sapsis, T. P., and Lermusiaux, P. F., 2009, "Dynamically Orthogonal Field Equations for Continuous Stochastic Dynamical Systems," *Physica D*, **238**(23–24), pp. 2347–2360.
- [459] Sapsis, T. P., and Lermusiaux, P. F., 2012, "Dynamical Criteria for the Evolution of the Stochastic Dimensionality in Flows With Uncertainty," *Physica D*, **241**(1), pp. 60–76.
- [460] Haller, G., 2001, "Distinguished Material Surfaces and Coherent Structures in Three-Dimensional Fluid Flows," *Physica D*, **149**(4), pp. 248–277.
- [461] Haller, G., 2002, "Lagrangian Coherent Structures From Approximate Velocity Data," *Phys. Fluids*, **14**(6), pp. 1851–1861.
- [462] Shadden, S. C., Lekien, F., and Marsden, J. E., 2005, "Definition and Properties of Lagrangian Coherent Structures From Finite-Time Lyapunov Exponents in Two-Dimensional Aperiodic Flows," *Physica D*, **212**(3–4), pp. 271–304.
- [463] Green, M. A., Rowley, C. W., and Haller, G., 2007, "Detection of Lagrangian Coherent Structures in 3D Turbulence," *J. Fluid Mech.*, **572**, pp. 111–120.
- [464] Mathur, M., Haller, G., Peacock, T., Ruppert-Felsot, J. E., and Swinney, H. L., 2007, "Uncovering the Lagrangian Skeleton of Turbulence," *Phys. Rev. Lett.*, **98**(14), p. 144502.
- [465] Brunton, S. L., and Rowley, C. W., 2010, "Fast Computation of FTLE Fields for Unsteady Flows: A Comparison of Methods," *Chaos*, **20**(1), p. 017503.
- [466] Farazmand, M., and Haller, G., 2012, "Computing Lagrangian Coherent Structures From Their Variational Theory," *Chaos*, **22**(1), p. 013128.
- [467] Kafiabadi, H. A., Chan, P. W., and Haller, G., 2012, "Lagrangian Detection of Aerial Turbulence for Landing Aircraft," *J. Appl. Meteorol. Climatol.*, **30**(12), pp. 2808–2819.
- [468] Shadden, S. C., Astorino, M., and Gerbeau, J. F., 2010, "Computational Analysis of an Aortic Valve Jet With Lagrangian Coherent Structures," *Chaos*, **20**(1), p. 017512.
- [469] Wilson, M. M., Peng, J., Dabiri, J. O., and Eldredge, J. D., 2009, "Lagrangian Coherent Structures in Low Reynolds Number Swimming," *J. Phys.: Condens. Matter*, **21**(20), p. 204105.
- [470] Green, M. A., Rowley, C. W., and Smits, A. J., 2011, "The Unsteady Three-Dimensional Wake Produced by a Trapezoidal Pitching Panel," *J. Fluid Mech.*, **685**, pp. 117–145.
- [471] Peng, J., and Dabiri, J. O., 2008, "The 'Upstream Wake' of Swimming and Flying Animals and Its Correlation With Propulsive Efficiency," *J. Exp. Biol.*, **21**(16), pp. 2669–2677.
- [472] Bollt, E. M., Luttmann, A., Kramer, S., and Basnayake, R., 2012, "Measurable Dynamics Analysis of Transport in the Gulf of Mexico During the Oil Spill," *Int. J. Bifurcation Chaos*, **22**(3), p. 1230012.
- [473] Lekien, F., Couillette, C., Mariano, A. J., Ryan, E. H., Shay, L. K., Haller, G., and Marsden, J. E., 2005, "Pollution Release Tied to Invariant Manifolds: A Case Study for the Coast of Florida," *Physica D*, **210**(1–2), pp. 1–20.
- [474] Mezić, I., Loire, S., Fonoferov, V. A., and Hogan, P., 2010, "A New Mixing Diagnostic and Gulf Oil Spill Movement," *Science*, **330**(6003), pp. 486–489.
- [475] Padberg, K., Hauff, T., Jenko, F., and Junge, O., 2007, "Lagrangian Structures and Transport in Turbulent Magnetized Plasmas," *New J. Phys.*, **9**(11), p. 400.
- [476] Froyland, G., and Padberg, K., 2009, "Almost-Invariant Sets and Invariant Manifolds—Connecting Probabilistic and Geometric Descriptions of Coherent Structures in Flows," *Physica D*, **238**(16), pp. 1507–1523.
- [477] Froyland, G., Santitissadeekorn, N., and Monahan, A., 2010, "Transport in Time-Dependent Dynamical Systems: Finite-Time Coherent Sets," *Chaos*, **20**(4), p. 043116.
- [478] Tallapragada, P., and Ross, S. D., 2013, "A Set Oriented Definition of Finite-Time Lyapunov Exponents and Coherent Sets," *Commun. Nonlinear Sci. Numer. Simul.*, **18**(5), pp. 1106–1126.
- [479] Dellnitz, M., Froyland, G., and Junge, O., 2001, "The Algorithms Behind Gaio—Set Oriented Numerical Methods for Dynamical Systems," *Ergodic Theory, Analysis, and Efficient Simulation of Dynamical Systems*, B. Fiedler, ed., Springer, Dordrecht, pp. 145–174.
- [480] Dellnitz, M., and Junge, O., 2002, "Set Oriented Numerical Methods for Dynamical Systems," *Handbook of Dynamical Systems*, Vol. 2, B. Fiedler, ed., Elsevier, Amsterdam, pp. 221–264.
- [481] Carlberg, K., Bou-Mosleh, C., and Farhat, C., 2011, "Efficient Non-Linear Model Reduction Via Least-Squares Petrov–Galerkin Projection and Compressive Tensor Approximations," *Int. J. Numer. Methods Eng.*, **86**(2), pp. 155–181.
- [482] Avellaneda, M., and Majda, A. J., 1990, "Mathematical Models With Exact Renormalization for Turbulent Transport," *Commun. Math. Phys.*, **131**(2), pp. 381–429.
- [483] Amsallem, D., Zahr, M. J., and Farhat, C., 2012, "Nonlinear Model Order Reduction Based on Local Reduced-Order Bases," *Int. J. Numer. Methods Eng.*, **92**(10), pp. 891–916.
- [484] Carlberg, K., Farhat, C., Cortial, J., and Amsallem, D., 2013, "The GNAT Method for Nonlinear Model Reduction: Effective Implementation and Application to Computational Fluid Dynamics and Turbulent Flows," *J. Comput. Phys.*, **242**, pp. 623–647.
- [485] Everson, R., and Sirovich, L., 1995, "Karhunen–Loeve Procedure for Gappy Data," *JOSA A*, **12**(8), pp. 1657–1664.
- [486] Willcox, K., 2006, "Unsteady Flow Sensing and Estimation Via the Gappy Proper Orthogonal Decomposition," *Comput. Fluids*, **35**(2), pp. 208–226.
- [487] Barrault, M., Maday, Y., Nguyen, N. C., and Patera, A. T., 2004, "An 'Empirical Interpolation' Method: Application to Efficient Reduced-Basis Discretization of Partial Differential Equations," *C. R. Math.*, **339**(9), pp. 667–672.

- [488] Chaturantabut, S., and Sorensen, D. C., 2010, "Nonlinear Model Reduction Via Discrete Empirical Interpolation," *SIAM J. Sci. Comput.*, **32**(5), pp. 2737–2764.
- [489] Chaturantabut, S., and Sorensen, D. C., 2012, "A State Space Error Estimate for POD-DEIM Nonlinear Model Reduction," *SIAM J. Numer. Anal.*, **50**(1), pp. 46–63.
- [490] Peherstorfer, B., Butnaru, D., Willcox, K., and Bungartz, H.-J., 2014, "Localized Discrete Empirical Interpolation Method," *SIAM J. Sci. Comput.*, **36**(1), pp. A168–A192.
- [491] Majda, A. J., and Kramer, P. R., 1999, "Simplified Models for Turbulent Diffusion Theory, Numerical Modelling, and Physical Phenomena," *Phys. Rep.*, **314**(4), pp. 237–574.
- [492] Majda, A. J., Harlim, J., and Gershgorin, B., 2010, "Mathematical Strategies for Filtering Turbulent Dynamical Systems," *Discrete Contin. Dyn. Syst.*, **27**(2), pp. 441–486.
- [493] Majda, A. J., and Harlim, J., 2012, *Filtering Complex Turbulent Systems*, Cambridge University Press, Cambridge, UK.
- [494] Maynard Gayme, D., 2010, "A Robust Control Approach to Understanding Nonlinear Mechanisms in Shear Flow Turbulence," Ph.D. thesis, California Institute of Technology, Pasadena, CA.
- [495] Marusic, I., and Hutchins, N., 2005, "Experimental Study of Wall Turbulence: Implications for Control," *Transition and Turbulence Control*, World Scientific, Singapore, pp. 207–246.
- [496] Smits, A. J., McKeon, B. J., and Marusic, I., 2011, "High-Reynolds Number Wall Turbulence," *Annu. Rev. Fluid Mech.*, **43**(1), pp. 353–375.
- [497] Cacuci, D. G., Navon, I. M., and Ionescu-Bujor, M., 2013, *Computational Methods for Data Evaluation and Assimilation*, Chapman & Hall, Oxford, UK.
- [498] Cordier, L., Abou El Majd, B., and Favier, J., 2010, "Calibration of POD Reduced-Order Models Using Tikhonov Regularization," *Int. J. Numer. Methods Fluids*, **63**(2), pp. 269–296.
- [499] Kapur, J. N., and Kevasan, H. K., 1992, *Entropy Optimization Principles With Applications*, 1st ed., Academic Press, Boston.
- [500] Noack, B. R., and Niven, R. K., 2012, "Maximum-Entropy Closure for a Galerkin System of Incompressible Shear Flow," *J. Fluid Mech.*, **700**, pp. 187–213.
- [501] Noack, B. R., and Niven, R. K., 2013, "A Hierarchy of Maximum-Entropy Closures for Galerkin Systems of Incompressible Flows," *Comput. Math. Appl.*, **65**(10), pp. 1558–1574.
- [502] Andrensen, B., 1983, "Finite-Time Thermodynamics," *Physics Laboratory II*, 1st ed., University of Copenhagen, Copenhagen, Denmark.
- [503] Noack, B. R., Schlegel, M., Ahlbom, B., Mutschke, G., Morzyński, M., Comte, P., and Tadmor, G., 2008, "A Finite-Time Thermodynamics of Unsteady Fluid Flows," *J. Non-Equilibr. Thermodyn.*, **33**(2), pp. 103–148.
- [504] Noack, B. R., Schlegel, M., Morzyński, M., and Tadmor, G., 2010, "System Reduction Strategy for Galerkin Models of Fluid Flows," *Int. J. Numer. Methods Fluids*, **63**(2), pp. 231–248.
- [505] Taira, K., 2015, private communication.
- [506] Watts, D. J., and Strogatz, S. H., 1998, "Collective Dynamics of 'Small-World' Networks," *Nature*, **393**(6684), pp. 440–442.
- [507] Barabási, A.-L., and Albert, R., 1999, "Emergence of Scaling in Random Networks," *Science*, **286**(5439), pp. 509–512.
- [508] Barabási, A.-L., 2009, "Scale-Free Networks: A Decade and Beyond," *Science*, **325**(5939), pp. 412–413.
- [509] Del Genio, C. I., Gross, T., and Bassler, K. E., 2011, "All Scale-Free Networks are Sparse," *Phys. Rev. Lett.*, **107**(17), p. 178701.
- [510] Barzel, B., and Barabási, A.-L., 2013, "Universality in Network Dynamics," *Nat. Phys.*, **9**(10), pp. 673–681.
- [511] Newman, M. E., 2003, "The Structure and Function of Complex Networks," *SIAM Rev.*, **45**(2), pp. 167–256.
- [512] Leonard, N. E., and Fiorelli, E., 2001, "Virtual Leaders, Artificial Potentials and Coordinated Control of Groups," *40th IEEE Conference on Decision and Control*, Orlando, FL, Dec. 4–7, Vol. 3, pp. 2968–2973.
- [513] Olfati-Saber, R., 2006, "Flocking for Multi-Agent Dynamic Systems: Algorithms and Theory," *IEEE Trans. Autom. Control*, **51**(3), pp. 401–420.
- [514] Balch, T., and Arkin, R. C., 1998, "Behavior-Based Formation Control for Multirobot Teams," *IEEE Trans. Rob. Autom.*, **14**(6), pp. 926–939.
- [515] Cortes, J., Martinez, S., Karatas, T., and Bullo, F., 2002, "Coverage Control for Mobile Sensing Networks," *IEEE International Conference on Robotics and Automation (ICRA '02)*, Washington, DC, May 11–15, Vol. 2, pp. 1327–1332.
- [516] Leonard, N. E., Paley, D. A., Lekien, F., Sepulchre, R., Fratantoni, D. M., and Davis, R. E., 2007, "Collective Motion, Sensor Networks, and Ocean Sampling," *Proc. IEEE*, **95**(1), pp. 48–74.
- [517] Milo, R., Shen-Orr, S., Itzkovitz, S., Kashtan, N., Chklovskii, D., and Alon, U., 2002, "Network Motifs: Simple Building Blocks of Complex Networks," *Science*, **298**(5594), pp. 824–827.
- [518] Luscombe, N. M., Babu, M. M., Yu, H., Snyder, M., Teichmann, S. A., and Gerstein, M., 2004, "Genomic Analysis of Regulatory Network Dynamics Reveals Large Topological Changes," *Nature*, **431**(7006), pp. 308–312.
- [519] Low, S. H., Paganini, F., and Doyle, J. C., 2002, "Internet Congestion Control," *Control Syst.*, **22**(1), pp. 28–43.
- [520] Doyle, J. C., Alderson, D. L., Li, L., Low, S., Roughan, M., Shalunov, S., Tanaka, R., and Willinger, W., 2005, "The 'Robust Yet Fragile' Nature of the Internet," *Proc. Natl. Acad. Sci. U.S.A.*, **102**(41), pp. 14497–14502.
- [521] Rahmani, A., Ji, M., Mesbahi, M., and Egerstedt, M., 2009, "Controllability of Multi-Agent Systems From a Graph-Theoretic Perspective," *SIAM J. Control Optim.*, **48**(1), pp. 162–186.
- [522] Liu, Y.-Y., Slotine, J.-J., and Barabasi, A.-L., 2011, "Controllability of Complex Networks," *Nature*, **473**(7346), pp. 167–173.
- [523] Lin, F., Fardad, M., and Jovanović, M. R., 2014, "Algorithms for Leader Selection in Stochastically Forced Consensus Networks," *IEEE Trans. Autom. Control*, **59**(7), pp. 1789–1802.
- [524] Cowan, N. J., Chastain, E. J., Vilhena, D. A., Freudenberg, J. S., and Bergstrom, C. T., 2012, "Nodal Dynamics, Not Degree Distributions, Determine the Structural Controllability of Complex Networks," *PLoS One*, **7**(6), p. e38398.
- [525] Brockett, R., 2012, "Notes on the Control of the Liouville Equation," *Control of Partial Differential Equations* (Lecture Notes in Mathematics, Vol. 2048), F. Alabau-Bousouira, R. Brockett, O. Glass, J. Le Rousseau, and E. Zuazua, eds., Springer, Berlin, pp. 101–129.
- [526] Hopf, E., 1951, "Statistical Hydromechanics and Functional Analysis," *J. Ration. Mech. Anal.*, **1**, pp. 87–123.
- [527] Bagheri, S., 2013, "Koopman-Mode Decomposition of the Cylinder Wake," *J. Fluid Mech.*, **726**, pp. 596–623.
- [528] Bagheri, S., 2014, "Effects of Weak Noise on Oscillating Flows: Linking Quality Factor, Floquet Modes and Koopman Spectrum," *Phys. Fluids*, **26**(9), p. 094104.